Rehydroxylation dating

by

Vincent Hare

A thesis submitted in partial fulfillment for the degree of Doctor of Philosophy

RLAHA
University of Oxford

October 2016

Statement of Originality

I declare that the work presented herein is my own. I confirm that:

- I know that plagiarism is wrong. Plagiarism is to use another's work and to pretend that it is one's own.
- I have used an accepted convention for citation and referencing. In this dissertation, each signicant contribution or quotation from the work or works of other people has been attributed, and cited or referenced.
- This dissertation is my own work.
- I have not copied the work of any other person; nor have I allowed, and nor will I allow, anyone to copy my work with the intention of passing it off as his or her own work.

"Whoever, in the pursuit of science, seeks after immediate practical utility, may generally rest assured that he will seek in vain. "

Hermann von Helmholtz (trans.)
Atkinson (1883) Popular Lectures on Scientific Subjects: First Series, at 29

Abstract

This thesis is concerned with a better understanding of issues which currently limit the precision, accuracy and robustness of rehydroxylation (RHX) dating. MC simulations and analytical expressions show that age uncertainties of previous studies are underestimates. The ratio of sample mass to balance resolution should be of the order of 10^{-6} or less for measurement precision under 1%. A combined measurement uncertainty of ~ 4 % should be possible, given well-designed experiments, appropriate samples, and a $t^{1/N}$ model with $N = 4$. Highly-fired materials have an age limit of $\sim$ Ma, but low α and y_{max} preclude dating materials such as porcelain. There is little correlation between non-stabilisation of m_2 and factors such as porosity, specific heat capacity or density. The strongest effect is that of sample dimension (thickness), which is found to cause long times to stage II mass gain following 105 ^{o}C heating - roughly proportional to the thickness squared, suggesting some long-lived contribution from Fickian diffusion. Another strong effect is acceleration of the rehydroxylation reaction upon cooling from high temperatures, which is also dependent on sample size. This causes long times to stage II, and inaccuracies in fitting α_{m}. Sample dimensions therefore pose a fundamental challenge for rehydroxylation dating by gravimetric analysis. Evidence is presented for a long-lived weakly-bound (T1) water regime in certain materials. A new apparatus for high-precision mass measurements of multiple samples under controlled conditions was used to investigate differences between meta-clay minerals, and to evaluate the efficiency of different pretreatments on fired clays of known age (1.1a). RHX age determinations, corrected for ELT, range from 30.1 $\pm$ 0.3 a to 1.51 $\pm$ 0.04, and some clear differences appear for different meta-clay minerals. FTIR spectra indicate that treatment with 0.5M HCl at 70 ^{o}C for 30 minutes causes rehydroxylation of clay minerals, but 0.1M HCl seems suitable. Organic removal by chloroform/methanol solvent extraction or H_2O_2 treatment avoids alteration of structural OH, but is not as effective as supercritical fluid extraction (SFE) in the case of lipids. The RHX age determination of a sample of Werra pottery (MAN07) was 169 $\pm$ 30 a, with an activation energy of 82.7 kJ mol^{-1} and at an ELT of 10.5 ^{o}C, which is not in agreement with the result obtained in previous studies. The relationship between the $t^{1/4}$ model and diffusion mechanisms is briefly discussed, and a discussion of the issues is entertained. Goodness-of-fit statistics are highest for a model with long-lived T1 and T2 regimes, but this mass gain behaviour is identical to that expected from an accelerated $t^{1/4}$ process and slow cooling. It is therefore not possible to exclude the possibility of a $t^{1/4}$ regime.

Acknowledgements

A great many people assisted with this project, in some way or another. In no particular order, I am very grateful to Prof. Murray Moinester for his ideas, enthusiasm and advice, and similarly to Dr. Yves Gallet and Dr. Maxime le Goff for the great deal of time and thinking they have put into RHX, which has yielded very important and fruitful ideas. Likewise, Prof. Christopher Hall has been a great help and has made many valuable suggestions and I have benefitted from our discussions. I would like to thank Dr. Moira Wilson, for bringing us to Manchester, for planting the seed and giving us a great deal to think about. Also thanks to Sarah-Jane Clelland.

At Oxford, I could not have completed this project without the help of Jon Temple, Department of Atmospheric Physics, to whom no technical request was too much, and who helped to construct and wire the chamber. Dr. Simon Calcutt assisted with chamber design. I learnt a great deal from Bob Sawala and Prof Martin Williams of the Department of Engineering, who helped to cast concrete. Paul Shelley at Brec engineering machined the parts I designed for the carousel, and Joe Graystone, RLAHA, helped with installation and general odd jobs. At RLAHA, Dr Mike Dee has kept me going through much sound advice and a willing ear. I am very grateful to Dr Thibaut Devièse and who has been essential in performing the SFE experiments, and a very fruitful collaborator indeed. I hope we will continue this research. I wish to thank my supervisor, Prof. Christopher Ramsey for many good suggestions, and for his patience and encouragement.

I am grateful to my new friends and collaborators at the Department of Physics, University of Leipzig, Dr. Christian Chmelik, Prof. Jörg Kärger and Prof. Dieter Freude, who are bringing an essential degree of understanding to the relationship between diffusion mechanisms and rehydroxylation phenomena.

I wish to give special thanks to Margaret Hayden for her help in casting the concrete, and for giving me balance of a different sort through these past years.

The financial support of the Clarendon Fund, and the OUP John Fell Research Fund are gratefully acknowledged. Without them I would not have neither the freedom to pursue my studies nor the new apparatus with which to do it.

To my father.

Preface

After the initial pioneering study of rehydroxylation dating, several global teams attempted to replicate the success of what seemed at the time to be a methodologically straightforward and powerful dating technique. However, very little agreement was reached, and for the past decade very few dates have been published. In part this may have been due to difficulties in measurement; characterising the chemical kinetics of such a slow process in fact poses a significant measurement challenge. Great instrumental control, and several months of measurements under constant conditions are necessary for accurate characterisation of even the most well-behaved materials, which is a difficult task for any field of metrology. But in the course of these studies it has also become clear that some of the underlying assumptions of the phenomenon of rehydroxylation in fired clays need to be reevaluated. The motivation is that, archaeological considerations aside, a dating technique is only as good as our fundamental knowledge of the physics and chemistry of the underlying time-dependent process. By way of analogy, radiocarbon dating would certainly prove less robust if we did not properly understand the carbon cycle, and the role of post-depositional processes of contamination. But it would be thoroughly untenable without appropriate knowledge of radioactive decay, and good measurement of the half-life of ^{14}C. It is in this spirit that this work has been undertaken. It is believed that understanding the issues of the rehydroxylation phenomenon is not only the key to future development of a robust dating tool for archaeological ceramics, but will also assist in establishing a new framework for understanding the long-term chemical changes of fired clays, with wider implications for geology, construction and material science.

Contents

List of Figures

List of Tables

Symbols

Symbol	Name	Unit of measure
y	fractional RHX mass gain	$\mathrm{g.g^{-1}}$
y_a	lifetime fractional RHX mass gain ($= m_\mathrm{a}/m_4$)	$\mathrm{g.g^{-1}}$
y_max	maximum lifetime fractional RHX mass gain	$\mathrm{g.g^{-1}}$
t	time	h
t_a	RHX age	hours (h) or years (a)
E_a	activation energy	$\mathrm{kJ.mol^{-1}}$
α	RHX rate constant ($= \alpha_m/m_4$)	$\mathrm{h^{-1/4}}$
α_m	measured RHX rate constant	$\mathrm{g.h^{-1/4}}$
α_e	effective lifetime RHX rate constant	$\mathrm{g.h^{-1/4}}$
α_0	RHX rate constant at temperature T_0	$\mathrm{g.h^{-1/4}}$
m_a	archaeological mass	g
m_2	equilibrium sample mass	g
m_4	RHX stage 2 intercept	g
m_cer	ceramic mass	g
m_nrc	non-refactory component mass	g
m_w0	type 0 water mass	g
m_w1	type 1 water mass	g
m_a	type 2 water mass	g
$\mathbf{R}$	universal gas constant	$\mathrm{mol.K^{-1}}$
T	temperature	K unless stated
$\bar{T}$	mean lifetime temperature	K unless stated
T_e	effective lifetime temperature	K unless stated
t_{99}	time to 99% saturation of m_w0	h

Chapter 1

Introduction

This thesis will evaluate several aspects of a new dating technique based on rehydroxylation in fired clays. Rehydroxylation (RHX) dating has its roots in a novel experimental study (Wilson et al., 2003) of long-term moisture expansion in structural ceramics, a phenomenon which is now thought to be the consequence of slow progressive rehydroxylation (Hamilton and Hall, 2012). In their study, Wilson et al. (2003) proposed a power law relationship between long-term expansive strain and time. In this model, rehydroxylation is best described by a quartic root ($t^{1/4}$) time dependence - a finding which suggests a transport process of sub-diffusion along restricted pathways in phyllosilicates (Savage et al., 2008). In addition, microgravimetric studies (Wilson et al., 2009; Mesbah et al., 2010; Tosheva et al., 2010) have claimed that the same power law relationship is evident in mass gain experiments, and that both moisture expansion and mass gain are the consequence of chemical rehydroxylation of thermally-altered clay minerals. It is ultimately the long-term, slow and progressive nature of the phenomenon which makes it suitable for a method of dating fired clays. Mass gain measurements afford a higher degree of precision and repeatability than measurements of expansive strain. Therefore, gravimetric methods were used to obtain the first published rehydroxylation ages applied to archaeological pottery and historical brick (Wilson et al., 2009, 2012). The dates obtained in these studies agreed with the known ages to within their quoted measurement uncertainty (0.5 - 1%). This agreement, for a range of materials, demonstrates support for the original model of long-term chemical rehydroxylation proposed by Wilson et al. (2003). However, other authors have called the power law relationship into question,

suggesting either discrepancies in data reduction or experimental methodology (Le Goff and Gallet, 2014a,b), intrinsic variability of the power law itself (Le Goff and Gallet, 2014c; Bowen et al., 2013), and/or multiple long-term processes which occur alongside rehydroxylation, which mask the process (Gallet and Le Goff, 2015). Arguably, these studies have shown that a clearer picture of the long-term time dependence of mass gain is yet to emerge, as does the relationship between mass gain, expansive strain, diffusion mechanisms, and the process of rehydroxylation. A better understanding of these issues is certainly required before further development of any dating method based on the process. This approach will form the basis of this thesis. The purpose of the following introduction is to outline the existing evidence for models of rehydroxylation, as well as the practical basis for RHX dating methodology, and identify the central outstanding questions.

1.1 The phenomenon of rehydroxylation in fired clays: historical models

Early studies investigated rehydration of fired clays under varying conditions of atmospheric moisture and temperature. This strategy was employed to determine the maximum level of saturation of a ceramic body. Mellor and Holdcroft (1911) first found that kaolin took up $\sim 2.5\%$ water under steam autoclave, a process that was apparently reversible upon reheating to 500^{o}C. Similarly, Laird and Geller (1919) later found that clays which had originally been fired to moderate temperatures between 600 and 700 ^{o}C could be rehydrated by boiling in water at 200 - 270 ^{o}C for 8-48 hours. They suggested that after this treatment the rehydrated clay resembled the raw clay, and that higher temperatures of original firing reduced the rate and extent of rehydration (Laird and Geller, 1919). A similar finding was made by Washburn and Footitt (1921). These early studies therefore seemed to provide good evidence that thermally-altered clays were in fact meta-stable materials. However, less was known about the mechanisms of rehydration, and how rehydration is related to clay mineral atomic structure. Laird and Geller (1919) identified that the water in the rehydrated clay was chemically recombined with

the ceramic matrix, since it was lost upon heating to high temperatures. In fact, the distinction of 'chemically combined' water as opposed to other forms of molecular water in clays goes back to the pioneering work of Le Châtelier (1887), who found that clay minerals such as montmorillonite and kaolinite all undergo two major endothermic reactions when heated; the first associated with the removed of adsorbed ('physisorbed') water at low temperatures ($\sim 100^{o}$C), and the second associated with the loss of structural hydroxyl (lattice water) at higher temperatures. In general, 'rehydration' is a broad term which describes the reversal of both behaviours, whereas 'rehydroxylation' is a specific term which refers to the recombination of hydroxyl molecules with sites within the sheet structure of clay minerals. Following these early studies, Schurecht (1928) and Schurecht and Pole (1929) identified that rehydration was responsible for the moisture expansion of ceramic bodies, and is therefore responsible for the cracking of glazes. Furthermore, he suggested that moisture expansion and rehydration is a long-term and progressive effect, and varies between different ceramics of different chemical composition. He considered that moisture expansion was reversible, and suggested that it might be possible to determine how much a ceramic body has expanded by reheating it to moderately high temperatures (Schurecht, 1928).

1.1.1 Expansion model of Hosking and Hueber (1958)

In the following decades, several studies (e.g. Mattyasovszky-Zsolnay (1946); Geller and Creamer (1941); Bullin and Green (1954)) examined moisture expansion and the cracking of glazes, mostly supporting the earlier findings of Schurecht (1928). In the nineteen fifties McBurney (1954) and others began to investigate moisture expansion as a possible cause of structural failure in building ceramics such as brick and tile (related in the review of Hamilton and Hall (2012)). Hosking and Hueber (1958) were among the first to suggest an empirical relationship between expansion and time, based initially on autoclave experiments of over 400 different specimens of fired clays of varying composition and structure. They suggested that strain might be predicted by the relatively simple relation:

$$\varepsilon(t) = \varepsilon_{\mathrm{T}}(1 - e^{-kt}) \ , \tag{1.1}$$

where $\varepsilon(t)$ is the percentage expansion at time t, ε_{T} is the total expansion, and k a constant. This paper also marks the first real attempt at understanding the underlying physical and chemical processes behind moisture expansion. Hosking and Hueber (1958) argued that the primary influence on the rate of expansion was the temperature of the reactive moisture. They found that the average rate of expansion changed ~ 1.8 times for each 10^{o}C rise in temperature, which led them to argue that the moisture expansion was controlled by a chemical reaction. The agreement between their experimental data and the above equation suggested that the reaction was first order, with ε_{T} essentially a function of the concentration of sites at which the reaction occurs. In general, this varied according to the temperature of original firing, with 'highly-burnt' materials exhibiting a slower rate. 'Lightly-burnt' samples showed a higher rate of expansion, and consequently reached a maximum level of expansion more quickly. All samples reached a constant expansion at large autoclave times, which motivated for the mathematical formulation of their model, with asymptotic expansion at large times approaching ε_{T}. They speculated that the reactive sites in 'highly-burnt' samples were vitreous components of the ceramic, whereas reactive sites in the 'lightly-burnt' materials were mainly amorphous silicates and clay minerals. A subsequent paper (Hosking and Hueber, 1959) also found a similar behaviour in several hundred laboratory specimens exposed to a range of (lower) laboratory temperatures and conditions, showing that a similar type of reaction, albeit much slower, was probably responsible for the long-term expansion seen in these materials.

1.1.2 The model of Cole (1961) and Cole (1962)

Cole (1961) also examined autoclave and lower-temperature expansion data for a mixture of fired kaolinite, mica and quartz and found that the autoclave expansion curves paralleled the lower-temperature curve, suggesting that a similar process occurs at both low and high temperatures. He suggested an alternative linear relationship between moisture expansion and the logarithm of time, for all materials fired between 800 and 1200 ^{o}C. He also found good agreement between this expression and both moisture

expansion and mass gain. In a subsequent contribution Cole (1962) suggested the following relationship based on the Elovich equation (Halsey, 1951; Low, 1960) applied to chemisorption of gases on solids:

$$q(t) = \frac{1}{b} ln\big(abt + 1\big) \ , \tag{1.2}$$

where $q(t)$ is the amount of gas adsorbed, a and b are constants, which are related to a parameter called the "time-offset" $t_0 = 1/ab$. This parameter is not measured directly, but suitable values of t_0 are chosen to optimise the fit. Higher values of t_0 were needed for materials fired at higher temperatures. Cole also suggested that the form of the above equation was consistent with a chemical reaction in which activation energy increases with progressive expansion. He suggested that this increase in activation energy was caused by reactions which occur at sites at increasing "depths below the surface of the reactable material" (Cole (1962) at 432).

1.1.3 The model of Wilson et al. (2003)

Wilson et al. (2003) first proposed a relationship between long-term expansive strain and the fourth root of time ($t^{1/4}$). Like previous authors, they subjected the materials to a range of environmental conditions, but their approach differed from previous studies in two main aspects: first, they included archaeological and historical bricks as well as modern bricks in their study in order to quantify lifetime expansion; and second, they monitored the expansive strain whilst bricks were still hot from the kiln. Wilson et al. (2003) claimed that a power law fit of the form

$$\varepsilon(t) = at^b \ , \tag{1.3}$$

with b determined as ~ 0.25 for a range of different fired clay materials, was a better description of the phenomenon of moisture expansion. Bricks aged under water at 20^{o}C for 104 days were found to have expansion rates which were similar to those of bricks aged at similar temperatures in air. This led them to claim that the reaction responsible for expansion is largely independent of relative humidity, provided that only some water

is available. Hall et al. (2011) also re-analysed the 35 year moisture expansion dataset of Zsembery et al. (2004), as well as 64 years of length measurements of a brick bench used by the National Physical Laboratory (U.K.) for standardising work. They also found agreement with a $t^{1/4}$ relationship.

Savage et al. (2008) described a process in which moisture expansion proceeded in two stages, both linear with $t^{1/4}$. In similarity to Cole (1961), they found agreement between measurements of mass gain and expansive strain. Similar gravimetric results were reported by Mesbah et al. (2010) and Tosheva et al. (2010). Comparison of strain measurements with diffusive-reflectance infrared Fourier transform spectroscopy (DRIFTS) and thermogravimetric mass spectrometry of fired clay brick was performed by Clegg et al. (2012). These authors found that the peak area under the OH stretching band envelope (roughly 3800-2600 cm^{-1}) increases after re-firing in accordance with a $t^{1/4}$ relationship. After an initial phase of rapid sorption (associated with the 3450 cm^{-1} and 3250 cm^{-1} peaks related to more weakly bound water), the 3620 cm^{-1} peak associated with structural OH begins to dominate. These authors, as well as Hall and Hoff (2012), therefore identified the underlying reaction responsible for both mass gain and expansive strain as *rehydroxylation* - a word apparently first used to describe the reversal of the well-studied dehydroxylation reaction in fired clays by Heller et al. (1962). Many authors had suggested that moisture expansion was partly due to chemical recombination of structural water in the form of OH^- groups, e.g. as evidenced by FTIR spectrosopy (Shoval et al., 1991) and oxygen stable isotope analysis (Nuñez et al., 2012), but Clegg et al. (2012) and Hall and Hoff (2012) identify both mass gain and moisture expansion as a consequence of long-term rehydroxylation, which obeys a $t^{1/4}$ dependence.

During the first stage identified by Savage et al. (2008), uptake of weakly-bound forms of water accompanies rapid rehydroxylation. This weakly-bound water, variously called 'physisorbed', 'capillary water', 'T0 water', 'pore water' or 'interplanar water', all of which are lost at relatively low temperatures, will rapidly diffuse into the micro-scale pores and inner surfaces of the fired clay matrix, and establish a pseudo-equilibrium with ambient humidity (at constant temperature). Additionally, in most clay minerals there exists more strongly-bound water (but not structural OH) which is lost upon heating

above 100 ^{o}C, but below 500 ^{o}C. Wilson et al. (2012) label this 'T1' water, and assume that it follows a similar time-dependence weakly-bound water. This first phase is rapid and transient; after a few hours or days, rehydroxylation (i.e. the recombination of clay mineral sheets with water to regain structural OH) begins to dominate moisture expansion and fractional mass gain, y, which similarly obeys a $t^{1/4}$ regime:

$$y(t) = \alpha(T)t^{1/4} \ . \tag{1.4}$$

The rehydroxylation rate constant α varies from about 0.00018 to 0.00075 h$^{-1/4}$ (Wilson et al., 2009, 2012) at common environmental temperatures. Its value depends on the temperature of original firing (Tosheva et al., 2010), as higher temperatures increase the degree of vitrification, and therefore reduce the number of sites available for rehydroxylation. The magnitude of changes proposed by the Wilson et al. (2003) model can be easily demonstrated. Consider a sample of fired clay that has a mass at dehydroxylation of 10g. Let us assume that $\alpha = 0.00075$ h^{-4} at the subsequent lifetime temperature, which we will assume is constant immediately after firing. Then, the percentage change in mass within the first hour should be given by Eq. 1 as $\alpha(1^{1/4} - 0^{1/4}) = 0.075\%$, or about 7500 μg. The mass change in the 100^{th} hour will be $\alpha(100^{1/4} - 99^{1/4}) \sim 59$ μg, which is two orders of magnitude smaller. This represents a scenario where α is very high. At the other extreme ($\alpha = 0.00018$h$^{-1/4}$), we can expect approximately 1800 μg within the first hour, and ~14 μg in the 100^{th} hour.

1.1.3.1 Relationship to transport mechanisms

Wilson et al. (2003) first suggested that the slow power-law kinetics of the rehydroxylation reaction may be linked with mechanisms of diffusive transport, a concept which was further elaborated by Savage et al. (2008). Both studies tentatively linked the $t^{1/4}$ behaviour to theoretical models of single-file diffusion (e.g. Levitt (1973)), which have predicted that the mean square displacement $\langle x^2 \rangle_{\mathrm{sf}}$ of a diffusing particle is proportional to $t^{1/2}$. Savage et al. (2008) described a scenario whereby a queue of molecules diffuse along a pathway sufficiently small that they cannot pass one another, and that an annihilation reaction of the form $A + B \rightarrow 0$ removes the leading molecule from the queue.

This allows the queue to advance a set distance until the next reaction site, which leads to $t^{1/4}$ kinetics because the distance travelled by the queue of molecules is proportional to the amount of reaction, and therefore mass gain/expansion.

Single-file diffusion is a special case of *anomalous diffusion*, whereby the mean square displacement $\langle x^2 \rangle$ of a single diffusing particle goes as t^n, with either $n < 1$ (subdiffusion) or $n > 1$ (superdiffusion). In recent years, several authors seem to have noted the presence of anomalous diffusion in thermally-altered clay minerals. Interestingly, Drozdov et al. (2003) identified anomalous diffusion in heated montmorillonite clay (90 ^{o}C) on the basis of gravimetric and strain measurements. Mazzucato et al. (1999) looked at the dehydroxylation of muscovite mica between 700-1000 ^{o}C by X-ray powder diffraction. They found that dehydroxylation kinetics are limited by a subdiffusive process, an idea which dates back to the work of Rouxhet (1970). Similarly, Tokiwai et al. (2010) used infrared spectroscopy study of the dehydroxylation kinetics of muscovite mica, heated to between 760-860 ^{o}C. They identified that the rate-limiting step in the dehydroxylation reaction most probably was a process of single-file ('mono-dimensional') diffusion.

1.1.4 Archaeological dating technique of Wilson et al. (2009) and Wilson et al. (2012)

The study of Wilson et al. (2003) on a range of historical bricks revealed that Roman brick samples showed the largest amount of lifetime expansive strain. This prompted a series of dating trials by these authors, based on the concept that if the lifetime expansive strain could be measured, along with the rate of expansion of the particular brick, then the proposed $t^{1/4}$ model could be used to predict the time since firing. Strain measurements were eventually abandoned in favour of micro-gravimetric measurements, on account of greater precision and repeatability.[1] Wilson et al. (2009) obtained promising results, in some cases with sub-decade precision. Their gravimetric technique relied on several reheating steps to determine the fraction T2 water with which the clay minerals had combined since the event of original firing, along with a rate determination at

[1] Related to the author by Moira Wilson, August 2012. See also Ince (2009)

several temperatures. The latter step allowed complete characterisation of the chemical kinetics of mass gain via measurement of activation energy.

Briefly, it will be useful to outline their gravimetric methodology in more detail. Wilson et al. (2012) define all possible components to the mass of archaeological fired-clays as the following:

> $\boldsymbol{m_{\mathbf{cer}}}$ - the inorganic mineral lattice, including refractory components which remain "after re-heating the sample to 500^{o}C until it reaches constant mass" (Wilson et al. (2012) at 3),
>
> $\boldsymbol{m_{\mathbf{nrc}}}$ - the 'non-refractory component mass', i.e. all substances other than water, including organic contaminants, food residues, etc., lost upon heating to 500^{o}C,
>
> $\boldsymbol{m_{\mathbf{w0}}}$ - all weakly-held molecular water, including adsorbed and capillary water ('T0 water'),
>
> $\boldsymbol{m_{\mathbf{w1}}}$ - molecular water removed during heating to 500^{o}C (chemisorbed molecular water, 'T1 water'), but not RHX water, and finally
>
> $\boldsymbol{m_{\mathbf{a}}}$ - the mass of water gained during the lifetime of the fired-clay ceramic as a result of RHX (Wilson et al., 2012) ('T2 water').

In this thesis, the terms 'T0', 'T1' and 'T2' water will also be used for the different water components. After drying to constant mass at 105^{o}C, only T0 water should be removed. In the revised method of Wilson et al. (2012), the sample is then allowed to take up weakly held molecular water at the same constant temperature and relative humidity at which subsequent RHX measurements are made. The final constant mass, in equilibrium with the measurement chamber, is called 'm_2'. Heating to 500^{o}C then removes all mass components except for m_{nrc}. Upon removal, the material begins to take up new amounts of T0, T1 and T2 water. After the uptake of of T0 and T1 is complete, 'stage II' is described by the power law:

$$m(t) = \alpha_{\mathrm{m}} t^{1/4} - m_4 \ . \tag{1.5}$$

After heating to 500^{o}C, the mass of weakly-held molecular water should be equal to the original mass of weakly-held molecular water taken up after heating at 105^{o}C. If the mass of chemisorbed water, T1, which is gained after reheating to 500^{o}C is similar to the mass of chemisorbed molecular water originally present in the sample before reheating, then Wilson et al. (2012) show that:

$$m_{\mathrm{a}} \approx (m_2 - m_4) \ ,$$

which means that the lifetime RHX mass gain will be the difference between the measured 'equilibrium' mass and m_4, the y-intercept of the $t^{1/4}$ power law when $t = 0$, following reheating to 500^{o}C. Since rehydroxylation is always accompanied by the uptake of T0 water in first stage of mass gain, and is therefore masked, m_4 is a purely theoretical quantity determined by the fit. Dividing the above equation by m_4 yields the lifetime fractional mass gain, y_a:

$$y_{\mathrm{a}} \approx (m_2 - m_4)/m_4 \ , \tag{1.6}$$

Inserting the above equation 1.6 into the gravimetric RHX rate equation 1.4, and rearranging yields the RHX age equation of Wilson et al. (2012):

$$t_{\mathrm{a}} = \Big(\frac{m_2 - m_4}{\alpha_m}\Big)^4 \ . \tag{1.7}$$

1.1.4.1 Measurement of activation energy, corrections for effective lifetime temperature

The above age equation 1.7 is only valid when the rehydroxylation rate constant α_m is measured in the laboratory at the same effective lifetime temperature (ELT) at which the ceramic object spent its life. However, in most cases the ELT is unknown, and has to be estimated. In order to correct for ELT, Hall and Hoff (2012) and Hall et al. (2013) recently presented a method that bears resemblance to the corrections used in obsidian

hydration dating (Friedman and Long, 1976; Michels et al., 1983). If a conventional solid state rate constant k is measured at some temperature T, and the activation energy E_a of the reaction is known, then the rate constant is expected to obey Arrhenius-type behaviour, i.e.:

$$lnk = -\frac{E_a}{\mathbf{R}T} \ . \tag{1.8}$$

Where **R** is the gas constant (**R**=8.314 J.mol^{-1}.K^{-1}), and E_a is the activation energy. In the Wilson et al. (2009) model, the rate constant k is defined as $(\alpha/y_{max})^4$, where y_{max} is the maximum value of y when the reaction is complete (Wilson et al., 2012). In practice, y_{max} does not need to be known, but an Arrhenius plot of α_m ratios, measured at three different re-heating temperatures, will suffice for the determination of E_a, since $k(T) \propto \alpha(T)$.

If the rehydroxylation reaction proceeds indefinitely, then y_{max} will be a purely theoretical quantity. Inserting this form of the rate constant into the above equation yields:

$$ln(\alpha/y_{max})^4 = -\frac{E_a}{\mathbf{R}T} \ . \tag{1.9}$$

Of course, a similar equation may be written for *any* value of the rate constant k_0, measured at corresponding temperature T_0:

$$ln(\alpha_0/y_{max})^4 = -\frac{E_a}{\mathbf{R}T_0} \ . \tag{1.10}$$

Subtracting Eq. 1.10 from Eq. 1.9 yields:

$$ln(\alpha/y_{max})^4 - ln(\alpha_0/y_{max})^4 = -\frac{E_a}{\mathbf{R}T} + \frac{E_a}{\mathbf{R}T_0} \ , \tag{1.11}$$

which may be simplified, eliminating y_{max}, to:

$$4ln(\frac{\alpha}{\alpha_0}) = -\frac{E_a}{\mathbf{R}}(\frac{1}{T} - \frac{1}{T_0}) \ , \tag{1.12}$$

alternatively:

$$\alpha = \alpha_0 e^{-\frac{E_a}{4\mathbf{R}}(\frac{1}{T}-\frac{1}{T_0})} \ . \tag{1.13}$$

In principle, the above equation can be used to correct α_m to α_{ELT} if both T_m and the ELT are known precisely (i.e. substitute these quantities for α_0 and α and T_0 and T in the above equation). In practice, it is more convenient to perform appropriate numerical integration of the differential equation $4y^3dy = \alpha(T)^4dt$ (derived from Eq. 1.4), with knowledge of E_a and the temperature history of the object ($T(t)$). Note that Moinester et al. (2014) recently propose a technique whereby measuring E_a, y_a and α_m for two samples of the same age, and at a minimum of three different temperatures, will allow for determination of the ELT which does not rely upon estimation using meteorological records. Their same-age-samples (SAS) protocol is yet to be tested, and since the mathematical details are beyond the scope of this introduction, they can be found in Appendix A.

1.2 Challenges identified by subsequent studies

Several teams (e.g. Le Goff and Gallet (2014b), Bowen et al. (2013), Burakov and Nachasova (2013)) have not been able to replicate the original results of Wilson et al. (2009) and Wilson et al. (2012). In part, this may be due to experimental issues and the effects of organic carbon and/or calcite. Wilson et al. (2013) first suggested that the presence of calcite may effect the estimation of stage II α_m measurements. Hamilton and Hall (2012) mention that decarbonated microcrystalline calcite may form portlandite under ambient conditions, which may skew mass gain/loss data. The importance of organic matter present in the ceramic matrix, which burns off upon reheating to temperatures as high as 500^{o}C, was stated by Wilson et al. (2012) and Hamilton and Hall (2012). Subsequently, Nümrich et al. (2015) investigated the effect in a range of

historical bricks by mass spectrometry measurements of the quantity m_{nrc}, which they found to be relatively high (0.05-0.55%). This is a large percentage of the mass of T2 water, which causes dates several thousand years too old. Nümrich et al. (2015) also suggest a pretreatment strategy based on acid-oxidation of the organic matter.

On the other hand, the failure to replicate the results of Wilson et al. (2003) may indicate systematic problems with the original $t^{1/4}$ model of rehydroxylation. A somewhat important, yet poorly understood assumption of the dating method is the universality of the 1/4 power. Authors have called the power law relationship into question, suggesting either discrepancies in data reduction or experimental methodology (Le Goff and Gallet, 2014a,b), intrinsic variability in the 1/4 power itself (Le Goff and Gallet, 2014c; Bowen et al., 2013), and/or uptake of weakly-bound water over long timescales, which leads to long-lived normal diffusion regime, i.e. $\langle x^2 \rangle \propto t$, which masks $t^{1/4}$ behaviour (Gallet and Le Goff, 2015). These authors have proposed alternative models, which will now briefly be considered.

1.2.1 Suggested model of Gallet and Le Goff (2015)

Gallet and Le Goff (2015) propose a similar model to Wilson et al. (2003), with the addition of an extra term which describes a normal diffusion regime (i.e. $t^{1/2}$). However, they envisage a scenario where T1 water and T2 water exhibit temporal variations on similar timescales; in other words, that transport of T1 water continues over timescales of several months/years. They suggest that this long-lived regime is responsible for the apparent non-stabilisation of m_2 after initial heating to 105 ^oC and several weeks measuring time, which has been noted to occur in many (if not most) ceramic samples (Le Goff and Gallet, 2014b; Gallet and Le Goff, 2015; Hare, 2012). The time taken for measurements of m_2 is currently one of the biggest obstacles to increasing the throughput and reliability of RHX dating. Gallet and Le Goff (2015) propose that the degree to which one process dominates over the other corresponds to the diversity and size distribution of available cracks/interlayer spaces, as well as the availability after each heating of vacant sites in the clay mineral matrix. In terms of mass gain, this means that observed time dependence is therefore neither $t^{1/2}$ or $t^{1/4}$, but combination of the

two (plus the initial rapid transport of T0 water):

$$y(t) = -\beta e^{-t/\tau} + \mu + \alpha_4 t^{1/4} + \alpha_2 t^{1/2} \ , \tag{1.14}$$

where β and τ are the respectively the amplitude and time constant of the first rapid stage of mass gain, and α_4 is analogous to α of Wilson et al. (2009), and α_2 is the mass gain rate for a normal diffusion regime.

1.2.2 Suggested model of Bowen et al. (2013)

Bowen et al. (2013) proposed a similar approach to combining sources of mass gain, but without a $t^{1/2}$ behaviour:

$$m(t) = -\beta'\left(1 - e^{-\tau' t}\right) + \alpha_4' t^{1/4} + \delta \ . \tag{1.15}$$

To evaluate the hypothesis that slow uptake of T0 water is superimposed on the rate of structural OH recombination, these authors calculate the theoretical time to 99% complete uptake (using the fitted values of τ') of T0 water as $-\ln(10^{-2})/\tau'$), which they calculate as lying between 5 and 16 hours for a range of pottery samples between ∼0.9 and ∼1.7 g, apparently contradicting the results of Gallet and Le Goff (2015).

To evaluate the models of Gallet and Le Goff (2015) or Bowen et al. (2013) may be problematic, as multi-parameter fits (with only two measurands) of the form of Eq. 1.14 and 1.15 are prone to overfitting. This may also may pose a significant challenge for any dating technique based on these models. Over and above the experimental issues of measurement and pretreatment, the most fundamental issue raised by the conflicting experimental data is the relation between the proposed $t^{1/4}$ dependence of mass gain/expansion in fired clays and sub-diffusive transport mechanisms.

1.3 Aims of this thesis

This thesis is concerned with better understanding the issues which currently limit the precision, accuracy and robustness of rehydroxylation dating. Chapter 2 examines the precision of the technique from a theoretical perspective, and presents a more thorough analysis of the different components of measurement error to gravimetric RHX age determinations. The dating results of Wilson et al. (2009) and Wilson et al. (2012) reported relatively small measurement errors, and the analysis presented here will identify the most significant contributions to the expected uncertainties in RHX age determinations, as well as some estimation of the timeframe over which the dating technique is applicable.

Since relatively little is known about how calcite/organic species affect rehydroxylation measurements, Chapter 3 presents an overview and discussion of both the existing evidence for structural changes in fired clay minerals and possible post-depositional processes in archaeological fired clays. The expected effects of the presence of calcite and organic carbon are also discussed. Following this, Chapter 4 then examines various pretreatment strategies for the removal of these species, based in part on the methods proposed by Nümrich et al. (2015). It will evaluate possible complications arising from different chemical pretreatments by FTIR spectroscopy of different fired-clay materials.

Chapter 5 examines the specific question of non-stabilisation of m_2 mass after heating at 105^{o}C, with the aim of understanding variable physical and chemical effects which may be responsible for this behaviour. A new multi-sample apparatus for the gravimetric analysis of rehydroxylation in fired clays under controlled conditions was constructed for these measurements. This apparatus is then used in the remaining chapters of this thesis. Chapter 6 then reports the preliminary results of RHX age determinations from both archaeological materials and clay reference samples of known composition, as well as those subjected to various pretreatment strategies.

Finally, via the evidence presented in this thesis, as well as previous studies, Chapter 7 will evaluate evidence for the variability of the proposed $t^{1/4}$ power law, and discuss the overall implications for the rehydroxylation dating method, as well as different models

of mass gain/expansive strain. In addition, some speculations are presented as to the variability of diffusive transport mechanisms with clay mineral microstructure.

Chapter 2

Theoretical aspects of error estimation in RHX dating

2.1 General overview[1]

There are several factors which determine the usefulness of an analytical dating method when applied to archaeological material. However, of primary importance is the precision it is likely to afford, as well as the age range over which it is expected to be appropriate. As **?** points out, scientific dating is both expensive and inherently destructive, and in order to determine if the technique will have any practical usefulness it first 'needs to be established that the likely error limits are good enough' (**?**, at 2). Of course, the ultimate test of a dating technique is comparison with alternative dating methods; analytical or otherwise. However, in the absence of verification studies, there are still theoretical/experimental considerations which pose fundamental limits to the technique. In radiocarbon dating, for example, the limits of measurement precision and the effective age range are set by a combination of counting statistics, measurement background, and the half-life of ^{14}C. Detected events follow a Poisson distribution, and the measurement precision for any one sample will go as $\sqrt{N}$, where (N) is the number of events detected. By increasing the sample mass shorter counting times are obviously needed to achieve

[1]This chapter formed the basis of the paper Hare (2015), and the findings are similar to that paper. It is included here because it is relevant to subsequent chapters, which will build on this framework.

the same level of precision. In modern high-precision laboratories, the limit is of the order of ∼20-30 years.

The aim of this Chapter is to investigate the theoretical limits to the RHX dating technique, as proposed by Wilson et al. (2009, 2012). Two methods will be explored: a conventional Taylor-series propagation of error, as well as a Monte Carlo-type approach. Of several recent pilot studies into rehydroxylation dating Bowen et al. (2011); Nachasova and Burakov (2012); Barrett (2013), none has attempted to quantify an expanded measurement uncertainty. Indeed, only one of the three (Nachasova and Burakov, 2012) present what could be called 'RHX ages', corrected via the determination of activation energies. Wilson et al. (2012) give the RHX age equation as:

$$t_{\mathrm{a}} = \left(\frac{y_{\mathrm{a}}}{\alpha}\right)^4 .$$

Noting that $y_{\mathrm{a}} = (m_2 - m_4)/m_2$, and that α is defined as α_{m}/m_2 the above equation may be rewritten as:

$$t_{\mathrm{a}} = \left(\frac{m_2 - m_4}{\alpha_{\mathrm{m}}}\right)^4 . \tag{2.1}$$

m_2 is the mean of the sample mass after equilibrium has been achieved with the T and RH of the environmental chamber. α_{m} is given by the slope of RHX mass gain $dy/dt^{1/4}$ in an RHX experiment, variations in which will chiefly depend on the stability of the temperature at which mass gain measurements are conducted - assuming constant relative humidity. Wilson et al. (2012) assume that the primary component of uncertainty in RHX age is that of the measured RHX gradient, α_{m}. In their study they approach the problem by determining a relative uncertainty in the measured gradient, $u(\alpha_{\mathrm{a}})/\alpha_{\mathrm{a}}$ by calculating

$$u(\alpha_m) = \frac{s}{\sqrt{(n-2)}} * \sqrt{\frac{n}{D}} ,$$

where n is the number of data points in a linear least-squares fit, s the L2 norm of the residuals, and D is given as

$$D = n\sum_{i=1}^{n} x_i^2 - \left(\sum_{i=1}^{n} x_i\right)^2 .$$

Measurement uncertainty in RHX age (1σ) is taken as $u(\alpha_\mathrm{a})/\alpha_\mathrm{a}$ multiplied by the RHX age (t_a) .This approach yielded uncertainties in a range of 15 to 60 years for a range of dates, the earliest of which was 59 AD, and the most recent 1624 AD. A better approximation of measurement uncertainty would be larger. Indeed, although the most significant component of uncertainty in RHX ages is predicted to be that associated with the measured RHX gradient, Wilson et al. (2012) point out that this approach does not represent an expanded uncertainty, which should take into account measurement error in all quantities used to determine RHX age. This would include m_2, m_4, activation energy E_a, as well as temperature terms. More importantly, it is also intuitive that this expression is inappropriate at recent timescales, when errors in m_2 and m_4 must become significant. There is also no *a priori* reason why errors about mean RHX ages should be normally-distributed. All these features deserve further investigation.

2.2 1^{st} Order Taylor-series approach

Given any quantity y which is function of several measured variables, i.e.

$$y = f(x, z, ...) ,$$

and assuming that the most probable value for the mean, $\bar{y}$, is calculated by $f(\bar{x}, \bar{z}, ...)$, and that the variables x, z, etc. all have sample variances, e.g.

$$s_x^2 \equiv \frac{1}{N-1}\sum_{i=1}^{N}(x_i - \bar{x})^2 ,$$

then it can be shown by Taylor-series expansion (Bevington and Robinson, 2003; Weisstein, 2012) that the sample variance in y is given by

$$\begin{aligned} s_y^2 = \quad & \frac{1}{N-1}\sum_{i=1}^{N}\Big[(x_i-\bar{x})^2\big(\frac{\partial y}{\partial x}\big)^2+(z_i-\bar{z})^2\big(\frac{\partial z}{\partial z}\big)^2 \\ & +2(x_i-\bar{x})(z_i-\bar{z})\big(\frac{\partial y}{\partial x}\big)\big(\frac{\partial y}{\partial z}\big)+...\Big] \qquad (2.2) \\ = \quad & s_x^2\big(\frac{\partial y}{\partial x}\big)^2+s_z^2\big(\frac{\partial y}{\partial z}\big)^2+2s_{xz}\big(\frac{\partial y}{\partial x}\big)\big(\frac{\partial y}{\partial z}\big)+... \qquad (2.3) \end{aligned}$$

where s_{xz} is the covariance given by

$$s_{xz} \equiv \frac{1}{N-1}\sum_{i=1}^{N}(x_i-\bar{x})(z_i-\bar{z}) \ .$$

Equation 2.2 is known in various guises as the *law of propagation of error*. If x and z are uncorrelated (which is often a reasonable assumption), and normally distributed, then $s_{xz}=0$, and the sample variance in y is given simply by the sum of the variances in x and z, weighted by the squares of the partial derivatives of with respect to either variable:

$$s_y^2 \approx s_x^2\big(\frac{\partial y}{\partial x}\big)^2+s_z^2\big(\frac{\partial y}{\partial z}\big)^2 \ . \qquad (2.4)$$

In fact, this can be derived for a function of *any* number of variables, e.g. for $y=f(x,z,w)$ this may be written as

$$s_y^2 = s_x^2\big(\frac{\partial y}{\partial x}\big)^2+s_z^2\big(\frac{\partial y}{\partial z}\big)^2+s_w^2\big(\frac{\partial y}{\partial w}\big)^2+\text{higher order terms} \ . \qquad (2.5)$$

The above equation is equally valid for the purposes of combining standard uncertainties (JCGM, 2008), likewise under the assumption that variables are uncorrelated and normally distributed. In the case of the RHX measurement procedure, m_2 is normally-distributed by definition, being a Type A evaluation of standard uncertainty based on repeat measurements of the equilibrium mass. There is also good evidence to suggest that both m_4 and α_a, obtained from fits to the RHX rate equation, are normally-distributed.[2] It is therefore provisionally likely that covariance is negligible, which is

[2] As related to the author by M. A. Wilson, June 2013.

assumed in the following analysis.

2.2.1 Without uncertainty in temperature

It will first be useful to apply Eq. 2.5 to the RHX age formula (Eq. 2.1) to yield an expression for the square of the combined standard uncertainty '$u^2_{t_\mathrm{a}}$' in RHX age t_a:

$$u^2_{t_\mathrm{a}} = \left(\frac{\partial t_\mathrm{a}}{\partial m_2}\right)^2 u^2_{m_2} + \left(\frac{\partial t_\mathrm{a}}{\partial m_4}\right)^2 u^2_{m_4} + \left(\frac{\partial t_\mathrm{a}}{\partial \alpha_\mathrm{m}}\right)^2 u^2_{\alpha_\mathrm{m}} + \dots \,. \tag{2.6}$$

Note that we do not include temperature error terms at this point; this forms the subject of the following section. Evaluating the partial derivatives in the above expression yields:

$$u^2_{t_\mathrm{a}} = \left(\frac{4(m_2-m_4)^3}{\alpha^4_\mathrm{m}}\right)^2 u^2_{m_2} + \left(\frac{4(m_2-m_4)^3}{\alpha^4_\mathrm{m}}\right)^2 u^2_{m_4} + \left(\frac{-4(m_2-m_4)^4}{\alpha^5_\mathrm{m}}\right)^2 u^2_{\alpha_\mathrm{m}} + \dots \,, \tag{2.7}$$

and taking the square root yields the combined standard uncertainty, which is an approximation of the 1σ error in RHX age:

$$u_{t_\mathrm{a}} = \sqrt{\left(\frac{4(m_2-m_4)^3}{\alpha^4_\mathrm{m}}\right)^2 u^2_{m_2} + \left(\frac{4(m_2-m_4)^3}{\alpha^4_\mathrm{m}}\right)^2 u^2_{m_4} + \left(\frac{-4(m_2-m_4)^4}{\alpha^5_\mathrm{m}}\right)^2 u^2_{\alpha_\mathrm{m}} + \dots} \,. \tag{2.8}$$

It is also possible to obtain a more concise expression for the error in RHX age as a function of the age. We note that since Eq. 2.1 can be rearranged as:

$$\frac{(m_2-m_4)^3}{\alpha^3_m} = t^{3/4}_\mathrm{a} \,, \tag{2.9}$$

this can be substituted into Eq. 2.8 to yield:

$$u^2_{t_\mathrm{a}} = \left(\frac{4t^{3/4}_\mathrm{a}}{\alpha_\mathrm{m}}\right)^2 u^2_{m_2} + \left(\frac{4t^{3/4}_\mathrm{a}}{\alpha_\mathrm{m}}\right)^2 u^2_{m_4} + \left(\frac{-4t_\mathrm{a}}{\alpha_\mathrm{m}}\right)^2 u^2_{\alpha_\mathrm{m}} + \dots \,. \tag{2.10}$$

Taking the square root of the above, and with simplification it may be shown that

$$\boxed{u_{t_\mathrm{a}} = \frac{4}{\alpha_\mathrm{m}} * \sqrt{(t_\mathrm{a}^{3/2})(u_{m_2}^2 + u_{m_4}^2) + t_\mathrm{a}^2 u_{\alpha_\mathrm{m}}^2}} \,. \tag{2.11}$$

2.2.2 Implications for the age range of the technique

Equation 2.11 may also be rearranged to yield an expression for relative uncertainties in RHX ages. Note that since $t_\mathrm{a}^{3/2} = t_\mathrm{a}^2.t_\mathrm{a}^{-1/2}$, Eq. 2.11 may be simplified further:

$$\boxed{\frac{u_{t_\mathrm{a}}}{t_\mathrm{a}} = \frac{4}{\alpha_\mathrm{m}} * \sqrt{\frac{(u_{m_2}^2 + u_{m_4}^2)}{t_\mathrm{a}^{1/2}} + u_{\alpha_\mathrm{m}}^2}} \,. \tag{2.12}$$

This expression is of some importance, since it predicts the range over which the RHX method should be useful. It may be noted that at very small t_a, the first term under the square root in the above expression will dominate, and consequently the relative error in RHX dates scales as $1/\mathrm{t}_\mathrm{a}^{1/4}$. Conversely, at large t_a, the first term under the square root will be negligible, and therefore the relative error will be approximately linear with time:

$$\frac{u_{t_\mathrm{a}}}{t_\mathrm{a}} \approx \frac{4u_{\alpha_\mathrm{m}}}{\alpha_\mathrm{m}} \,. \tag{2.13}$$

It may be noted that the above expression is similar to that assumed to be used in Wilson et al. (2012), with the exception of multiplication by a factor of 4. For practical purposes of dating, the linear increase in error at large times is very slow, so that for typical values of α_m reported by these authors we can expect a minimum relative error of $\sim 0.5\%$, which translates to an increase of 10 years in error every 2000 years or so. However, the relative error in RHX dates of very *recent* material increases sharply according to the power law (although usually on timescales $\ll$ a few days or so).

We may also note that by definition,

$$\alpha_{\mathrm{m}} \equiv \alpha m_4 \ , \tag{2.14}$$

and so the relative percentage error at large t_{a} becomes

$$\boxed{\frac{u_{t_{\mathrm{a}}}}{t_{\mathrm{a}}} \times 100 \simeq \left(\frac{400}{m_2}\right)\left(\frac{u_{\alpha_{\mathrm{m}}}}{\alpha}\right)} \ . \tag{2.15}$$

In addition, therefore, at large times the relative uncertainty in RHX dates is directly proportional to the measured RHX rate constant, and inversely proportional to the RHX rate constant itself. It is also inversely proportional to the absolute mass of the sample. This is because RHX water can only take up a theoretical maximum of about 4% of the total sample mass (stoichiometrically, for a pure clay mineral), and consequently m_4 is approximately equal to the total mass of the sample used in the dating experiment. Although it must be stressed that this equation is an approximation of the true relative uncertainty, it is nevertheless a useful expression for comparing baseline uncertainty in RHX age, as well to optimise the design of future experiments. Since the above expression neatly combines several concepts in RHX dating, it will be convenient to assign to it a symbol, 'Φ', which is dimensionless:

$$\boxed{\Phi \equiv \left(\frac{400}{m_2}\right)\left(\frac{u_{\alpha_{\mathrm{m}}}}{\alpha}\right)} \ . \tag{2.16}$$

For example, Table 2.1 compares the theoretical minimum relative uncertainty in RHX ages ('Φ') across a range of current experimental setups. By using a nominal value of α of 0.00023 $\mathrm{h}^{-1/4}$ (i.e. the same material used across different investigations) it is possible to compare the inherent precision afforded by each system. Note that $u_{\alpha_{\mathrm{m}}}$ is essentially limited by the resolution of the balance/microbalance.

It will be seen that there is a dramatic range in relative uncertainty, from 580% to <1%, which is primarily the result in a mismatch between balance resolution and sample size. For measurement precision under 1% the ratio of the two should be of the order of 10^{-6} or less.

TABLE 2.1: Comparison of minimum relative uncertainty in RHX age, Φ, between studies.

Study	$\boldsymbol{\alpha}$ $(h^{-1/4})$	$\boldsymbol{u_{\alpha_m}}$ $(g.h^{-1/4})$	$\boldsymbol{m_4}$ (g)	$\boldsymbol{\Phi}$
Wilson et al. (2012)	0.00023	0.000001	4	0.7
Barrett (2013)	0.00023	0.0001	3	60
Bowen et al. (2011)	0.00023	0.001	3	580
Ince (2009)	0.00023	0.001	120	15
Hare †	0.00023	0.00001	20	0.9
Gallet & Le Goff ‡	0.00023	0.00001	3	6

†: Proposed system (University of Oxford, 2014). ‡: personal communication.

2.2.3 Including temperature terms

Equation 2.16 represents a theoretical minimum percentage error in RHX age. However, a more complete expression for the combined uncertainty u_{t_a} would naturally take into account errors in the temperature T_m associated with α_m, as well as the errors in the estimated effective lifetime temperature T_e. It may be noted that Eq. 2.1 may be written as an explicit function of both by replacing α_m with α_m(T), which has the form:

$$t_{\mathrm{a}} = \Big(\frac{m_2 - m_4}{\alpha_{\mathrm{m}} * e^{-\frac{E_{\mathrm{a}}}{4\mathbf{R}}(\frac{1}{T_e} - \frac{1}{T_m})}}\Big)^4 , \tag{2.17}$$

which is in turn more concisely written as:

$$t_{\mathrm{a}} = \frac{e^{\frac{E_{\mathrm{a}}}{RT_e}}}{e^{\frac{E_{\mathrm{a}}}{RT_m}}}\Big(\frac{m_2 - m_4}{\alpha_{\mathrm{m}}}\Big)^4 . \tag{2.18}$$

Following the methodology of the previous section, the Taylor-series approach (Eq. 2.5) yields a more complete expression for an expanded uncertainty:

$$u^2_{t_{\mathrm{a}}} = \left[\frac{-4t_{\mathrm{a}}^{3/4}}{\alpha_{\mathrm{m}}}\right]^2 u^2_{m_2} + \left[\frac{-4t_{\mathrm{a}}^{3/4}}{\alpha_{\mathrm{m}}}\right]^2 u^2_{m_4} + \left[\frac{-4t_{\mathrm{a}}}{\alpha_{\mathrm{m}}}\right]^2 u^2_{\alpha_{\mathrm{m}}} \tag{2.19}$$

$$+\left[\frac{-t_{\mathrm{a}}}{\mathbf{R}(T_e - T_m)}\right]^2 u^2_{\mathbf{E}_{\mathrm{a}}} + \left[\frac{-E_{\mathrm{a}}t_{\mathrm{a}}}{\mathbf{R}T_e^2}\right]^2 u^2_{T_e} + \left[\frac{-E_{\mathrm{a}}t_{\mathrm{a}}}{\mathbf{R}T_m^2}\right]^2 u^2_{T_m}. \tag{2.20}$$

This expression includes an additional three terms. If we neglect all other terms than that of the uncertainty mean lifetime temperature, we can derive the following:

$$\frac{u_{t_a}}{t_a} \times 100 \geq \frac{-100 E_a u_{T_e}}{\mathbf{R} T_e^2} \ . \tag{2.21}$$

The term on the right is the minimum relative uncertainty in RHX age due to uncertainty in lifetime temperature history. It may be noted in passing that this is identical to the error term presented for lifetime temperature history in Wilson et al. (2012). If the uncertainty in effective lifetime temperature is around 0.1^oK, then the contribution of this term to the relative uncertainty in t_a is of the order of 0.6%, given a likely effective lifetime temperature of around 13^oC and an activation energy E_a for the rehydroxylation reaction of around 70 kJ.mol^{-1}. This translates to about half a year in 100 years, 5.5 years in 1000 years, etc. (effectively 1σ).

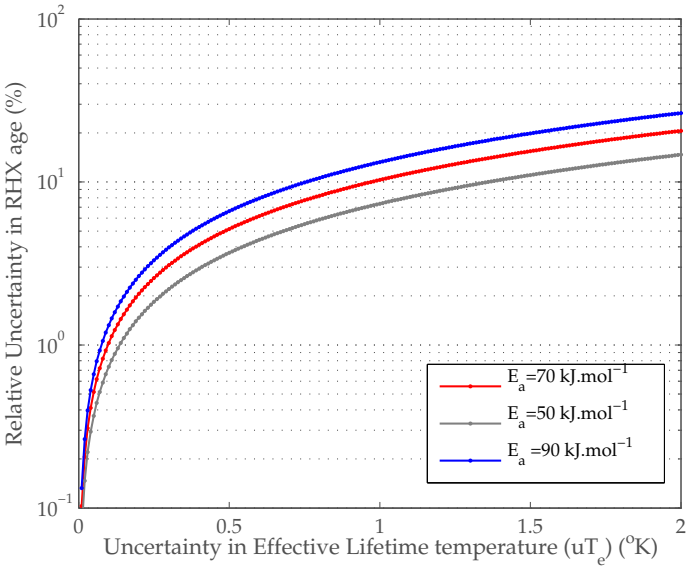

FIGURE 2.1: Minimum uncertainty in RHX age as a function of ELT uncertainty for different activation energies.

A graph of this is shown in Figure 2.1, in which this is plotted for three different activation energies in the range of those previously determined for the RHX reaction. Changing the actual effective lifetime temperature itself is negligible in comparison with

changing the activation energy, which itself does not greatly affect the order of magnitude of the relative uncertainty in RHX age (as seen below). The curve is sharpest at lower uT_e, and flattens out at around the 10% level towards higher $\mathrm{uT}_e(i.e.1^o\mathrm{C})$.

It should be noted that although the above expression for expanded standard uncertainty in RHX ages (i.e. Eq. 2.9) represents a better approximation of the 'true' uncertainty, there are undoubtedly more powerful methods of estimation which are better suited to this task.

2.3 Comparison with a simple Monte Carlo approach

Another approach is to propagate uncertainties using Monte Carlo-type simulations (Bevington and Robinson, 2003; Dunn and Shultis, 2012). The rationale behind this is to assume underlying distributions (i.e.*probability density functions*) for each random variable in a set $\mathbf{x} = x_1, x_2, x_3$, etc.. Each component random variable x_j, $j = 1, ..., x_n$ can either be discrete or continuous. To determine the expected mean $\langle z \rangle$ and variance $\sigma(z)$ of some function z of $\mathbf{x}$, where multiple x_i are distributed according to the joint probability density function $f(\mathbf{x})$ over the entire "volume" V, one essentially performs an integral

$$\langle z \rangle \pm \sigma(z) = \int_V z(\mathbf{x}) f(\mathbf{x}) \mathrm{d}\mathbf{x} \pm \sqrt{\int_V (z - \langle z \rangle)^2 f(\mathbf{x}) \mathrm{d}\mathbf{x}} \simeq \bar{z} \pm \sqrt{\frac{\bar{z^2} - \bar{z}^2}{N}} \tag{2.22}$$

Here the Monte Carlo estimate is formed by $\bar{z} = (1/N) \sum_{i=1}^{N} z(\mathbf{x_i})$, where N is the number of samples of $\mathbf{x_i}$ (or 'histories') drawn from the joint PDF (Dunn and Shultis, 2012). As applied to propagation of uncertainty, this PDF can be generated by assuming each random variable is drawn from its own independent PDF. In the case of RHX ages, this PDF can be determined by assuming that m_2, m_4 and α_m follow normal distributions with known mean and variance, and by sampling several hundred thousand times over the RHX age equation (Eq. 2.18). The resulting PDF may then be used to determine a Monte Carlo estimate of the mean and variance of the RHX age according the above formulation. This approach is useful in that it (a) requires no approximation to be made

by way of neglecting higher-order terms in the Taylor-series approach, (b) yields more information about *distribution* of likely dates, and (c) can be refined computationally in terms of a Bayesian framework, as is currently done for radiocarbon.

For example, a simple Monte Carlo estimate of an RHX age is shown below in Figs. 2.2 and 2.3, in the absence of temperature uncertainty (i.e. according to Eq. 2.1). This assumes in the first figure that m_2, m_4 and α_m are all drawn from normal distributions of continuous random variables ($\mathcal{N}(\mu, \sigma)$) of $\mathcal{N}(30.1, 0.001)$, $\mathcal{N}(30.3, 0.001)$ and $\mathcal{N}(0.024, 0.000079)$ respectively. The result is obviously a very recent date. The figure alongside it shows the same estimate, but this time with variances in the masses m_2 and m_4 which are one order of magnitude higher. This causes a broadening of the PDF, but also non-normality. All simulations of the PDFs of RHX ages presented here are best described by the gamma distribution:

$$f(x) = \frac{1}{\beta\Gamma(\alpha)}\left(\frac{x}{\beta}\right)^{\alpha-1} e^{-x/\beta} \ , \tag{2.23}$$

where $\Gamma(\alpha)$ is the gamma function defined by

$$\Gamma(\alpha) = \int_0^\infty x^{\alpha-1} e^{-x} \mathrm{d}x \ . \tag{2.24}$$

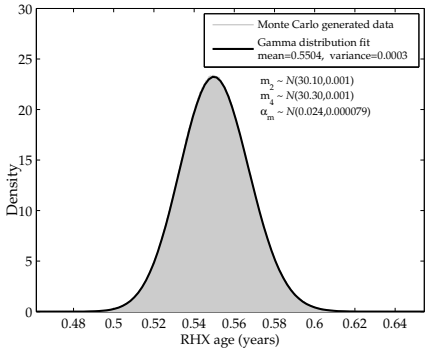

FIGURE 2.2: Monte Carlo propagation of measurement uncertainty for a theoretically very recent RHX date (in the absence of uncertainty in temperature).

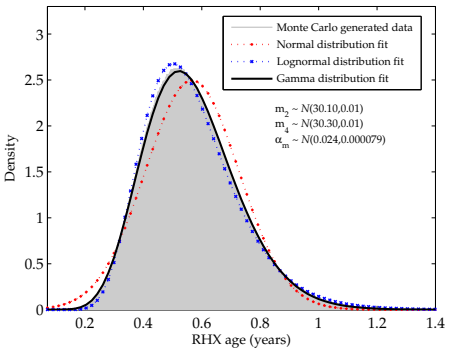

FIGURE 2.3: The same approach, but now with one order of magnitude higher uncertainty in the masses m_2 and m_4. Note that the pdf is now skewed.

2.4 Uncertainty in lifetime temperature history

This method for propagation of measurement uncertainty can be extended to include error in effective lifetime temperature history. Monte Carlo simulations on temperature-corrected RHX ages (shown in Fig. 2.4) show a systematic increase and broadening in simulated RHX age PDFs with a 0.1^oC stepped increase in error in T_e estimation. The estimates of each mean age are increased at intervals of approximately 7 years (1% of the value of t_a, which is in good agreement with the theoretical curve shown in the previous seciton). The expanded distributions correspond to about a 4.5% relative uncertainty in RHX age (at 68% confidence), and are thus one to two times more than confidence bounds given by the conventional Taylor-series approach (but nevertheless of the same order of magnitude).

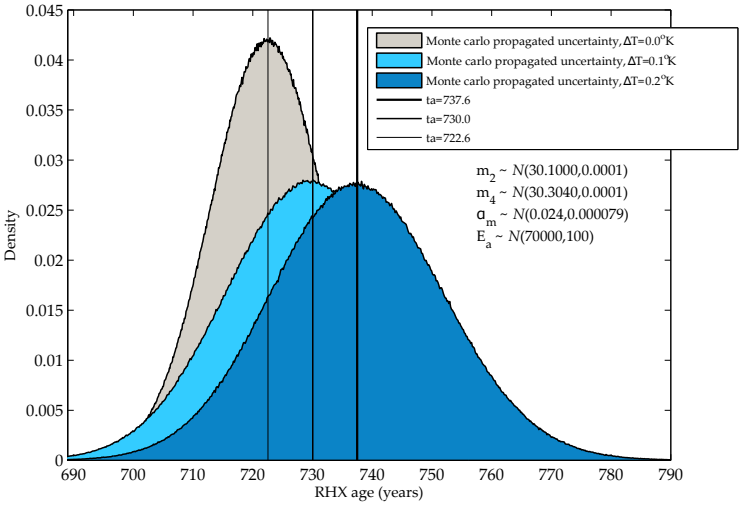

FIGURE 2.4: Probability density functions for three simulated dates at temperature errors of 0.0^oC, 0.1^oC and $0.2\ ^oC$. The result is to shift the entire distribution, which also becomes broader. The amount by which this mean is shifted at an activation energy of 70 $kJ.mol^{-1}$ is approximately 1% of t_a, in agreement with the analytical expression displayed in Fig. 2.1.

2.5 Implications for measurement and age range of the technique

If repeated simulations are performed sequentially for increasing m_2 (and therefore increasing t_a), then combined measurement and temperature uncertainty may be plotted as a function of RHX age. In Figure 2.5 (a-d) these are plotted as the percentage uncertainty (negative and positive) of the RHX age over a range of ages. The Monte Carlo propagated uncertainty (yellow regions, representing the relative percentage uncertainty (at 95% confidence) is compared with the Taylor-series approach (red lines) of a theoretical sample with parameters. These parameters are generally held constant from Fig. 2.5(a) to Fig. 2.5(d), with the exception of u_{m_2} and u_{m_4}, which are increased systematically from 0.0001 (Fig. 2.5(a)) to 0.1 (Fig. 2.5(d)), and u_{T_e}, which is 0.5 ^{o}C in Fig. 2.5(b), but 0.1 in all other subfigures.

The effect of increasing uncertainty in m_2 and m_4 can clearly be seen as a broadening of the confidence bounds at very recent RHX ages, which is non-symmetric in the case of the numerical method (a consequence of the Gamma distribution), as well as a large increase in the magnitude of percentage uncertainty (i.e. 20% in Fig. 2.5(c) would correspond to roughly $\pm$40 years (2σ) at an RHX age of 200 years. The Taylor-series estimates are in rough agreement with the numerical method, with the clear exception of Fig. 2.5(b), where the uncertainty in effective lifetime temperature is considerably greater (0.5^{o}C). The Monte Carlo approach yields fairly constant relative uncertainty of just under 10% (2σ), that is approximately $\pm$10 years in 100, 100 years in 1000, 1000 years in 10000, etc. This agrees with the linear nature of the minimum relative uncertainty predicted by the Taylor-series, i.e. Φ (Eq. 2.16) at large t_a. The extreme cases of Fig.2.5(c) and (d) are unlikely given the level of precision in m_2, m_4, but are nontheless presented here as an illustration.

In most cases we should be able to estimate the effective lifetime temperature to within 0.5 ^{o}C. The ELT is somewhat similar to an average temperature, in that the oscillation of daily and seasonal temperature variations will lead to increased mass gain at higher T, and decreased mass gain at lower T. However, mathematically at least, the extra mass

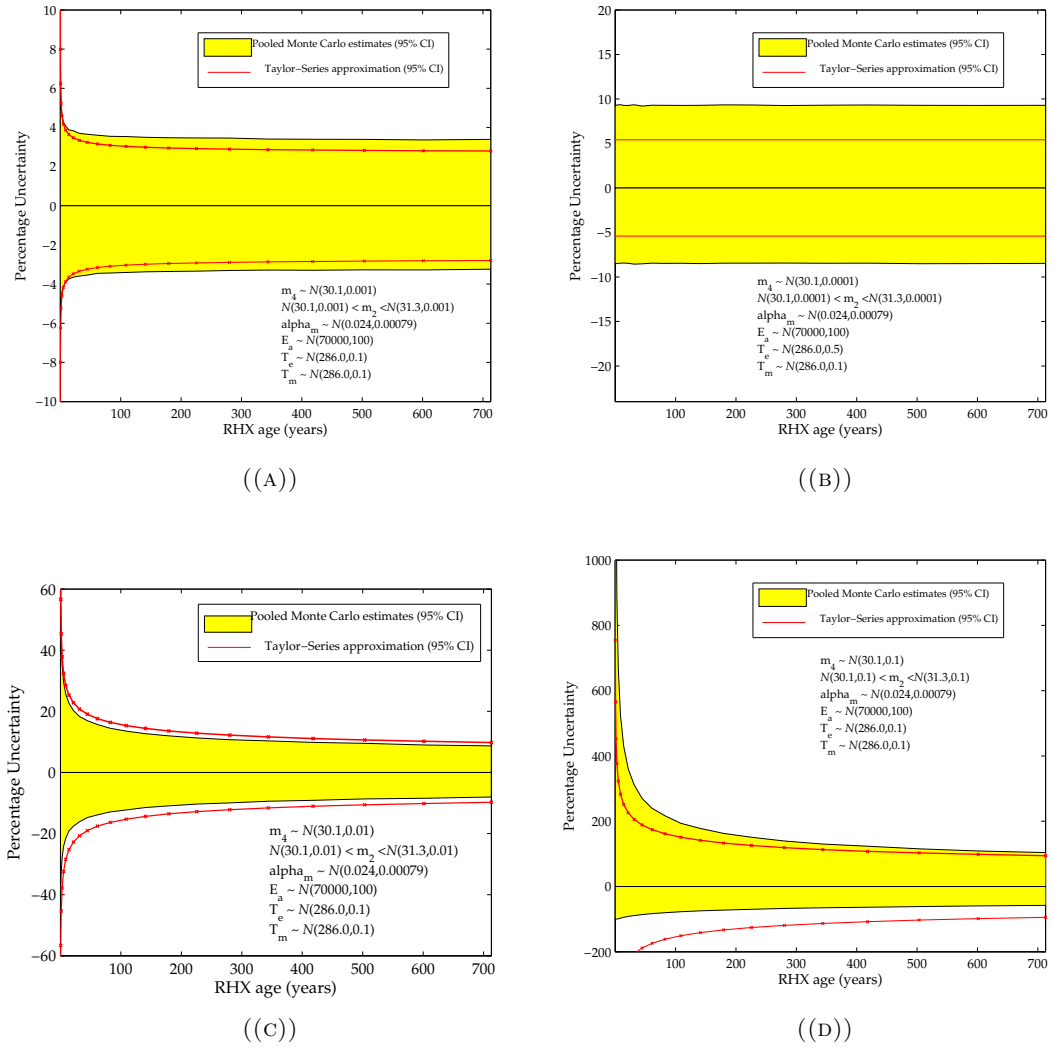

FIGURE 2.5: Comparison of Monte Carlo propagated uncertainty (yellow regions, representing the relative percentage uncertainty (at 95% confidence) with the Taylor-series approach (red lines) of a theoretical sample with parameters $m_4 = 30.1$g, $\alpha_{\mathrm{m}} = 0.024 \pm 0.00079$g.h^{-1}, $E_{\mathrm{a}} = 70$kJ.mol^{-1}, T_e, T_m=286.0 K. u_{m_2} and u_{m_4} are 0.0001, 0.001, 0.01 and 0.1 in (b), (a), (c) and (d) respectively.

gain at temperatures higher than the arithmetic mean will not completely compensate for the mass gain at lower T, since ELT is the fourth power mean $\left\langle \alpha(t)^4 \right\rangle^{1/4}$ of α over the temperature history (Hall et al., 2013). Uncertainty in ELT might well be higher (perhaps as high as 1 or 2 ^{o}C), for several scenarios. The first would be if an object is moved to a different geographical area over several decades. Another scenario is one where archaeological pottery is regularly used for cooking, particularly under lower temperatures (100-300 ^{o}C) where dehydroxylation is not predominant.

In other words, the magnitude of the uncertainty associated with lifetime temperature effects is likely to be influenced primarily by geographic latitude, use for cooking, and also to some extent burial (although this effect is merely expected to dampen the amplitude of temperature oscillations). Hall et al. (2013) point out that cumulative rehydroxylation mass gains of buried objects are less sensitive to short-term temperature variations than objects at other locations (i.e. building materials). For brick buildings, there will be relatively large oscillations in daily temperature, which will vary from one side of a building to another, i.e. from bricks exposed to direct sunlight in south facing walls (in the Northern Hemisphere) to those in full shade. Since the location of archaeological/historical bricks on an old building is largely unknown, and this variation is likely to be of the order of several degrees, the effect on α_{ELT} may be a significant source of uncertainty.

Additionally, there is a minimum level of uncertainty associated with the *calibration error* of temperature measurements. This may be thought of as an error of accuracy (or 'tolerance') rather than of precision. The temperature sensor in laboratory rehydroxylation experiments will be different from that which is used to assess lifetime temperature at a particular geographical location, and consequently this needs to be considered as part of the uncertainty budget of an RHX age determination. Generally speaking, a typical platinum resistance temperature detector (RTDs) has a tolerance in the range of $\pm$ 0.12% of resistance at 0 ^{o}C (for a class B RTD according to the IEC-751 standard). For a 100 Ω platinum RTD, this translates to about $\pm$ 0.3 ^{o}C. For an uncalibrated standard type J or K thermocouple, the typical tolerance is higher, at about 1 ^{o}C.

2.6 Expression for useful age range of the technique

Some consideration shall now be made of the useful age range of the technique. In the model of Hosking and Hueber (1958), expansion is asymptotic, approaching the total value ε_{T} in the limit $t \rightarrow \infty$. Although the power law model of Wilson et al. (2003) is not asymptotic, there must be some point at which the rehydroxylation reaction is complete. Beyond this, any RHX age determination is regarded as a minimum age (and

consequently, the age limit of the technique). If rehydroxylation is indeed a process of recombination of structural hydroxyl, then the upper limit to fractional mass gain $y_{\max}$ is set by the number of available sites in the clay mineral. Hall et al. (2013) point out that we currently have no way of knowing this value. However, it may still be possible to give some estimate of the age limit.

Looking at the model of Wilson et al. (2003), one might suppose the following simple relation to hold over the entire lifetime of the ceramic at some ELT:

$$t_{\max} = \left(y_{\max}/\alpha_{\mathrm{ELT}}\right) . \tag{2.25}$$

Additionally, one might describe the underlying chemical kinetics in the following general formalism, applicable to solid state chemical reactions (Hall et al., 2013; Vyazovkin and Wight, 1997):

$$\frac{d\zeta}{dt} = k(T)f(\zeta) , \tag{2.26}$$

where ζ is the extent of reaction given by y/y_{max}, and $k(T)$ is the solid state rate constant. Therefore, Hall et al. (2013) identify the reaction model as $1/(4\zeta^3)$. Given the differential equation for the Wilson et al. (2003) model, $4y^3dy = \alpha(T)^4dt$, one may obtain:

$$\frac{d\zeta}{dt} = \frac{(\alpha_{\mathrm{ELT}}/y_{\max})^4}{4\zeta^3} , \tag{2.27}$$

which by comparison with Eq. 2.26 implies that the rate constant $k(T)$ is $(\alpha_{\mathrm{ELT}}/y_{\max})^4$. Since $k(T)$ can also be decribed by the Arrhenius relationship $k(T) = A^{-1}exp(E_{\mathrm{a}}/\mathbf{R}T_{\mathrm{e}})$ (Eq. 1.8), with A being a pre-exponential factor, it is identified that:

$$t_{\max} = A^{-1}exp\left[\frac{E_{\mathrm{a}}}{\mathbf{R}T_{\mathrm{e}}}\right] . \tag{2.28}$$

Either Eq. 2.24 and Eq. 2.28 may be used to assess the useful age range of the technique. The complication is that A and y_{max} are unknown, in essence depending on the reversibility of the rehydroxylation reaction. However, it is still possible to give an estimate a value for $t_{\max}$. For example, consider a clay with hypothetical $y_{\max}$ of 2%. Using Eq. 2.24 $t_{\max}$ lies between 10 000 and 1000 years for an α_{ELT} of between 0.0002

and 0.0004 $h^{-1/4}$. At these values of t_{max}, and a slightly conservative estimate of combined measurement uncertainty of 10% (Fig. 2.5a), at the large time limit, the combined uncertainty would be of the order of 1000 years and 100 years across the stated range of α_{ELT}.

For a pure kaolinite clay mineral ($2Al_2Si_2(OH)_4$), y_{max} has a maximum value of 0.1295 by stoichiometry, which may give t_{max} greater than 100 000 years, over the entire range of measured α_{ELT} (Wilson et al., 2009, 2012). Highly-fired materials (at temperatures in excess of ~1000 ^oC) are likely to have a lower number of sites available for rehydroxylation, due to the collapse of clay mineral structure, and the formation of high-temperature phases such as spinel and mullite. At lower firing temperatures, the ceramic matrix may maintain a degree of structural integrity ('meta-clay', explored in more detail in Chapter 3.), and consequently the number of sites approaches the theoretical value as determined by stoichiometry (for a pure clay, at least) for the completely rehydroxylated clay mineral.

It will be briefly noted that if the power law model of Wilson et al. (2003) is modified to contain a variable power, i.e. $y_a = \alpha(T)t^{1/N}$, then the above Eq. 2.28 will remain the same, but Eq. 2.24 will become $t_{max} = (y_{max}/\alpha_{ELT})^N$.

2.7 Summary

This chapter presented theoretical limits to the RHX dating technique. Results from a conventional Taylor-series propagation of error, as well as a Monte Carlo-type approach show that minimum uncertainties vary across several orders of magnitude in recent experimental studies of rehydroxylation in archaeological ceramics. Arguably, most studies of rehydroxylation dating are therefore poorly-designed tests of the dating method, since they have combined measurement uncertainties which are greater than several tens of percent. Several practical steps may lead to greater precision in RHX age; most notably reducing the ratio of microbalance resolution to sample mass to less than parts-per-million (ppm) level.

On the basis of several arguments presented for lifetime temperature effects, it seems reasonable to expect a minimum uncertainty in ELT of 0.3^{o}C (i.e. from sensor tolerance and/or unknown effects of variable solar heating on structural ceramics, for instance). From Fig. 2.1 this translates to between 1 and 3 % of the age of the ceramic, for different values of E_a. Uncertainty in ELT is ultimately the most significant contributor to combined uncertainty, and these error estimates therefore set the fundamental limit to the technique. Further investigation and better methods of stochastic simulation are undoubtedly needed for robust estimation of ELT, but this is unfortunately beyond the scope of the current work.

Expressions for the age limit of the technique were presented, along with some calculations. The age limit varies quite significantly for different values of α_{ELT}, as well as $y_{\max}$. When $y(t) = y_{\max}$, all rehydroxylation sites are filled, and the rehydroxylation age will be a minimum estimate of the date of original firing. These calculations show that highly-fired materials are likely to have an age limit of several hundred thousand years, but these measurements will be significantly more challenging because these materials will have low α and $y_{\max}$. One such example would be highly-fired materials like porcelain, which are probably well beyond the limits of practical rehydroxylation measurements by microgravimetry.

Chapter 3

Chemical change and post-depositional processes in archaeological fired-clays

Rehydroxylation is the primary mechanism of long-term chemical weathering of archaeological fired-clays. Hydroxyl water which recombines with the matrix after firing may well account for up to $\sim 4.5\%$ of the ceramic body by weight, as determined by thermogravimetric analysis (Shoval and Paz, 2013) as well as saturation by steam autoclave (Mellor and Holdcroft, 1911; Wilson et al., 2003). However, it is not the only chemical process by which the ceramic may become altered. Indeed, the combination of clay mineral chemistry - specifically, the degree of substitution and variation in the molecular lattice - with their use and burial in archaeological contexts contributes to great complexity in the interactions which may take place after firing. At present, post-depositional processes in archaeological ceramics have received little attention, as pointed out by Pollard and Heron (2008), Freestone (2001) and others. The tendency has been to treat archaeological ceramics as immutable objects, whereas the reality, as we shall explore, is quite the opposite. The purpose of this Chapter is thus to explore the complexity of possible reactions undergone by archaeological ceramics during and after firing.

Additionally, it will be useful to explore the practical implications of these interactions on the RHX dating method. Since the current RHX method is based on gravimetry, molecular species which have entered (or been leached from) the ceramic matrix after firing are expected to affect dates either by overestimating (or underestimating) the mass measured after heating the ceramic to 500^{o}C, or by exhibiting sorption properties which may compete with the RHX process. For example,Wilson et al. (2012) recently report the presence of 0.67% organic carbon by weight in a sample of Anglo-Saxon loomweight, which effectively overestimated the RHX date by 1172 years. When compared to the decadal-scale precision potentially offered by the RHX measurement procedure, organic contamination appears to be a significant effect. Wilson et al. (2013) also point out that the presence of calcite contributes to non-linearity in stage I mass gain, presumably due to recarbonation of lime after firing, but also potentially partly due to hydration. These complications may well be resolved by effective pretreatment with a base (for organics) and acid (for calcite), but it is first important to consider in greater detail the theory of thermal and post-depositional processes undergone by archaeological ceramics, as well as the current evidence from archaeological and experimental studies. An experimental investigation of pretreatment protocols for the RHX method forms the subject of the following Chapter 4.

3.1 Overview: Mineralogy, hydration and the changes taking place on heating

The chemical structure of clay minerals has been intensively studied over the past century, and is well reviewed by Grim (1968), Bergaya et al. (2006) and Heller-Kallai (2006) (among others). However, it will be useful to give a brief overview.

Most clays minerals are layer-type aluminosilicates. They consist of alternating layers, each of which is comprised of a combination of a silica sheet (linked SiO_4 tetrahedra, with non-bridging oxygens rising above the basal plane), bonded to a plane of Al^{3+} ions. Each aluminium ion is octahedrally coordinated by hydroxyl and oxygen molecules. And each unit layer (the combination of tetrahedral SiO_4 and octahedral Al) is in turn bound

to other similarly-orientated layers, primarily by van der Waals' interactions/hydrogen bonding, but also by electrostatic attraction and extraneous ions, which are usually exchangeable in the case of hydrated clay minerals (Grim, 1968). Much of the utility of clays arises from the van der Waals forces/hydrogen bonding, which makes it easy for the layers to 'slip and slide' over one another, and renders the material plastic.

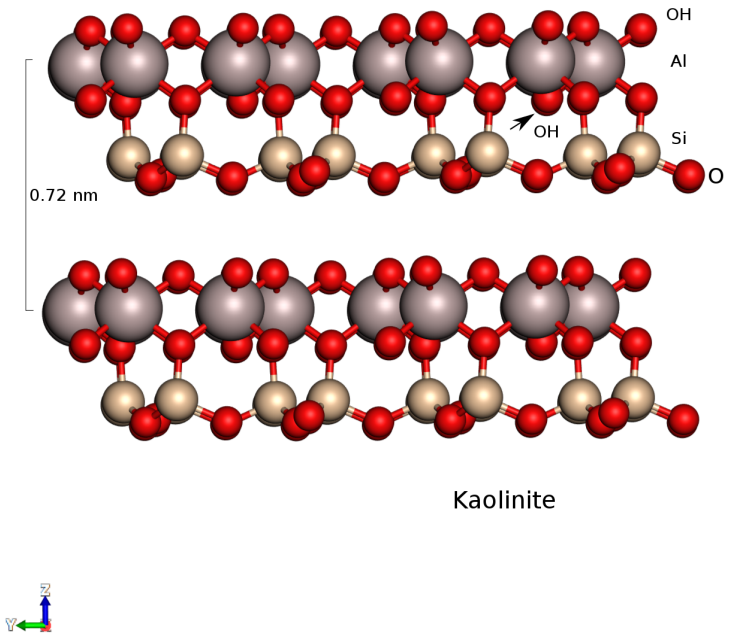

FIGURE 3.1: Layer structure of 1:1 clay mineral (kaolinite). Diagram shows location of Si tetrahedral layer and Al octahedral layer in the yz plane. x direction is into the page. Made with molview (http://molview.org, accessed 10/10/2016)

However, this simple description belies much complexity; the degree of substitution of both Si and Al, as well as variation in the geometry of unit layers leads to considerable variation upon the clay mineral theme. For example, kaolinite/China clay is a 1:1 or 'dimorphic' mineral, meaning that it has one tetrahedral and one octahedral sheet. The general formula for kaolinite is $Al_2(Si_2O_5)(OH)_4$, with the apices of the Si tetrahedra projecting onto the base plane of the octahedral Al sheet, effectively replacing two thirds of the hydroxyl ions. However, in the case of the smectites (e.g. montmorillonite) there is an additional layer of Si tetrahedra, orientated in an opposite direction to that of the first,

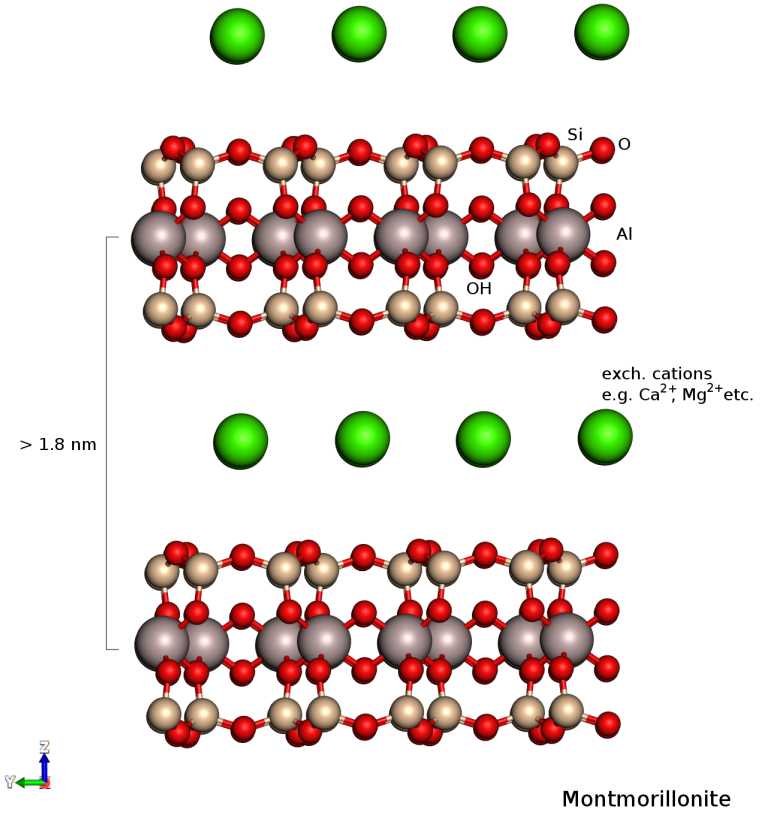

FIGURE 3.2: Layer structure of 2:1 clay mineral (montmorillonite). Orientation as in previous figure.

and both tetrahedral layers 'sandwich' the plane of Al^{3+} ions. These are called 2:1 or 'trimorphic' minerals. The general formula for montmorillonite is $Al_2Si_4O_{10}(OH)_2.nH_2O$, however this is perhaps a simplification since there is normally considerable substitution (either Al^{3+} replacing Si^{4+}, or a divalent cation of appropriate size such as Fe^{2+} or Mg^{2+} substituting for Al^{3+}). This in turn creates charge imbalance in the lattice which has to be satisfied by the presence of exchangeable cations on the interlayer plane (among other things). This property is of significance when considering the interactions of clay minerals with organic molecules (Theng, 1979), something which shall be explored in greater detail below. Other 2:1 minerals, such as muscovite ($KAl_2(AlSi_3)O_{10}(OH)_2$), may also have potassium substitution for Al^{3+} within the octahedral sheet, as well as OH^- and F^- between the layers. A further variation on the 2:1 structure are 2:1:1 layer minerals ('tetramorphic') such as chlorite, in which each trimorphic layer alternates with an hydroxide sheet.

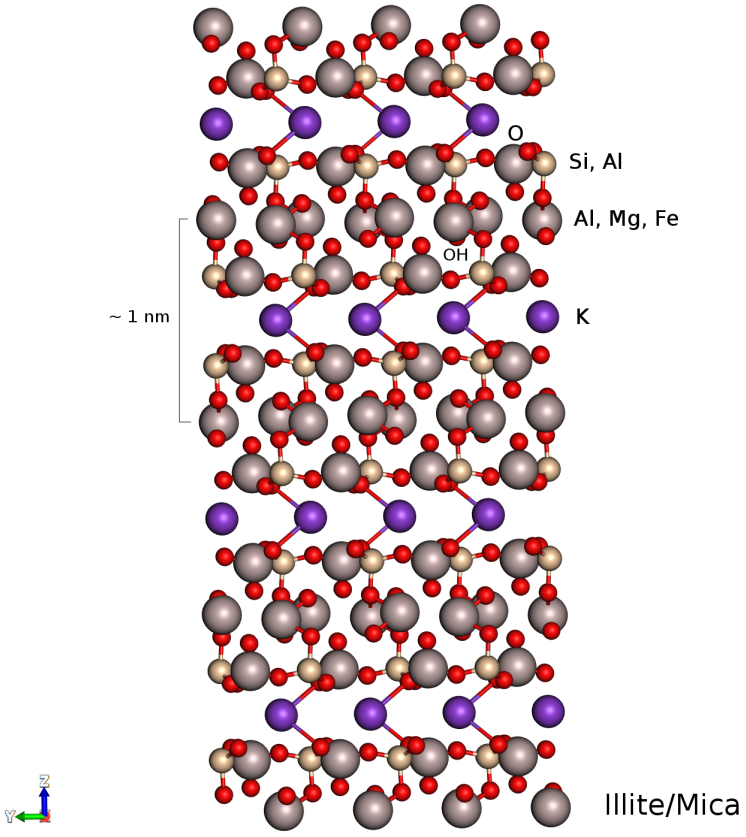

FIGURE 3.3: Layer structure of 2:1 clay mineral (illite/mica). In these clay minerals the interlayer space is occupied by poorly-hydrated potassium cations. Orientation as in previous figure.

If the variation within the clay minerals is one thing; the complexity of pedogenic clays is quite another. Compositionally, these may contain several clay minerals (although the predominant minerals of archaeological interest would be kaolinite and illite, and perhaps sometimes montmorillonite and chlorite), with different sheet layers either randomly or regularly interstratified (Theng, 1979). Products of geochemical weathering, such as carbonates ($CaCO_3$) and iron hydrates ($Fe_2O_3.H_2O$) often also form part of the clay matrix (Magetti, 1982), as do complex organic molecules (e.g. 'ball clays' are predominantly kaolinite, but with a substantial organic component - up to 16% - in the form of lignite (Holdridge, 1959)). Various minerals such as quartz, mica and pyrite are also usually present. With regard to the composition of archaeological ceramics, the conceptual difference between pedogenic clays and clay minerals is thus highly relevant (as pointed out by Pollard and Heron (2008), at 112). Any structural changes upon heating are not only influenced by the source clay minerals themselves, but also by the

presence of non-clay minerals in the material - a factor which has not previously been adequately explored in previous investigations of the RHX method.

3.1.1 The clay-water system

The most important change undergone by clays upon heating is loss of water. Post-firing, the material begins to take up water again. However, there are several types of water present in clays. Grim (1968) originally distinguished between water which is driven off at low temperature, and OH lattice water generally lost at temperatures higher than 300^{o}C. He divided the low-temperature water into three categories: (1) pore water and adsorbed water on the edges of discrete particles in the clay mineral; (2) interlayer water between the unit layers which is generally bound by weak hydrogen and van der Waals' forces; and (3) water at tubular openings present in sepiolite-type minerals (Grim, 1968). Of the three, the former two are more relevant to this discussion. Whilst interlayer water requires slightly higher temperatures to be driven off, pore water is more easily removed at around 100^{o}C (Heller-Kallai, 2006). In the case of pedogenic clays, from which archaeological material is drawn, we may also wish to add water which forms a hydration shell around adsorbed cations which are present in the interlayers.

3.1.2 Sorption and specific surface area

The rate of water adsorption depends primarily on the porosity, which is of course related to the degree of crystallinity and the specific surface area (SSA) (Wilson et al., 2013; Bowen et al., 2011), but also on the cation exchange capacity (particularly within soils). Clay minerals are of course inherently colloidal; that is they have a large surface area per unit weight. Therefore, it should be expected that the greater the SSA the longer it takes for hydration of the interlayers to occur, since there are more sites which to occupy. Wilson et al. (2013) recently presented data from archaeological pottery and brick which show a large range of SSA between 0.78 $m^2.g^{-1}$ (Samian ware) to 35.0 $m^2.g^{-1}$ (low-fired loom-weight), which is strongly dependent on both the temperature and duration of firing (Mesbah et al., 2010). Their data seems to suggest that, as expected, larger SSA leads to longer times for initial sorption of weakly-bound water. Practically, SSA should

not affect RHX dates themselves, since there is good experimental evidence to suggest that the RHX reaction is so slow as not to be limited by supply of water at all (Wilson et al., 2003, 2009). However, experimentally they may cause greatly extended measurement times (as it takes longer for equilibration of weakly-bound water in high SSA material).

From a theoretical point of view, there should also be an effect due to variation in underlying clay mineralogy. Montmorillonite is predicted to have the highest SSA of clay minerals, due in part to its trimorphic structure, but also due to the high degree of substitution within the lattice (Theng, 1979). This is supported by studies of internal reflectance spectroscopy (Mulla et al., 1985), as well as bulk-gas (N_2) and liquid adsorption methods (Macht et al., 2011). The latter authors determined values of SSA for illite and montmorillonite of 112 $m^2.g^{-1}$ and 475 $\pm$ 2 $m^2.g^{-1}$ respectively (liquid adsorption), whereas Mulla et al. (1985) determined the SSA of various montmorillonites as between 605 and 800 $m^2.g^{-1}$. Kaolinite had a much lower SSA at around 35 $m^2.g^{-1}$. It is not known exactly why these are much higher than that of the fired clays, but the most plausible explanation is the collapse of interlayers upon firing may reduce SSA. In any case, it may be of significance to note that the SSA of montmorillonite is two orders of magnitude higher than that of kaolinite, and that the presence of this clay mineral in archaeological ceramics might lead to extended measurement times.

3.1.3 Dehydroxylation temperatures of clay minerals, and changes in lattice structure on firing

When clays are first fired, dehydroxylation occurs at a range of temperatures in different clay mineral groups (from about 500 to 700^{o}C), naturally depending on particle sizes (Grim, 1968) and on the bond strengths of OH^- groups within the different structures of the phyllosilicates (Bergaya et al., 2006; Molina-Montes et al., 2008). For example, montmorillonite, a 2:1 clay, requires higher temperatures for dehydroxylation (Heller-Kallai, 2006). Differential thermal analysis curves show a peak corresponding to loss of lattice hydroxyl water at around 500 to 600^{o}C, the exception being smectite, which seems to have a broader range (Grim, 1968). The raw material used for bricks or pottery will typically be comprised of a mixture of clay minerals, and the exact temperature range

will therefore depend on the starting composition, as well as the heating regime (Heller-Kallai, 2006). However, in typical archaeological or historical material, there is no reason to believe that dehydroxylation should not proceed to completion (or near completion), since even low-fired earthenware generally would have exceeded dehydroxylation range. It is important however to note that these are all *ranges*. A small fraction of water (2-3%) is retained by kaolinite at 525^{o}C, and this is gradually lost to around 800^{o}C (Grim, 1968). De Keyser (1939) first showed that complete dehydroxylation can be achieved by simply extending heating times. In his study he found that, even at temperatures as low as 350^{o}C, 200 hours of extended heating was enough to remove all hydroxyl water.

If fired-clays are reheated, there is good evidence to suggest that the removal of recombined hydroxyl water may take place at slightly lower temperatures than the original hydroxyl water - a phenomenon first noted by Grim (1948) which is observed in kaolinite, illite and montmorillonite, and which is probably related to structural changes upon firing (Muller et al., 2000). Differential thermal analysis shows a dehydroxylation peak for rehydrated kaolin at around 70^{o}C lower than the previous heating, which may be due to the splitting or original crystals into smaller domains on reheating. 450-550^{o}C is now generally accepted to be the temperature range at which any subsequent dehydroxylation will start to occur (Hamilton and Hall, 2012), but longer heating regimes may be necessary for certain samples.

The precise structural nature of dehydroxylated (or partially dehydroxylated) clays minerals is complex, and is currently an active research area. Loss of OH^- water from the matrix is generally associated with a preferential change from octahedral to tetrahedral coordination in the Al^{3+} plane (Molina-Montes et al., 2008), although there are other possible variations that depend on the degree of substitution, as well as the presence of cations in the interlayer (Derkowski, 2012), which is also known to affect the degree of rehydroxylation. Vitrification or the formation of high-temperature phases of silica (SiO_2) and alumina (γ-Al_2O_3) obviously also act to reduce the RHX rate (Tosheva et al., 2010; Mesbah et al., 2010) after firing.

3.2 Chemical effects of use and burial on the ceramic matrix

3.2.1 Clay-organic reactions

$\boldsymbol{m}_{\mathbf{nrc}}$ in the terminology of Wilson et al. (2012) refers to any substances other than water lost upon reheating. By far the most significant of these with regard to archaeological pottery (buried or otherwise) is likely to be organic molecules. The source of these compounds varies greatly, from unfired elemental carbon/hydrocarbons of geological origin (0.05-0.2% by weight according to Zaitseva et al. (2009)), to charcoal and temper added to the original clay mix, to humic compounds derived from the soil, to proteins and degraded animal fats (mainly *n*-alkanoic acids and monounsaturated *n*-alkenoic acids, (Craig et al., 2004)). The chemical variety of these compounds leads to considerable complexity in the range of theoretical interactions with hydrated clay minerals. Less is known about their interaction with fired-clays. The formation of (hydrated) clay mineral-organic complexes has been fairly extensively reviewed by Theng (1979). It seems that organic molecules may be bound on the sheet surface or in the interlayers by a combination of van der Waals and weak hydrogen bonds, or may form stronger bonds with the clay minerals by ligand exchange. An example of the latter would be the incorporation of carboxylate group of organic polymers into the coordination shell of the aluminium layer (Parfitt et al., 1977). In dehydrated clays, alcohol groups may be preferentially coordinated directly to exchangeable cations in the clay matrix (Theng, 1979). The degree to which all these reactions occur is influenced by the soil pH (if buried), the net charge on the clay mineral surfaces and porosity of the ceramic fabric. The degree to which the collapsed interlayer rehydrates (and consequently expands) must also have an effect.

Of primary importance to the RHX dating method is the degree to which these compounds are removed upon reheating, which will clearly depend on the bond energies, and the duration of the heating regime. Elemental analysis performed by Johnson et al. (1987) has shown that oxidation-resistant organic carbon remains in archaeological fired-clays at temperatures as high as 800-1000^{o}C (30 minute firing duration), although,

on the other hand, extended heating times of 7.5 hours or longer at even lower temperatures (700^{o}C) are known to be enough to cause oxidative-weight loss of graphite and diamond powder (Crumpton et al., 1996). With regard to the RHX procedure, where samples are routinely heated to 500^oC for several hours/days, weight loss due to oxidation of strongly bound/oxidation-resistant carbon is therefore expected to be present.

Humic acids and other organic macromolecules may be removed by reaction with an alkali such as NaOH, but oxidation-resistant forms of carbon are probably less easily removed. Bird and Gröcke (1997) presented an experimental study of the effectiveness of both acidified dichromate (0.1M $K_2Cr_2O_7$ in 2M H_2SO_4) and basic peroxide reagents for oxidation of different carbon sources. They found that after an initial rapid loss of carbon, approximately ∼3% of highly-resistant carbon remained in the samples after several hundred hours of treatment (60^{o}C). With regard to RHX, if this carbon is burnt off at extended reheating times, but is not easily removed by reagents, then any protocol which seeks to pretreat for organic contamination would leave a small amount of carbon, which, if combusted, would make RHX ages erroneously old. Since limiting the reheating time is not an option (as all OH^- molecules with which the ceramic has recombined over its lifetime must be driven off), it needs to be established that the residual oxidation-resistant carbon is negligible in comparison to the RHX water m_a, or else corrections to the RHX age must be made. An investigation of these effects forms Chapter 4.

3.2.2 Other reactions

Apart from hydration and the adsorption/absorption of organic molecules, archaeological fired-clays also undergo a host of reactions after firing. Hamilton and Hall (2012), Wilson et al. (2013) and Shoval and Paz (2013) draw attention to the possible effects of calcite in rehydroxylation dating of ceramics. Calcite, which forms a common temper in ceramics, is converted into CaO from about 700 degrees or higher. After firing, the lime then undergoes hydration to $Ca(OH)_2$. It may then also recarbonate to $CaCO_3$, which itself may be leached from the ceramic matrix in acidic environments such as many soils (Freestone, 2001). Shoval and Paz (2013) also point out that there may be significant

extra mass lost upon to reheating to moderate temperatures, which is associated with the decarbonation of either fine particles of calcite, or larger fragments of limestone, chalk and/or mono-crystalline calcite. Another degree of complexity comes from the fact that the lime may react with the clay, to form high temperature Ca-silicates. On the basis of FTIR spectra of non-calcareous and calcareous ceramics Shoval et al. (1991) pointed out that this reduces the amount of OH^- present in archaeological pottery, and therefore "the rehydroxylation process and reconstruction of clay minerals take place in noncalcareous pottery after higher temperatures than in calcareous one[s]." (Shoval et al. (1991), at 1589). This is potentially a highly significant effect, as we shall examine in more detail in a later chapter.

Iron oxides may also hydrate, as do high-temperature silica phases (by either ion exchange or network dissolution). Heimann and Maggetti (1981) show that one such phase - gehlenite ($Ca_2Al_2Si_2O_7$ - is often present in modern ceramics, but is not present in ancient comparable sherds, which may be an indication of extensive hydration and partial loss to the burial environment. This should not be a great concern for the RHX dating method, as there is no *extra* loss of mass upon reheating. However, the presence of hydrated phases of carbonates or iron oxides would undoubtedly contribute to extra mass loss.

On the other hand, the hydrated clay mineral products of geochemical weathering could also form part of the archaeological fired-clay. Although unlikely, secondary clay minerals might enter the macro/microscopic pore structure of some archaeological ceramics during burial. When the sherds are subsequently refired, this may influence the RHX age by greater apparent loss of OH^- groups, and hence produce an age which is too old. Decomposition of high-temperature plagioclase feldspars might also lead to clay mineral (montmorillonite and calcite) neoformation within the ceramic matrix after firing (Shoval et al., 1991).

3.3 Predicted effects of contaminants on the RHX dating technique

Conceptually there are two ways in which species may interfere with the gravimetric procedure. First, molecules which may enter the ceramic matrix after firing, but before measurement. Species in this category, which are burnt off after laboratory dehydroxylation at 500^{o}C, may act to increase the apparent difference between the as-received "equilibrium" mass m_2 and the post-500^{o}C mass m_4. For the purposes of discussion, these may be called 'category A' contaminants. This causes erroneously old dates. Second, 'category B' contaminants are species present in the ceramic matrix may also exhibit physisorption or chemisorption of atmospheric moisture on timescales which may cause an apparent increase in the RHX constant, α_{m}, during mass gain measurements in the laboratory. This causes erroneously young dates.

3.3.1 Category A contaminants

Archaeological pottery usually has complex histories of usage and/or burial. The ceramic matrix may have accumulated residues from cooking or storage, and further additions may have occurred in the geochemical environment. We indentify these primarily, but not exclusively, as (1) cooking and storage residues: fatty acids, proteins, other organic macromolecules; and (2) contaminants from burial: humic acids, unfired clay minerals, products of reactions between exchangable cations present in the interlayers and the surrounding soil.

A partial list of the latter would be: thenardite (Na_2SO_4), halite (NaCl), darapskite ($Na_3(NO_3)(SO_4).nH_2O$), eugsterite ($Na_4Ca(SO_4)_3.2H_2O$), konyaite ($Na_2Mg(SO_4)_2.5H2O$), wattevilleite ($Na_2Ca(SO_4)_2.4H_2O$), bloedite ($Na_2Mg(SO_4)_2.4H_2O$), gypsum ($CaSO_4.2H_2O$), calcite ($CaCO_3$), antigorite ($Mg_{48}Si_{24}O_{85}(OH_{62})$), brucite ($Mg(OH)_2$).

Thenardite (Na_2SO_4), for example, is known to be a common weathering product in brick, particularly in high urban areas (Hughes and Bargh, 1982). Most of these species are soluble, and therefore should be removed by ultra-pure water. Calcite, which is

insoluble, should not pose a problem since thermal decomposition of calcite takes place at around 848^{o}C, and hence it is unlikely that extra mass would be lost lost at lower temperatures due to calcination.

In general, more strongly-bound molecules which have entered the matrix after the event of firing (but which are not removed during the 500^{o}C step) should not in principle affect RHX dates since there is no extra loss in mass after reheating.

3.3.2 Category B contaminants

Compounds which undergo hydration include the following:

- Calcium sulfate. Anhydrous $CaSO_4$ hydrates to Gypsum ($CaSO_4.2H_2O$). This is reversible by heating to 200^{o}C. Heating to higher temperatures (250^{o}C) forms β-anhydrite, which does not undergo hydration. There is therefore expected to be little effect on the post-500 ^{o}C step. However, this may still effect the estimation of equilibrium archaeological mass m_2.
- Haematite. This forms limonite: $2Fe_2O_3 + 3H_2O \rightarrow 2Fe_2O_3.H_2O$
- Magnetite. This forms ferrihydrite ($5Fe_2O_3.9H_2O$)
- Bauxite. $Al_2O_3 + 3H_2O \rightarrow Al_2O_3.H_2O$
- Olivine. There is a range of reactions here, but olivine is not likely to be a common constituent of fired-clay ceramics. One reaction is the transformation of fayalite into magnetite: $3Fe_2SiO_4+2H_2O \rightarrow 2Fe_3O_4+3SiO_2+3H_2$. Another is the transformation of Forsterite into serpentine: $2Mg_2SiO_4 + 3H_2O \rightarrow Mg_3Si_2O_5(OH)_4 + Mg(OH)_2$.

Goethite (FeO(OH)) has also been previously noted in pottery (Mata et al., 2002), as well as the hydrated mineral jarosite (Secco et al., 2011). All these reactions (with the exception of calcium sulphate) could potentially contribute to mass gain after reheating, effectively increasing the measured RHX constant, α_{m}, and causing erroneously young dates. The relative magnitude of these effects is still not known, and clearly depends

upon the degree of reversibility of the hydration reactions after reheating, as well as redox conditions during heating. If they are irreversible then there should be little effect on α_m. If they are reversible, then all but calcite are most likely negligible in comparison to rehydroxylation, for the main reason that carbonates form a fairly common component of most archaeological pottery and brick. More detailed investigation is definitely needed to determine the effect of calcite on the RHX gravimetric procedure.

In addition to hydration reactions, there are also oxidation reactions undergone by iron oxides embedded in the ceramic matrix:

- Iron(II) oxide (Wüstite) to haematite. $4FeO + O_2 \rightarrow 2Fe_2O_3$

- Magnetite to haematite. $4Fe_3O_4 + O_2 \rightarrow 6Fe_2O_3$

These reactions are spontaneous and favoured at low temperatures. They would contribute to mass gain under oxidising conditions if wüstite and magnetite are indeed present.

Finally, there is a reaction which may fall into both categories (A) and (B). Burakov and Nachasova (2013) claim that iron hydroxides are transformed into magnetite (and haematite) with the exudation of water during firing, which "distorts the pattern of water accumulation." Iron(II, III) hydroxyide and iron(III) hydroxide (or their hydrates) may form magnetite and haematite respectively by the following reactions:

- $3Fe(OH)_2 \rightarrow Fe_3O_4 + H_2 + 2H_2O$ (under a reducing atmosphere)

- $2FeO(OH) \rightarrow Fe_2O_3 + H_2O$ (haematite formation)

- $2Fe(OH)_3 \rightarrow Fe_2O_3 + 3H_2O$ (haematite formation).

The forward reactions may contribute to an overestimation of hydroxyl groups lost on reheating, thereby causing erroneously old dates (category A). Archaeomagnetic analysis performed by these authors on one sample of brick with a high magnetite content showed that 40 mg out of 65 mg lost by the sample could be attributed to hydroxl groups from hydrated iron(III) oxide (Burakov and Nachasova, 2013). These authors claim that this resulted in an RHX age of 10,980 BC, as opposed to a corrected date of 1725 AD (i.e. Category A type contamination). The measurement uncertainty associated with their experimental setup is not provided, but if the role played by chemical weathering of magnetite/haematite is indeed significant, then the presence of this mineral may pose an obvious challenge to pretreatment/correction protocols. Since these authors do not give more information is not known whether unintentionally large measurement uncertainty (600% in the case of Bowen et al. (2011) - see Chapter 1) might have caused this overestimation.

Iron hydroxyides would be less easily removed by chemical pretreatment. If it is not possible to remove the contaminants by any reasonable means, then an accurate procedure for the quantification of these contaminants (and appropriate correction) should be developed. Where possible, category A and B contaminants should be removed using a standardised procedure which should be readily extensible to archaeological pottery, with minimal damage to material aesthetic. A promising alternative in any event would be to use N_2 gas in both the reheating and the rehydroxylation steps to prevent excessive oxidation. In the process of heating oxygen will nevertheless be liberated from the ceramic *itself*, so this approach may not be sufficient in and of itself. An experimental investigation of these effects forms the subject of the following Chapter.

Chapter 4

Investigation of pretreatment strategies for rehydroxylation dating

4.1 Motivation

Recent work by Nümrich et al. (2015) has emphasised the need for mandatory removal of organic carbon from samples selected for rehydroxylation dating. The need has arisen because the method proposed by Wilson et al. (2009) relies upon mass gain as a proxy for rehydroxylation rate. Hydroxyl content cannot be measured directly by current methods. Any additional change in mass upon reheating which is not attributed to dehydroxylation (such as that associated with the combustion of humic acids, lipids, etc.) may therefore affect the determination of m_{a} (m(OH) in Nümrich et al. (2015)). As discussed in the previous chapter, this is one way in which an RHX age determination may be erroneously old. In addition, any change in mass other than that attributed to rehydroxylation will affect the accuracy of a rehydroxylation rate determination. This latter class of interferents tend to cause erroneously young ages. The hydration of lime (formed by calcination of carbonate, which may be diagenetic, or originally added as temper), first proposed by Wilson et al. (2013), is one such possible effect. The calcination temperature

of carbonates is nominally 825 ^{o}C, but prolonged heating at much lower temperatures, particularly in atmospheres in which the partial pressure of CO_2 exceeds equilibrium CO_2 pressure, will also yield CaO (and, upon rehydration, $Ca(OH)_2$). Therefore, reheating to 500^{o}C as part of the rehydroxylation dating procedure will result in the incomplete formation of $Ca(OH)_2$, which will skew mass gain.

It is clear that the presence of certain interferents exerts significant effects on the accuracy of rehydroxylation dating. Therefore, in the absence of direct measurements of hydroxyl content, the removal of both calcite and organic carbon is an essential prerequisite for accurate dates. The subject of this chapter is therefore the removal of calcite and organic carbon from samples selected for rehydroxylation dating; the efficiency of various chemical pretreatments and their associated affects on the ceramic matrix.

There are three minimum conditions which must be met by such a pretreatment protocol:

- Organic carbon and carbonate which remains after pretreatment should be less than $\sim 1/10^5$ of the total mass of the sample selected for analysis. This is the required precision in m_a for an RHX determination with combined uncertainty less than $\sim$5%, as outlined in the numerical simulation of uncertainties (Chapter 2);

- structural OH remains unaffected by chemical reagents;

- any reaction by-products must themselves be removed from the ceramic matrix.

A central problem which any such investigation must overcome is that archaeological ceramics may display high intra- and inter-sample variability in underlying mineralogy, as well as organic carbon and/or carbonate content. As a consequence, meaningful comparison of the efficiency of several techniques, and their different effects on underlying mineralogy is problematic. A new experimental strategy is therefore introduced to test the efficiency of wet chemical pretreatments at removing both calcite and organic carbon. This strategy involves adding small known amounts of calcite and organics to small

replicate samples of identical fired-clays of very well-known composition. The effects of different pretreatments are thus easily investigated by standard infra-red spectroscopic techniques, and serve as a reference point for comparison with archaeological materials.

4.2 The mid infra-red spectra of clay minerals

The infra-red spectra of clay minerals have now been studied at length for many decades, and for a more thorough introduction the reader is directed to the reviews of Farmer and Russell (1964), Farmer (1974), Madejová and Komandel (2001) and Madejová (2003). For the current purpose it will suffice to outline the general features of the IR spectra of the clay minerals which predominate archaeological ceramics (namely kaolin and smectite group minerals), as well as changes upon heating. The mid infra-red region (4000-400 cm^{-1}) is of particular interest from a diagnostic point of view, as well as with regard to distinguishing between molecular water and structural hydroxyl groups.

4.2.1 Assignment of functional groups, and structural changes upon heating

4.2.1.1 Frequencies between 3750 and 3500 cm^{-1}

In layer silicates absorption in this part of the infra-red is due to hydroxyl groups. Bands attributed to structural OH groups generally occur at higher frequencies (3600 to 3700 cm^{-1}), whereas the OH stretching of adsorbed water is visible as a broad shoulder at the lower end of this range (~3400 cm^{-1}, see Figure 4.1). The latter region is strongly associated with the peak attributed to the deformation vibration of water at 1640 cm^{-1}, and this peak disappears together with the broad shoulder at 3400 cm^{-1} upon heating to ~200 ^{o}C (Serratosa, 2013; Madejová, 2003). On the other hand, the bands attributed to OH groups between 3600 and 3700 cm^{-1} do not show much change at these temperatures (Wolff, 1963), but are completely lost upon heating to 600 ^{o}C, in fresh samples of kaolin and montmorillonite. In kaolin minerals, the well-defined high frequency OH bands (see Table 4.1 below) are each assigned to a distinct type

of hydroxyl, whereas montmorillonite has a single peak at around 3626 cm^{-1}. The precise positions of these bands seem to vary slightly with several factors, including the the degree to which surface hydroxyl groups are associated with interlayer cations, the degree of interaction with the oxygens of the next unit layer, or various structural perturbations which arise from substitutions within the octahedral or tetrahedral sheets.

In fired clays and archaeological materials, the spectra in this region are an indication of the degree of rehydroxylation, but may also reflect the presence of organics. Clegg et al. (2012) observed changes in this region in clay ceramics immediately after firing by diffuse reflection (DRIFTS) method in combination with thermogravimetry mass spectrometry. These authors identify the 3620 cm^{-1} band in a sample of brick as the inner hydroxyl associated with the octahedral sheet, and as such a reliable indication of the degree of rehydroxylation. They find that the intensity of this band increases in accordance with the kinetic model of Wilson et al. (2003).

Figures 4.1a and 4.1b clearly show the effect of firing and subsequent uptake of both weakly-bound and strongly-bound water for montmorillonite and kaolin in this region.

4.2.1.2 Frequencies between 1150 and 400 cm^{-1}

In this region spectra are dominated by deformation and stretching vibrations associated with the underlying mineralogy of the tetrahedral/octahedral sheets. The strongest band is seen at around 1023 cm^{-1} for montmorillonite and 1003 cm^{-1} for kaolinite, and are attributed to Si-O stretching. Upon heating, this band increases in frequency slightly for kaolinite, but not for montmorillonite. In kaolinite a strong band attributed to the deformation vibration of structural OH is present at 912 cm^{-1}, which disappears upon heating to 800 ^{o}C.

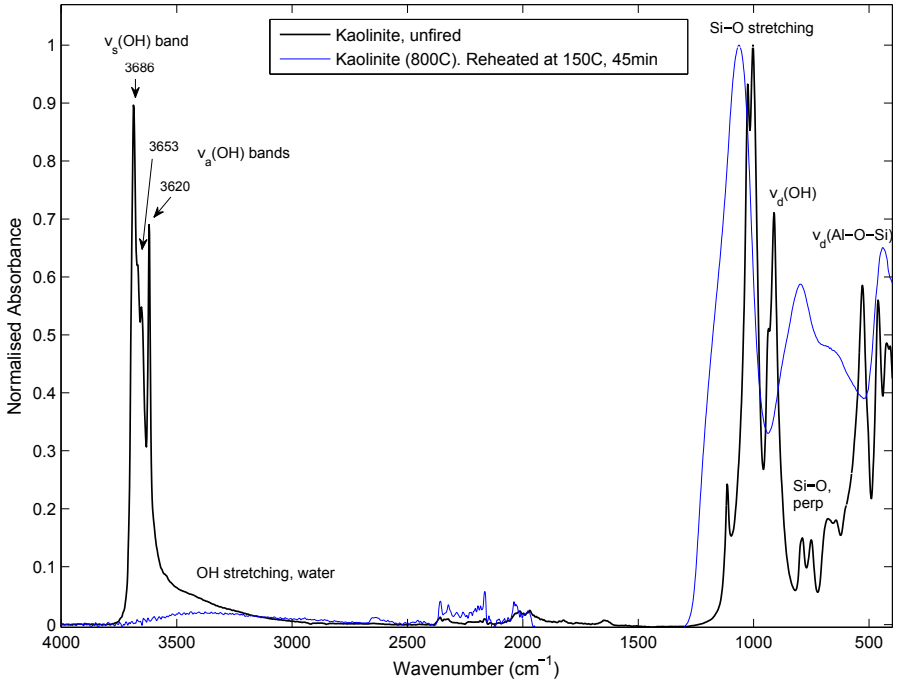

((A))

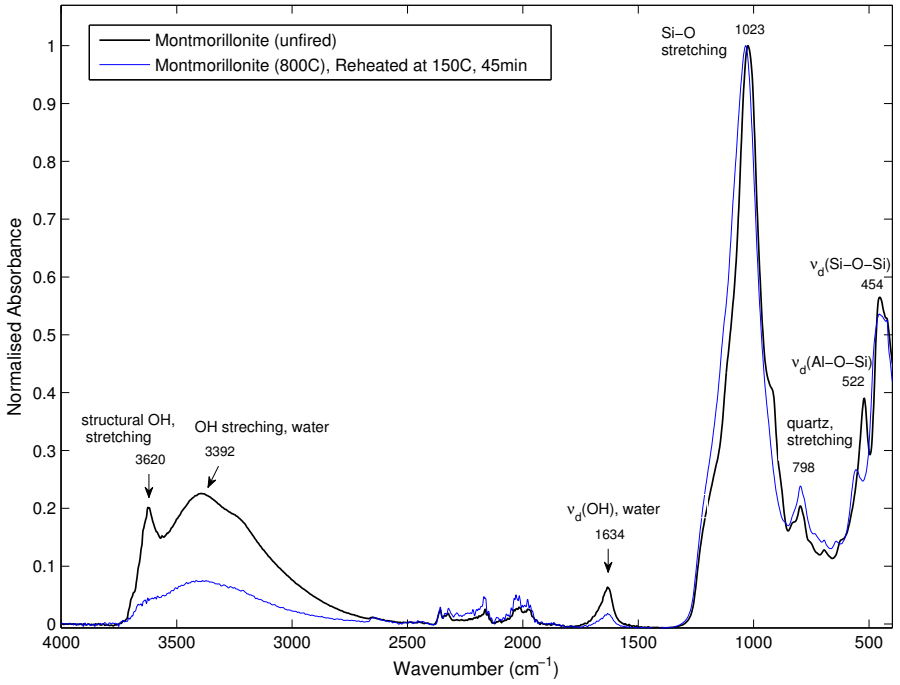

((B))

FIGURE 4.1: MIR spectra of kaolin (A) and montorillonite (B) standards used in this study. Blue curves show the spectra after firing at 800^{o}C for two hours, and subsequent incubation at 150^{o}C for 45 minutes, showing rehydroxylation in the 3750 to 3500 cm^{-1} frequency range.

TABLE 4.1: Mid infra-red absorption bands of unfired kaolinite and montmorillonite, compiled from Madejová and Komandel (2001), Serratosa (2013) and Farmer (1974).

Wavenumber (cm^{-1})	Assignment	Material
3689	inner-surface OH stretching (in-phase vibration)	Kaolinite
3669	inner-surface OH stretching (anti-phase vibration)	Kaolinite
3651	inner-surface OH stretching (anti-phase vibration)	Kaolinite
3626	structural OH stretching	Montmorillonite
3619	inner OH stretching	Kaolinite
3618	structural OH stretching	Montmorillonite
3457†	OH stretching, water	Kaolinite
3393	OH stretching, water	Montmorillonite
1629 - 1640†	OH deformation, water	Montmorillonite
1635†	OH deformation, water	Kaolinite
1115	Si-O stretching (longitudinal mode)	Kaolinite
1116	Si-O stretching (longitudinal mode)	Montmorillonite
1103	Si-O stretching	Montmorillonite
1102†	Si-O stretching (perpendicular mode)	Kaolinite
1027	Si-O stretching (in-plane)	Kaolinite
1005	Si-O stretching (in-plane)	Kaolinite
937	inner-surface OH deformation	Kaolinite
913	Al-Al-OH deformation	Montmorillonite
912	inner OH deformation	Kaolinite
885	Al-Al-OH deformation	Montmorillonite
885	Al-Fe-OH deformation	Montmorillonite
837	Al-Mg-OH deformation	Montmorillonite
788	Si-O	Kaolinite
798	Si-O stretching of silica	Kaolinite
751	Si-O, perpendicular	Kaolinite
684	Si-O	Montmorillonite
681	Si-O, perpendicular	Kaolinite
645	Si-O	Kaolinite
541	Al-O-Si deformation	Kaolinite
520†	Al-O-Si deformation	Montmorillonite
472†	Si-O-Si deformation	Kaolinite
466†	Si-O-Si deformation	Montmorillonite
432†	Si-O deformation	Kaolinite

† Measurement by KBr method. Unless otherwise stated, all other measurements are ATR.

4.3 Experimental

4.3.1 Materials

Clay standards were prepared from high purity kaolin (Fischer Scientific, 10010220) and montmorillonite K-10 (Acros Organics, via Fischer Scientific, 15250309), formed into pastes with the addition of milli-Q water (Millipore Corporation). Montmorillonite K-10 is a 2:1 phyllosilicate of the smectite group, commonly used as a catalyst in many industrial applications, prepared from source clay by calcination and reaction with a strong mineral acid. The kaolin and montmorillonite pastes were then formed into small ∼1 g pellets (see Figure 4.1). Internal calcite standard was obtained by crushing Iceland

spar, approximately 0.1 g of which was added to a sub-selection of clay pellets, and fired at 800^{o}C for 2 hours, cooling in air. IR spectra were then recorded. Following firing, a selection of acid pretreatments were preformed using 0.5M and 1M HCl at 70^{o}C (as recommended in Nümrich et al. (2015)) for 30, 60 and 90 minutes respectively. During the duration(s) of this treatment, control samples of pure and calcite-tempered fired clay standards were also kept at 70^{o}C for comparison. All samples were then dried at 102^{o}C under N_2, and IR spectra recorded again.

To simulate the effect of addition of lipids (as expected in cooking or storage), 15 μL of internal olive oil standard was pipetted onto a sub-selection of fired pellets, and IR spectra recorded. The olive oil was fairly easily adsorbed. Ultrasonication at 40^{o}C for three 15 minute intervals was then performed in a solution of chloroform/methanol (1:1), draining and rinsing each time. Samples were then dried under a stream of N_2 and IR spectra recorded again. In addition, another set of lipid-contaminated clays were then heated to 150^{o}C for 2 hours, and the same chloroform/methanol extraction procedure performed for comparison.

In addition to small pellets for IR measurements, several larger ($\sim$10 g) kaolinite and montmorillonite standards were also fired for rehydroxylation dating, with known amounts of lipid and calcite added. These samples were kept under known conditions of temperature (23.1 $\pm$ 0.2 ^{o}C) and relative humidity (31 $\pm$ 0.3 %) after firing. This was to measure the practical effect of RHX interferents on dates obtained by the rehydroxylation method, as recent dates (greater than a few weeks) of acceptable precision should be possible according to the simulations performed in Chapter 2.

4.3.2 ATR FT-IR specroscopy

Fourier transform infra-red spectroscopy was performed on a Cary 640 spectrometer (Agilent) equipped with a mid-IR ceramic source, an extended range KBr beamsplitter and DLaTGS detector (spectral range 9000-375 cm^{-1}). The spectrometer was coupled to an attenuated total reflectance (ATR) accessory (GladiATR single reflection diamond, PIKE technologies). After drying, fired clay pellets were lightly crushed with

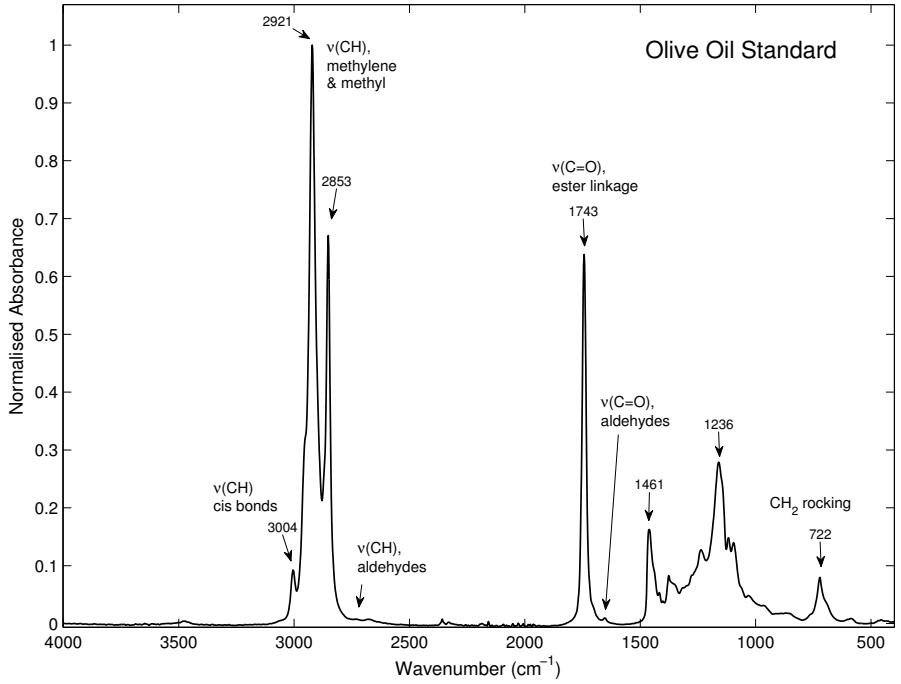

((A))

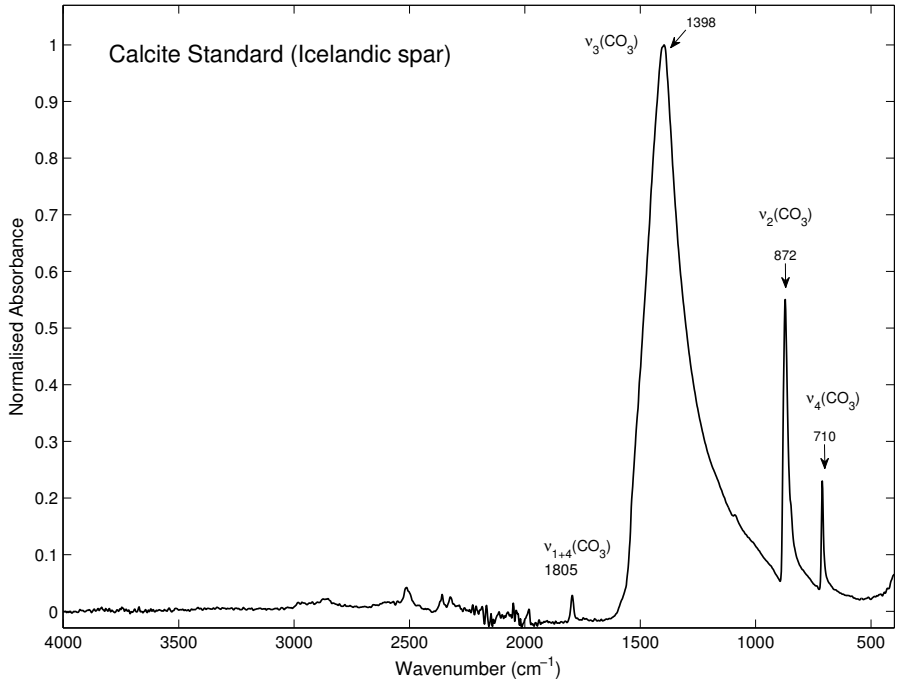

((B))

FIGURE 4.2: MIR spectra of olive oil (A) and calcite (B) standards used in this study. Assignment of lipid functional groups follows Dobson (2001), and calcite follows White (1974).

agate mortar and pestle. Three absorption spectra (64 scans each) at 4 cm^{-1} resolution were measured sequentially for 1 mg aliquots from each pellet immediately after

crushing, with backgrounds obtained between each spectrum. Spectra were baseline corrected using the Varian Resolutions Pro Software (Agilent) using two wavenumbers (4000 and 2550 cm^{-1}) for which no IR bands were present for any of the materials. Replicate spectra were then combined, and normalised to the highest peak (assigned to Si-O stretching in the case of all materials). Peak heights were fitted using a custom script written in MATLAB, which utilises code for the fitting of Lorenzians to spectral data written by Tom O'Haver, University of Maryland (available at https://terpconnect.umd.edu/~toh/spectrum/PeakFindingandMeasurement.htm, accessed April 2015).

4.3.2.1 Indices for alteration of structural OH and absorbed water

The following index is proposed as an indication of alteration structural OH. It is hypothesised that structural OH may either be gained thermally or by chemical alteration (or by both). For each chemical pretreatment, a control sample is therefore placed in milli-Q water at the same temperature, and dried under the same conditions as the pretreated sample. In order to determine if a particular chemical treatment has an effect on structural OH *other* than that which is expected to occur by thermo-rehydroxylation, the height of the peak assigned to the inner-OH stretching mode (A_s) is subtracted from the height of the corresponding peak for the control sample (A_c). The ratio is then expressed as a percentage of the peak height for the control sample (A_c). This quantity is called $A_{OH,T2}$:

$$A_{OH,T2} = 100 \times (A_s - A_c)/A_c. \tag{4.1}$$

Another similar index, called $A_{OH,T1}$ is used to describe the effect of pretreatment on T1 water, and is calculated off the height of the diffuse band for the OH-stretching vibration of absorbed water at 3400 cm^{-1}.

4.3.2.2 Index for removal of calcite

Two indices are considered as a semi-quantitative measure of the amount of calcite removed by pretreatment. Here two peak heights are considered, corresponding to the OH stretching band at 3640 cm^{-1} associated with the formation of $Ca(OH)_2$ upon reheating, and the broad region between 1400 and 1500 cm^{-1} associated with the chemisorption of CO_2 on $Ca(OH)_2$ and the ν_3 stretching mode associated with the CO_3^{2-} ion. These are called R_{Ca1} and R_{Ca2} respectively. The two indices are calculated by subtracting the peak height ratio of the untreated control sample from the treated sample ratio, and expressed as a percentage.

4.3.2.3 Index for removal of lipid

Similarly, three indices are constructed for lipids as semi-quantitative measures of the amount of lipid removed by chloroform/methanol extraction. These indices are based on the three strongest peaks in the spectrum of olive oil adsorbed onto clay minerals standards: the 2921 and 2853 cm^{-1} bands corresponding to ν(CH) vibrations of methylene and methyl groups, and 1737 cm^{-1} peak corresponding to ν(C=O). These indices are labelled R_{l1}, R_{l2} and R_{l3} respectively.

4.3.3 A note on physical preparation of samples

Since structural OH is the species of interest in rehydroxylation dating, it follows that any pretreatment strategy should avoid removing or introducing OH into the ceramic structure. Pretreatment includes any mechanical/physical alteration of the sample (including cutting or grinding or powdering), which is necessary for samples which are too large to measure. The question arises as to the affect of mechanical processing on structural OH. Dellisanti and Valdré (2008) studied the thermal behaviour and structural alteration of unfired kaolinite, talc and montmorillonite powders by mechanical treatment by planetary ball mill in vacuum at 25^{o}C. They find that dehydroxylation temperature decreases linearly with milling time of the order of several hours, which is combined with a progressive decrease in mass loss at temperature between 400-800^{o}C

for kaolinite, 500-750^{o}C for montmorillonite and 800-1250^{o}C for talc. This is consistent with loss of structural OH. XRD analysis show an increase and broadening of the $FWHM_{001}$ with milling time, indicating some loss of layer stacking. These authors suggest that changes occur primarily in the octahedral sheet during the early stages of milling, whereas the deformation of tetrahedral sheets only takes place at much longer times. Frost and Kristof (2004) also found evidence for structural changes in kaolinite upon grinding, beginning with the breaking of hydrogen bonds between adjacent layers. Dry grinding (i.e. thermal-mechanical alteration) resulted in the decrease of position and intensity of the 3668 and 3652 bands (corresponding to stretching of inner-surface OH), which were completely absent from spectra in one hour. The position of the single inner-OH vibration band at 3619 was not affected, but intensity also reduced with progressive grinding. Conversely, the OH-stretching bands of water showed progressive increase upon grinding.

These studies apply to unfired clay minerals. However, very little study has been made of the mineralogical effect of mechanical grinding on the structural OH in fired clays. Similar effects are to be expected in these materials, but it may be that they take longer, given the increased bond strengths caused by firing. In light of the above, solid archaeological samples instead of powdered samples should be used as a matter of course to avoid alteration of structural OH. For samples where reduction of overall mass is necessary given experimental constraints, thermal-mechanical alteration of fired clays is currently minimised by cutting using a water cooled geological saw, and thorough but gentle wet-sanding of the cut edges performed using conventional silica sandpaper and milli-Q water. This methodology has been successfully used for archaeomagnetic analysis for several decades to avoid the alteration of magnetic mineralogy, which also serves as an indication of alteration of the ceramic matrix. However, the extent of thermo-mechanical alteration of fired clays in the context of rehydroxylation dating is still an open question which deserves more research.

Analysing solid archaeological samples using FTIR is almost impossible; samples are required to have very good contact with the crystal surface when using ATR absorbance

methods, and are too strongly absorbing without the addition of KBr using transmission methods. Both methods necessitate powdering of solid samples. With regard to the present experiments, preliminary comparison of ATR-FTIR spectra between carefully-formed *solid* samples of clay standards (the wet paste formed directly over the ATR diamond before firing to ensure good contact with the crystal in subsequent measurement) and those gently crushed by mortar and pestle showed no significant differences in the lattice OH stretching and water OH stretching regions. The spectra display high reproducibility. Therefore, we can be confident that ATR is an appropriate technique for this study, as long as prolonged grinding is not used to prepare samples.

4.4 Pretreatment strategies assessed by infrared spectroscopy

4.4.1 Removal of calcite

4.4.1.1 Efficiency

IR spectra of calcite-added kaolin show rapid and visible features associated with the formation of calcium hydroxide via lime upon heating to 800 ^{o}C. First, a well-defined peak at 3640 cm^{-1} associated with the hydroxyl stretching vibration, and second, a broader split absorption band between 1400 and 1550 cm^{-1} which is primarily assigned to the ν_3 stretching mode of CO_3^{2-} (see Figure 4.3). Calcination results in a broadening of the latter peak, an effect which has been linked with the chemisorption of CO_2 in the form of monodentate carbonate ions (Kalinkin et al., 2005). In all samples, treatment with 0.5M HCl at 70^{o}C for 30 minutes, following the recommendation of Nümrich et al. (2015), removed any presence of the 3640 cm^{-1} peak, as well as the split absorption band between 1400 and 1550 cm^{-1}. Treatment with 1M HCl had a similar effect.

With regard to calcite-added montmorillonite, it is interesting to note that there is no evidence of either the 3640 cm^{-1} peak or the 1400 to 1550 cm^{-1} band appearing upon firing to 800^{o}C. It is possible that this is due to the high specific surface area of montmorillonite (and the larger interlayer spacing), which may effect the partial pressure of CO_2 within the ceramic upon firing. Another explanation is that the calcite

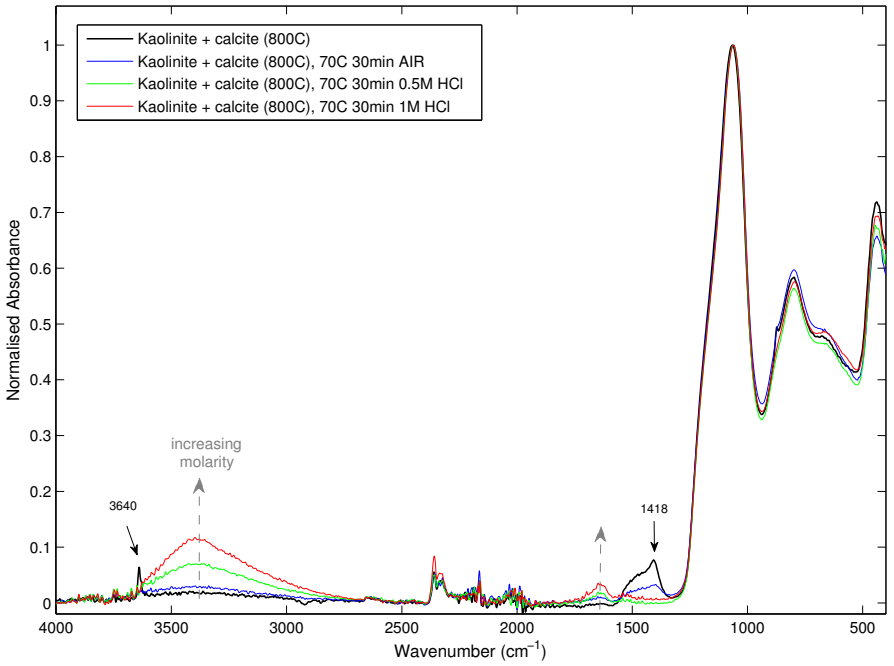

((A))

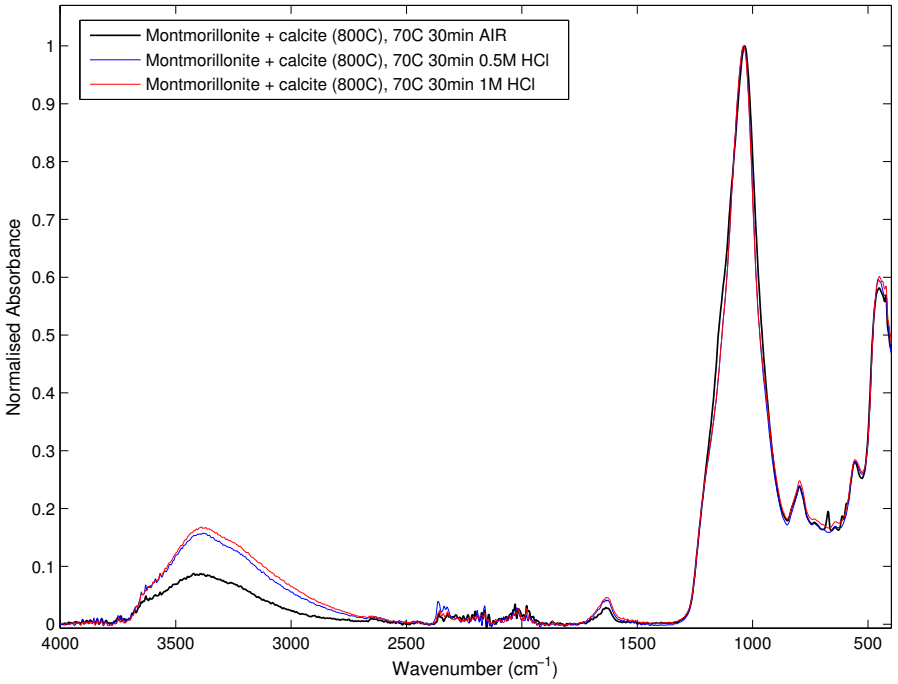

((B))

FIGURE 4.3: The effect of pretreatment with HCl of different concentrations on the IR spectra fired clay standards, performed at the same temperature and duration. (a) Calcite-tempered kaolin. (b) Calcite-tempered montmorillonite.

dissociated and formed stable complexes with the montmorillonite structure. A faint peak present in this spectrum at 710 cm^{-1} may be assigned to the ν_4 mode of CO_3^{2-}.

This peak disappears completely upon treatment with HCl.

4.4.1.2 Evidence for alteration of OH groups

The most notable effect visible in Figure 4.3a/b is the increase in the broad absorption peak at ~3400 cm^{-1} associated with the OH stretching vibrations of adsorbed water. This peak increases in both kaolin and montmorillonite standards with the molarity of the acid, but not necessarily with the duration of treatment. The concomitant increase in the band attributed to the deformation vibration of OH of adsorbed water at 1640 cm^{-1} also points to strong changes in adsorbed water with molarity. These changes are greater than those expected from simple thermal rehydroxylation. Since this water is not lost upon prolonged heating to 105 ^{o}C, but is removed at heating to higher temperatures, it will contribute to significant mass loss in the rehydroxylation procedure ('chemisorbed' water is considered negligible in the method of Wilson et al. (2012)). A strong acid therefore should be avoided.

With regard to the 3620 cm^{-1} band presumed to be diagnostic of the structural OH groups of ultimate interest (Clegg et al., 2012), it is clear from Figure 4.3 that there is at least *some* small additional rehydroxylation which may be attributed to treatment by strong mineral acid, at least in montmorillonite. Further tests are needed to assess the statistical significance of this effect. Temperature, too, may be an important effect. 70 ^{o}C, as recommend by Nümrich et al. (2015) may be too high.

4.4.1.3 Mechanisms for acid attack on fired clays

There is considerable information available on the mechanism of acid attack on clay minerals, but very little on fired clays. In general, strong acid treatment of unfired clay minerals is associated with the liberation of aluminium and/or silicon from the mineral layers, with great dependency on pH and duration of treatment. Ostrom (1961) found that 0.3M HCl or 0.1M acetic acid produced no discernible effects on the X-ray diffraction data, as opposed to 0.33M acetic acid and 0.5M HCl, which produced a slight effect. Pask and Davies (1945) studied the solubility of powdered kaolinite upon boiling

in 20% H_2SO_4 before and after firing to 800^{o}C. They found that pre-firing the material to these temperatures in fact increased the solubility of aluminium relative to unfired kaolinite. They found that solubility then decreases at higher temperatures (>950^{o}C), associated with the formation of high-temperature phases such as mullite.

4.4.2 Removal of lipids

4.4.2.1 Efficiency

The spectra of lipids added to clay standards are shown in Figure 4.4. The 2921 and 2853 cm^{-1} bands corresponding to ν(CH) vibrations of methylene and methyl groups, and 1737 cm^{-1} peak corresponding to ν(C=O) are clearly defined, along with the hydroxyl stretching region and other features associated with the underlying clay mineralogy. Ultrasonication in chloroform/methanol for 45 minutes causes partial reduction in the absorbance bands associated with the lipid functional groups. The removal indices R_{l1} for kaolinite and montmorillonite (as shown in Table 4.2) are -71% and -87% respectively for unheated samples. This index is generally in good agreement with the index R_{l2} (-72% and -89%).

When samples are heated to 150 ^{o}C for 2 hours, the peak heights of the 2921, 2853 and 1737 cm^{-1} bands show a clear reduction. When the chloroform/methanol treatment is performed on these heated samples, a significant reduction in the efficiency of lipid removal is observed. The effect is most pronounced for montmorillonite (R_{l1} and R_{l2} of -13% and -11%, indicating very little of the degraded lipid is removed). The difficulty of removal suggests the formation of relatively stable clay-organic complexes, which are not removed by heating at low temperatures (i.e. 105^{o}C) but are probably lost at higher temperatures. This is another significant challenge to rehydroxylation pretreatment. Longer ultrasonication (of the order of several hours) is likely to be necessary for archaeological ceramics with significant residues. Alternatively, the use of strong wet oxidation with H_2O_2, NaOCl or NaBrO may improve the extraction efficiency.

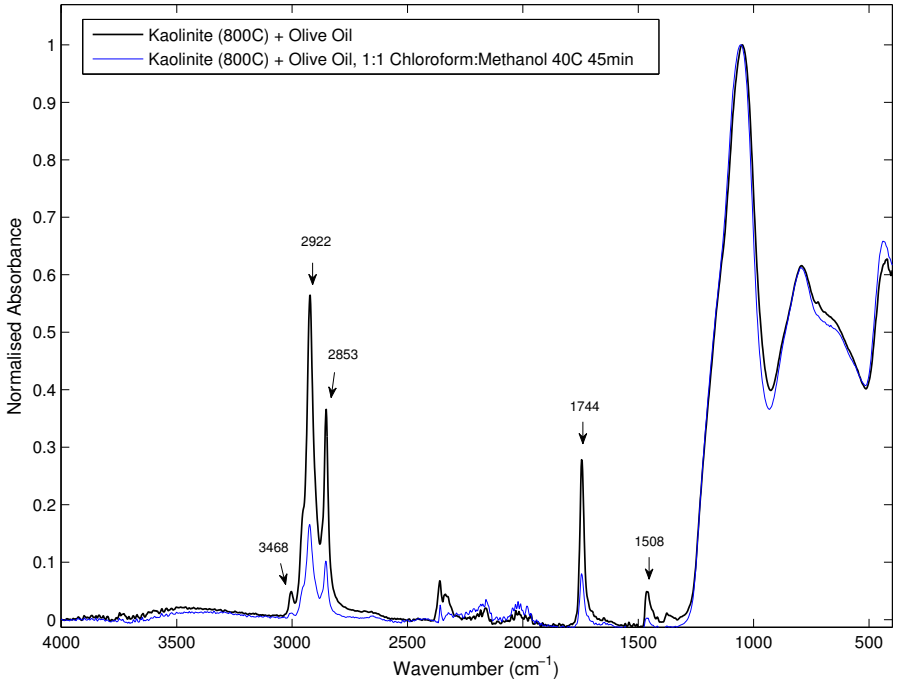

((A))

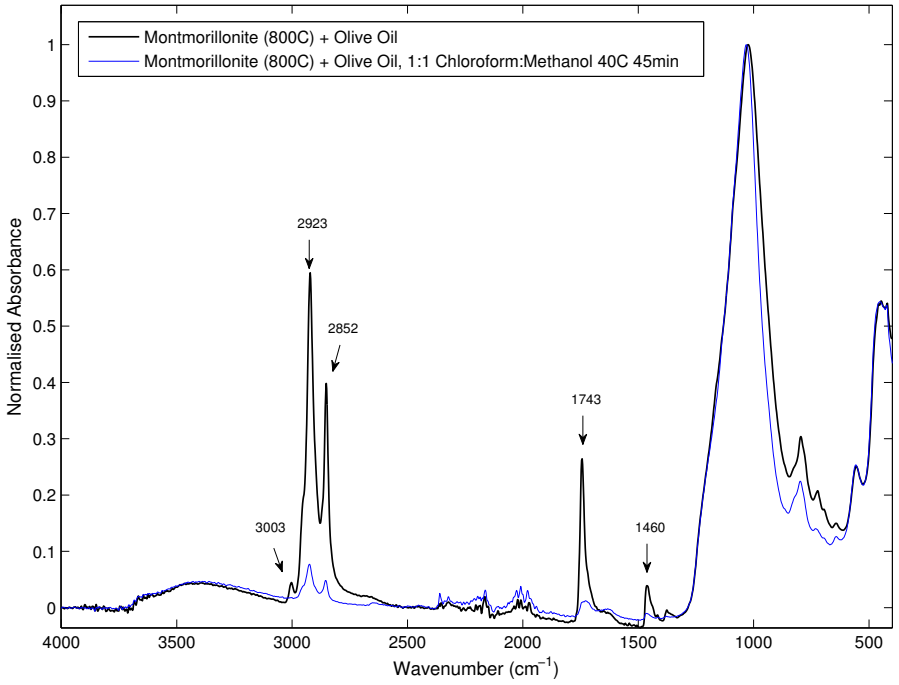

((B))

FIGURE 4.4: The effect of ultrasonication in chloroform/methanol for 45 minutes at 40^{o}C on the removal of lipid from kaolin and montmorillonite standards (unheated after addition of olive oil). (a) Kaolin. (b) Montmorillonite.

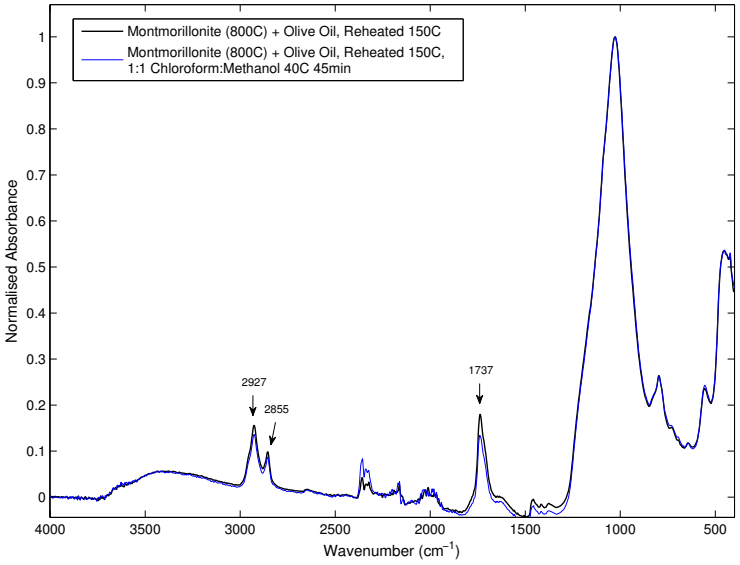

FIGURE 4.5: IR spectra of olive oil adsorbed onto montmorillonite and heated to 150^{o}C, before and after ultrasonication in Chloroform/Methanol.

4.4.2.2 Evidence for alteration of OH

From the IR spectra, there is no clear evidence for any significant differences in the absorbances of peaks attributed to structural OH (3640 cm^{-1}) or absorbed water OH (∼3400 cm^{-1}) between chloroform/methanol-treated standards and their control counterparts. Furthermore, no peaks indicating either chloroform or methanol residues in the fired-clay matrix are present. This particular treatment therefore seems to be suitable for a pretreatment methodology. Longer treatment times may be more effective at removing lipid to well below 1%. Of course, the error associated with peak fitting ATR-FTIR spectra is likely to be no better than 1%, and to discern any subtler effects it may be necessary to measure the amount of burn off more precisely, either by mass spectrometry or by gravimetric analysis. However, this analysis shows that IR spectroscopic methods are a powerful tool for initial optimisation and quality control.

4.4.3 Possible use of supercritical CO_2 for pretreatment of archaeological ceramics

Supercritical fluid extraction is a potentially minimally-invasive pretreatment technique for removal of organics from ceramics. Supercritical fluids (SFs) are gases or liquids

TABLE 4.2: Indices for extraction efficiency and alteration for extraction of olive oil from a selection of fired-clay standards by ultrasonication in Chloroform/Methanol (1:1) for 45 minutes at 40^{o}C, assessed by infra-red spectroscopy.

Material	R_{l1} (%)	R_{l2} (%)	$A_{OH,T1}$
Kaolin	-71 ± 1	-72 ± 1	-3 ± 1
Kaolin†	-44 ± 1	-46 ± 1	1 ± 2
Montmorillonite	-87 ± 2	-89 ± 9	-6 ± 2
Montmorillonite†	-13 ± 1	-11 ± 2	-2 ± 1

† Heated, together with olive oil, at 150^{o}C for 2 hours.

which are brought above their critical temperatures and pressures. The properties of SFs make them good at penetrating a porous matrix. When SFs are combined with an appropriately-chosen co-solvent, molecules of interest can be targeted for extraction. CO_2 is a common SF used for extraction purposes, because it forms a SF at relatively convenient temperatures (> 31 ^{o}C), and at pressures above 7.4 MPa.

Previous work by Van Ham-Meert (2015) showed order of magnitude improvement in extraction efficiencies by SFE when compared with conventional solvent extraction (chloroform/methanol). One disadvantage of conventional solvent extraction is that they usually require a sample to be powdered. SFE therefore has potential when used as a pretreatment method for removing organics from samples for rehydroxylation dating, since it should offer significantly higher extraction efficiency, without the need for sample destruction.

The purpose of this brief test was to determine if SFE is suitable to remove organic contaminants, specifically lipids, whilst avoiding extra dehydroxylation or rehydroxylation of the clay mineral portion of the ceramic matrix. As in previous experiments, the peak heights of structural OH and T1 water are monitored by ATR-FTIR, and the indices $A_{OH,T1}$ and $A_{OH,T2}$ are reported.

4.4.3.1 Materials

The materials here comprise four samples of neolithic pottery from three sites in the Baikal region, Russia. All samples have different ages. Sample UST2 comes from the site of Ust' Karenga, dated at 12 ka B.P.. Another two samples, PL2 and PL4 come from the site of Popovkii, dated at $\sim$ 6 ka BP and $\sim$ 4 ka BP respectively. Another sherd

comes from the site of Shamanka II, which is not properly dated. Van Ham-Meert (2015) obtained large quantities of lipids (between 0.8 and 7.5 mg per 100 mg) in all these sherds by SFE. Analysis by GC-MS showed a range of unsaturated fatty acids (both even and odd), and a limited number of mono-unsaturated fatty acids. Cholesterol was found in all sherds, which is an indication the pottery was used for cooking and/or storage of animal products. The presence of unsaturated fatty acids also indicate plant oils.

4.4.3.2 Methods

The SFE extraction was previously performed by Van Ham-Meert (2015), and further details may be found in that work. Briefly, SFE was performed on all samples using a modified supercritical fluid chromatography instrument (SP-2086, Jasco). 16 % by volume EtOH:H_2O (95:5) was used as co-solvent with supercritical CO_2 at 50 ^{o}C and 30 MPa for 3 hours. Samples were then allowed to dry for several weeks under laboratory conditions. Triplicate ATR-FTIR spectra were obtained on lightly crushed aliquots of (a) SFE treated pottery, and (b) pottery left untreated by SFE. FTIR spectra were baseline corrected and processed as in the previous sections.

4.4.3.3 Evidence for alteration of OH

The spectra of one sample is shown in Fig. 4.6, before and after SFE treatment. There are very small changes visible in the region between 2500 and 3500 cm^{-1}, which are sometimes evident in other samples. The effect is not consistent. Unfortunately, the broad shoulder in this region does not allow for peak fitting for the lipid indices R_{l1} and R_{l2}. However, for all samples it is still possible to obtain the values of $A_{OH,T1}$, which are presented in Table 4.3. The results are slightly inconsistent. For three samples (PL4, SHAMII and UST2), there is a reduction in height of the broad $\sim$ 3370 cm^{-1} peak, which are differences of between 0.5 and 6 %. For one sample, PL2, the peak hight increases by 12 %. For the first three samples, there may be several reasons for the reduction in the height of this peak, including (a) loss of OH groups associated with lipids, and (b) variability of T1 water within the sample, which is not fully averaged by triplicate measurements. More measurements would be necessary to rule out (b). As a

general feature, the shoulder from 3300 to 2500 cm^{-1} becomes smoother in all samples treated by SFE, which would suggest the loss of OH is partially associated with loss of lipids.

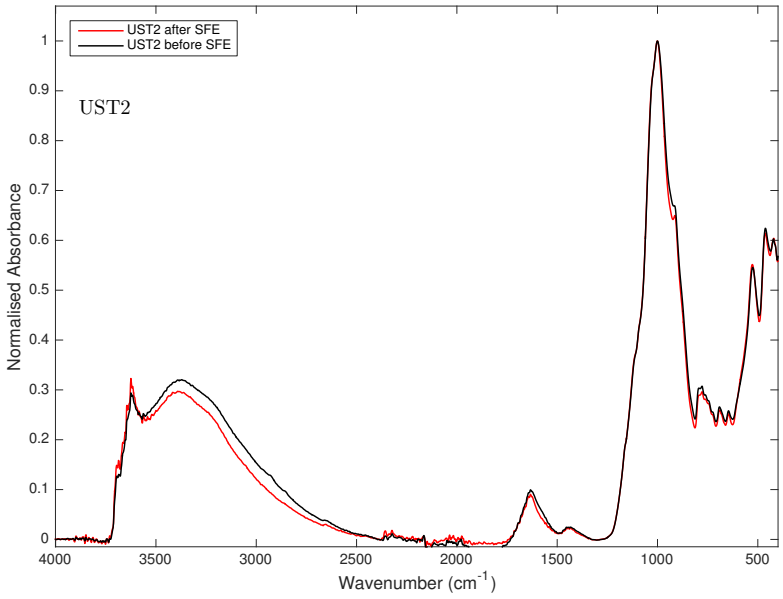

FIGURE 4.6: ATR-FTIR spectra of ceramic sample UST2, before and after supercritical fluid extraction (SFE).

The spectra for UST2, shown in Fig. 4.6, is the only sample for which a clear ~ 3620 cm^{-1} structural OH peak can be discerned. Interestingly, it is also the oldest sample. For the other three samples this peak is only visible as a shoulder. Because UST2 has a clear peak, it is possible to assess whether structural OH is gained/removed by SFE. A value of $A_{OH,T2} = 3.20 \pm 0.06$ % is obtained for this sample, which suggests some rehydroxylation occurred during SFE. This may be due to the higher temperatures of SFE extraction (50 ^oC, 3 hrs), which accelerate the mass gain via the Arrhenius nature of the rate constant α. It may also be due to variability between different parts of the sherd, which are not properly averaged by the triplicate measurements. More experiments are need to investigate this effect further.

TABLE 4.3: Indices for samples of neolithic pottery from the Baikal region, Russia, treated by supercritical fluid extraction.

Material	$A_{OH,T1}$ (%)	$A_{OH,T2}$ (%)
PL2	12 ± 5	-
PL4	-0.5 ± 0.2	-
SHAMII	-5 ± 2	-
UST2	-6 ± 3	3.20 ± 0.06

Note that a 3.2 % difference in m_a will lead to an error in rehydroxylation age determination of the order of several hundred years for the oldest ceramic samples. However, given the high extraction efficiency, it may still be valid to apply to samples which have very high quantities of lipids, since the effect of lipid burn off may be greater. Alternatively, the FTIR quantification may be used to correct RHX age determinations for the effects of SFE. Further experiments will be performed in Chapter 6 to investigate the effect of SFE on RHX determinations performed on modern samples of terracotta. The benefit of this material is it can be homogenised before firing, and similar amounts of lipid can be added to subsamples of the material. Potentially, SFE provides a more efficient alternative to other forms of organic pretreatment, if the effect on structural OH is minimal. Both of the methodological modifications on terracotta should provide a better test of the the extent to which SFE causes re- or de-hydroxylation.

Chapter 5

Factors affecting non-stabilisation of equilibrium sample mass (m_2)

This chapter investigates the causes of spurious m_2 mass gain in rehydroxylation dating. This behaviour is described as a failure to achieve constant stabilised mass at the m_2 estimation step after several weeks of measurement at constant temperature and relative humidity. In previous investigations (Hare, 2012), about 10 out of 16 samples of historical brick failed to achieve constant mass after one month of measurement following heating to 105^{o}C. These 10 samples exhibited marked mass gain (of the order of 10^{-5} g h^{-1} for ~60 g samples) after four weeks. The 'non-equilibration' effect is somewhat unexpected, since 105^{o}C is generally thought to remove only weakly-bound T0 water, which should be relatively rapidly regained upon removal from the oven. The time taken for measurements of m_2 is currently one of the biggest obstacles to increasing the throughput and reliability of RHX dating. Measurement times in excess of 3-4 weeks for accurate m_2 measurement clearly make the technique impractical, and understanding the cause of this behaviour is therefore necessary to improve RHX dating.

This effect has been described by Le Goff and Gallet (2014a) for samples of pottery from Syria and Gallet and Le Goff (2015) for samples of Samian from Lezoux in France. Cultrone et al. (2004) conducted moisture sorption experiments after heating samples of both calcareous and non-calcareous clay bricks. They found that calcareous bricks lost

'free' (T0) water slower than the non-calcareous clay bricks, and that uptake was also slower, in some cases. They attributed this to the transformation of calcite into CaO (or CaO +MgO), creating a highly porous system with small pores. Additionally, Le Goff and Gallet (2014a) point out that non-stabilisation of m_2 seems to be present for some samples of Werra earthenware from Enkhuizen, Netherlands, originally dated by Wilson et al. (2012). However, there is currently no good explanation for the behaviour, and apart from Gallet and Le Goff (2015) and related papers, there has been no systematic investigation of the factors which may influence non-stabilisation of a wide range of materials.

5.1 Preliminaries

There are three main explanations for non-stabilisation of m_2 after heating to 105 ^{o}C, including;

- Physical effects. Here, uptake of T0 water which is removed at 105 ^{o}C might be slower for materials of different dimension or porosity.
- Thermal effects. In this scenario, acceleration of the underlying rehydroxylation reaction during reheating and subsequent slow cooling of the ceramic leads to long-term mass gain which persists for several weeks.
- Chemical effects, including the long-term chemisorption of T1 water within clay minerals, as well as due to those species responsible for mineral hydration.

With regard to physical effects, both Gallet and Le Goff (2015) and Bowen et al. (2013) point out that sorption of T0 water should be best described by a Lagergren kinetic rate equation of the form:

$$m(t) = m_{\text{eq}}\left(1 - e^{-t/\tau}\right) , \tag{5.1}$$

where m_{eq} is the final mass under isothermal (equilibrium) conditions. This function explicitly introduces the saturation of T0 water, and so cannot account for the non-stabilisation behaviour. Bowen et al. (2013) fitted mass gain data to the above expression, which allowed them to calculate the time to 99% mass gain (pseudo-stabilisation) as

$t_{99} = -\tau ln(10^{-2})$, which ranged between 5 and 16 hours for a range of pottery samples between 0.9 and 1.7 g.[1] However, these authors mention little about non-stabilisation. An alternative expression may be based on a first principles derivation for molecular diffusion from Fick's second law

$$\frac{\partial C}{\partial t} = D\frac{\partial^2 C}{\partial^2 x} \tag{5.2}$$

In a thin sheet of thickness L, and assuming constant diffusivity D, Eq. 5.2 can be solved in the form of an infinite series (Crank, 1956)

$$\frac{m(t)}{m_{\text{eq}}} = 1 - \frac{8}{\pi^2}\sum_{n=0}^{\infty}\frac{1}{(2n+1)^2}exp\big[-(2n+1)^2\frac{\pi^2 Dt}{L^2}\big] \ , \tag{5.3}$$

which is also asymptotic in the long time limit, where m_{eq} is the mass at saturation. This may be rearranged to yield an approximation for t_{99} which is

$$t_{99} = 0.445\frac{L^2}{D} \ . \tag{5.4}$$

This implies some dependence on sample thickness, which has not yet been experimentally confirmed. In some sense this is complicated to assess, because it requires measurements on a set of samples of homogenous composition, and archaeological samples are unlikely to be homogenous. On the other hand, if T0 uptake is a subdiffusive process, then uptake will be slower and less dependent on sample thickness. Savage et al. (2008) studied mass gain and expansion in a freshly fired clay brick, and suggested that the first phase after firing (when T0 sorption is presumed to be the rate-limiting step) indicated a separate $t^{1/4}$ process, although in principle the power does not need to be 1/4.

With regard to thermal effects, a sample heated to 105^{o}C will take a certain time to cool. During this time, temperatures are higher, which accelerates the rehydroxylation reaction. The time taken to cool will depend on several complex factors, including dimensions, porosity, density, heat capacity (and therefore ultimately depends on the composition of the object). With regard to simulation of these effects, cooling may be

[1] Here t_{99} is the terminology of Bowen et al. (2013), and is used here for consistency.

approximated by Newton's Law:

$$T(t) = (T_\mathrm{i} - T_\mathrm{f})e^{-t/\Lambda} + T_\mathrm{f} \tag{5.5}$$

Which relates the temperature at time t to T_i and T_f, the initial and final temperatures of the object. Λ is a time constant which depends on density, ρ, specific heat capacity c, and some heat-transfer coefficient H. These are seldom measured for fired-clay ceramics, but with appropriate calculation or approximation of these variables it may be possible to model the cooling behaviour of specimens. This temperature curve can then be used to model rehydroxylation mass gain via numerical integration of the differential equation $4y^3dy = \alpha(T)^4dt$ (derived from Eq. 1.4), with knowledge of the activation energy. In this 'thermal' scenario, the non-stabilisation of mass gain after heating to 105 ^{o}C may show some dependence on sample porosity, density or specific heat capacity. No measurements have yet been conducted to determine these quantities, although Barrett (2013) considered the effect of cooling from 500 ^{o}C for measurement of α_m and m_4. He suggested a practical approach of obtaining accurate fits to non-linear stage II mass gain by including a *time-offset*, t_0 in the rehydroxylation mass gain relation of Wilson et al. (2012):

$$m(t) = \alpha(T)(t + t_0)^{1/4} + m_4. \tag{5.6}$$

With regard to chemisorption of T1 water, Gallet and Le Goff (2015) suggest on the basis of strain dilatometry experiments that this may be attributed to long-term recovery of T1 ('chemisorbed') water content, which they say may be lost by heating to temperatures as low as 105 ^{o}C. Their claim is strengthened by the observation that there seems to be a systematic increase in the gradient of (logarithmic) mass gain with a increasing reheating temperature from 60 ^{o}C to about 450 ^{o}C, whereupon the gradient is relatively constant for higher temperature reheatings.[2] This is the range of temperatures over which T1 water may be lost upon initial firing, and non-stabilisation of m_2 may therefore be due to a long-lived uptake of T1 water upon subsequent reheating. If this is the case, then

[2]below temperatures higher than the original firing temperature, which will cause further structural changes.

chemisorption is expected to be greater within certain clay minerals which potentially have greater amounts of T1 water, such as smectites.

Another possible cause of chemisorption of T1 water is the long-term hydration of thermally-altered minerals which may form the non-clay mineral component of the ceramic matrix. The fragments of Samian in Gallet and Le Goff (2015) show compositions dominated by anorthite, albite, quartz, and hematite, but in their study no clear mineralogical changes were detected in X-ray diffraction spectra in response to laboratory heating at various temperatures, which suggests, together with the strain dilatometry experiments, that hydration of T1 water is more likely to occur in the clay minerals themselves.

Apart from the study of Gallet and Le Goff (2015), no authors have yet attempted to make any explicit links between mineralogical variation and observed non-stabilisation of m_2. In this chapter, gravimetric evidence for m_2 mass gain of a variety of archaeological and pure fired clays will be compared with FTIR spectra, energy-dispersive X-ray spectroscopy (EDS), SEM, and various measurements of porosity and specific heat capacity. Simulations will also be performed to help assess which factors (physical/thermal/chemical) are responsible for non-stabilisation behaviour.

5.2 Materials & Methods

5.2.1 Archaeological and clay mineral selection

Samples of clay minerals include montmorillonite K-10 and kaolinite (Fisher Scientific, U.K.), with negligible Ca and organic content, which were formed into 10g samples with the addition of milli-Q water. In addition, powdered calcite from a sample of crystallised Icelandic calcium carbonate obtained from the Natural History Museum, University of Oxford, was added to another sample of montmorillonite. The mass of carbonate added to this sample was 0.6324 $\pm$ 0.0002 g, comprising roughly 10 % of the clay mass. These clay samples were fired in a muffle furnace (RHF1500, Carbolite) at 825 ^{o}C on 31 January 2015. The heating rate was as follows: 5 ^{o}C/min until 493 ^{o}C,

whereafter the rate was 3 ^{o}C/min until 825 ^{o}C, which was held constant for 7 hours. 825 ^{o}C was chosen for two reasons: first, it is high enough for dehydroxylation, but not too high as to cause the formation of significant high-temperature phases such as mullite and spinel. Second, it is sometimes regarded as the temperature at which significant decarbonation of carbonate occurs. Samples were removed from the oven at 550 ^{o}C and thereafter placed in a sealed incubator (S.I.60, Stuart Scientific, U.K.). Internal temperature and RH were recorded by a data logger (OM-43, Omega Engineering, Inc.) with accuracies given by the manufacturer as 0.4 ^{o}C and 0.4 % for relative humidity.

As a test of possible thickness effects on early stage mass gain, three samples of homogenised unfired terracotta clay[3] were formed into disks of varying thicknesses (4.2 $\pm$ 0.2 mm, 6.4 $\pm$ 0.2 mm and 9.2 $\pm$ 0.2), but similar nominal masses ($\sim$ 3.8 $\pm$ 0.1 g). Additionally, a replicate sample of the first disk with the same dimensions (4.2 $\pm$ 0.2 mm, $\sim$ 3.8 g) was prepared. All terracotta was fired on 26 January 2016 for 7 hours at 800 ^{o}C. Samples were removed at 550 ^{o}C and placed in the apparatus for microgravimetric measurements (see section below). However, whereas the first three samples of terracotta were allowed to cool to chamber temperature relatively slowly, the replicate sample was rapidly quenched in milli-Q water, kept as close as possible to the chamber temperature (17.5 ^{o}C), and then dried under a stream of N_2 for 5 minutes. This was to test whether a rapid cooling has an effect on the early stage rate gain.

Additionally, the materials analysed here included seven historical bricks and one tile ($\sim$ 50 g each), for which gravimetric measurements were previously conducted after heating to 105 ^{o}C for 2 hours (Hare, 2012). Mass gain curves for these samples were obtained in 2012 by measurement with an analytical laboratory balance (GR-200, A&D Corporation, Japan), 0.1 mg repeatability, which was kept in the sealed incubator at 22.6 $\pm$ 0.1 ^{o}C, and relative humidity of 58.6 $\pm$ 0.1 %, maintained by saturated solution of sodium bromide positioned in the chamber under airflow maintained by the incubator fan. In addition, three samples of archaeological pottery (MAN037, MAN037/2 and MAN038) from two different samples of Werra ware were also provided by Dr Moira Wilson, and were subsamples of the same materials dated in Wilson et al. (2012) (but

[3]Fresh terracotta clay was kindly provided by Dr Moira Wilson.

not previously dehydroxylated). These materials were first wet-cut using a diamond-tipped circular saw, and were then cleaned of paint and surface residues whilst wet using a scalpel. The surface of each sample was then wet-sanded by hand using a fresh piece of silicon carbide sandpaper and milli-Q water, and allowed to dry. Mass gain of these samples was observed after subsequent drying with N_2 gas, as well as after heating to 105^{o}C for 3 hours in a specially-built apparatus (see below).

5.2.2 Apparatus for microgravimetric measurements

The author designed an apparatus for the automatic measurement of several samples of fired clay under conditions of constant temperature and R.H. The full details of this novel design are perhaps beyond the scope of this work, and the construction of this apparatus will be related at another time. However, it will suffice to give a general description. The apparatus consists of a microbalance with 22 g capacity and 0.001 mg readability (WXSS26 high precision weigh module, Mettler Toledo Inc.) inside a custom environmental chamber which was machined from solid aluminium. Gas streams enter the chamber base (which is 40 x 370 x 240 mm) through specially-designed channels which circulate the gas gently around the chamber (without disturbing the balance). The base sits on 8 Peltier ('TEC') modules (490-1288, RS components) rated at 19.2 W (8 A, 3.8 V). The Peltiers are wired in series, and controlled by a pulse-width modulation (PWM) programmable controller (PR-59, Laird Technologies, Plc.) in proportional-integral-derivative (PID) mode, and capable of supplying a peak DC voltage of 30 V (15 A). This is slightly below the maximum rating of the 8 Peltier elements. PID settings were tuned manually by trial-and-error approach (P = 200, I = 0.1, D = 2). The Peltiers pump heat from the chamber into a solid copper plate embedded in a block of concrete. The underside of the copper plate is connected to copper piping which winds into the concrete, and through which fluid chilled at 6 ^{o}C (dilute ethylene glycol) is circulated. This acts to transfer the heat from the copper to the concrete. The concrete base sits on 6 passive vibration isolation pads (50 x 50 x 19mm) (Super W, Mason UK, Ltd.), which ensure dampening at frequencies above $\sim$ 11 Hz, given the mass of the concrete + chamber, as well as the compressibility of the pad material. The concrete block thus

acts as both vibration isolation for the microbalance, as well as a heatsink for the Peltier elements.

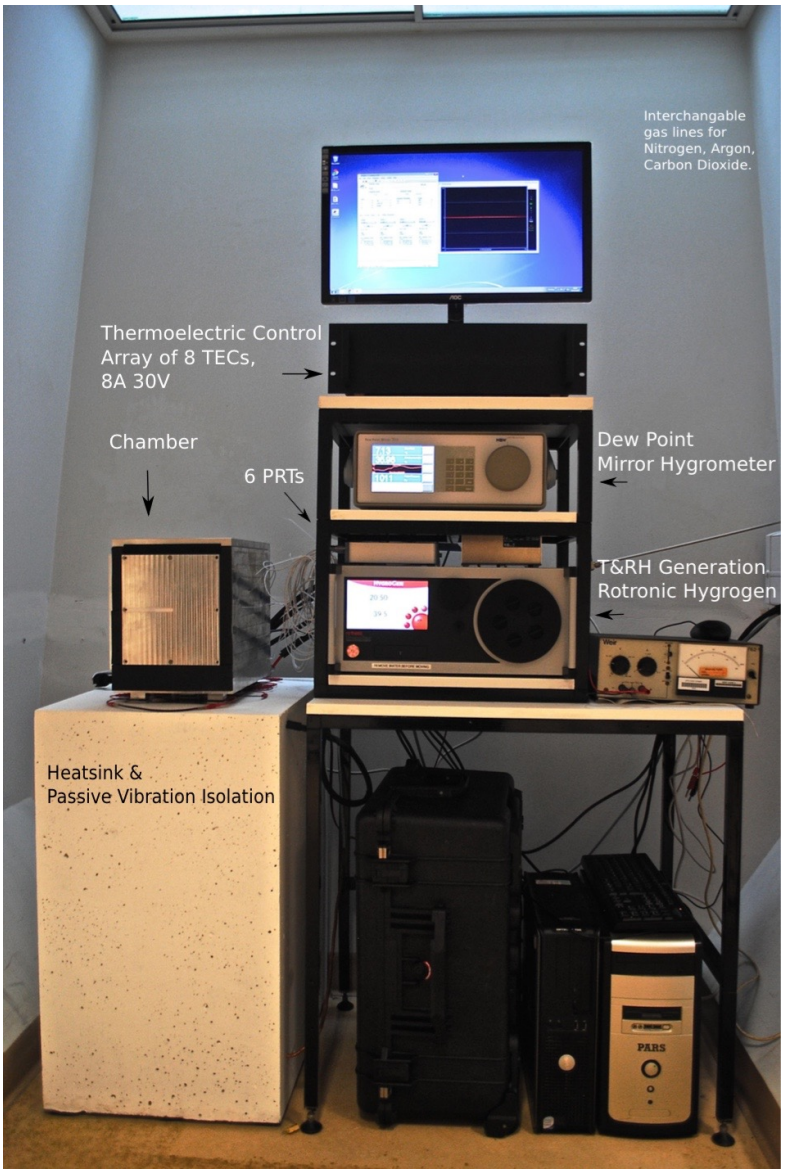

FIGURE 5.1: Experimental apparatus for gravimetric RHX measurements. Chamber rests on heatsink and passive vibration isolation (left), and is supplied by humidity generator and monitored by dew point mirror hygrometer (right).

The chamber is insulated from the laboratory and the concrete heatsink by polystyrene. Given the dimensions of the chamber and the polystyrene it is possible to perform a simple calculation to determine the heat transfer required to bring the chamber down from 22 ^{o}C to 5 ^{o}C. The polystyrene foam has a thermal conductivity of around 0.033 W m^{-1} K at 25 ^{o}C and thickness 0.01 m, and the chamber has a surface area S of 0.389 m^2. The thermal conductivity of pure aluminium is around 237 W m^{-1} K, which means

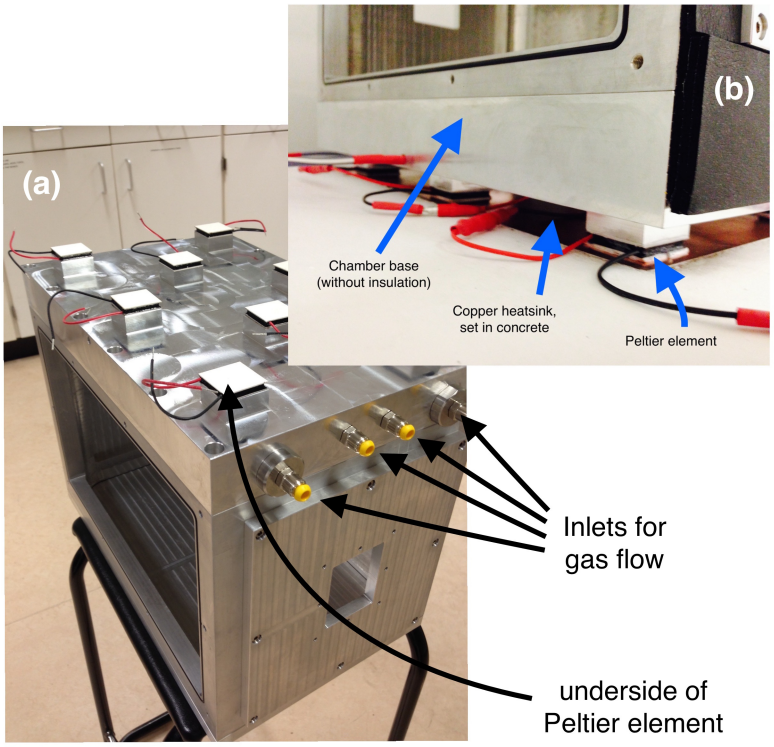

FIGURE 5.2: (a) Underside of chamber (upside down), without isolation, showing Peltier elements, and (b) showing the contact with the copper plate and chamber base.

that the overall heat transfer rate, K, is $(1/(1/237)+1/237+0.01/0.013) = 1.29\text{W m}^{-2}$ K. The amount of heat entering the insulated chamber at a steady-state temperature difference of $\Delta T = (25-5) = 20\ ^o\text{C}$ is calculated as $Q_1 = SK\Delta T = 0.389\times1.29\times20 = 10$ W, without internal sources. Heat sources inside the chamber include the microbalance as well as a single DC motor (6 rpm, 12V, 1A, ServoCity, USA), which drives the carousel mechanism. A conservative estimate of the heat transfer provided by internal sources in continuous operation is $\sim$ 5 W, which means that the total necessary heat absorption by the Peltier elements is about 15 W at a temperature difference of 20 ^{o}C. This is approximately the limit of the Peltiers, wired in series, and supplied with 8 A and 30 V. Under these conditions, the waste heat generated by the Peltiers is about 45 W, which is well within the capacity of the copper and concrete heatsink. [4]

A carousel was designed to operate off the DC motor. A Geneva mechanism converts the continuous motion of the DC motor (speed about 6 rpm) into intermittent motion,

[4]Specifications may be found at http://docs-europe.electrocomponents.com/webdocs/144a/0900766b8144a9a5.pdf. Accessed June 2016

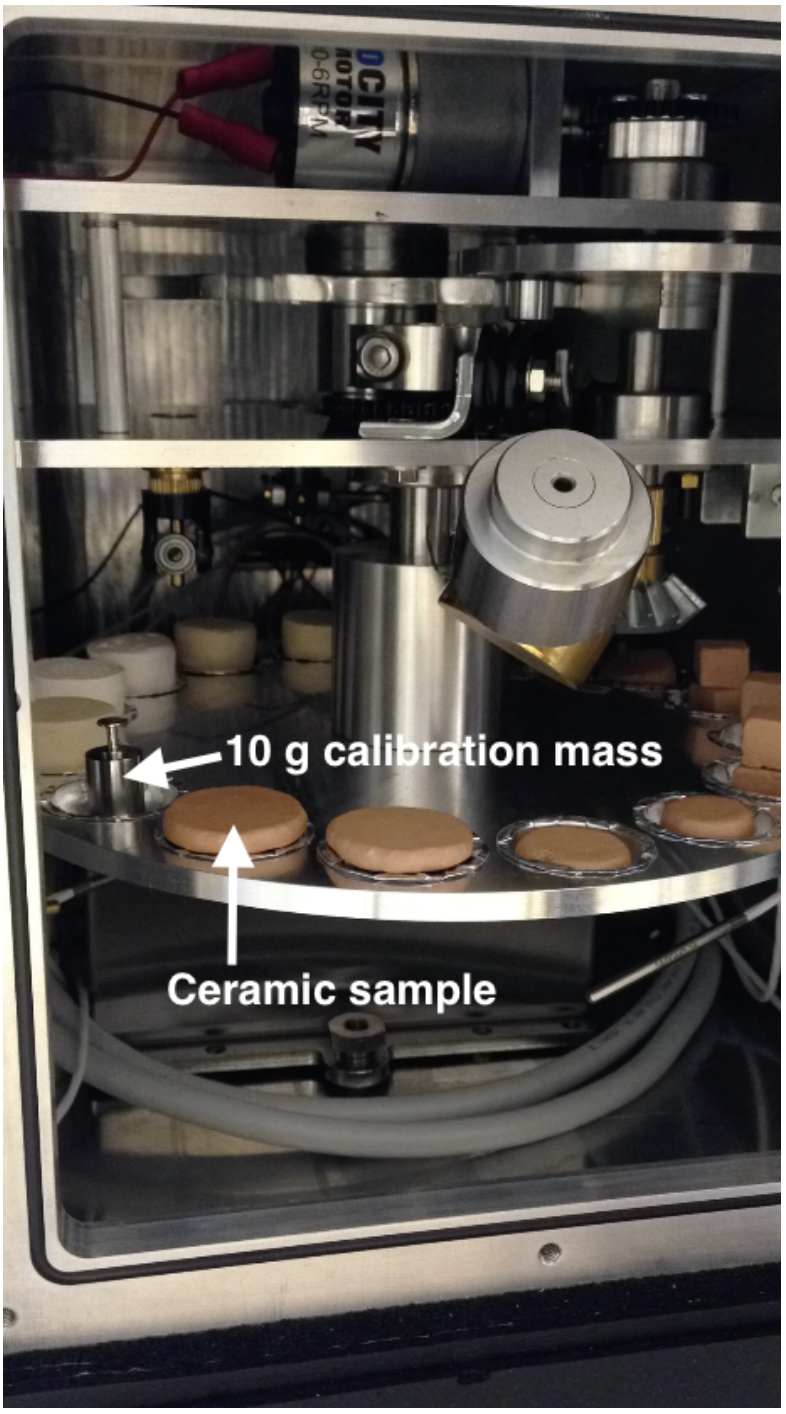

FIGURE 5.3: Carousel mechanism and microbalance inside chamber. 10 g calibration mass is indicated. A Geneva mechanism drives the carousel and is powered by 12 V DC motor in continuous operation.

which operates a 16 place carousel via a 2:1 gear. The entire mechanism operates very slowly; a single gravimetric measurement is made every 5 minutes or so. The length of measurement time means that transient disturbances in the instrument (e.g. caused by sub-11 Hz vibration) can be avoided. Custom aluminium weighing boats

were manufactured, and cleaned by ultrasonication in 1:1 chloroform/methanol, and then placed in the carousel. One weighing boat always contained a 10 g stainless steel calibration mass for comparison, measured approximately every 80 minutes.

With regard to humidity control and measurement, the 6 mm gas inlets which enter the base of the chamber were supplied by two instruments. First, humidity was controlled by a generator based on a two stream wet/dry system (Hygrogen2, Rotronic UK), rated at a control stability of 0.02 ^{o}C between 0 and 60 ^{o}C, and 0.1 % R.H.. This instrument has several advantages over a saturated salt solution, notably the ability to choose a RH set point at anywhere between 2 and 99 %. Humidity was quantified by the second instrument, a chilled mirror hygrometer (973, MBW Calibration Ltd.), which was capable of measuring dew/frost point over a range of -50 to 100 ^{o}C ambient temperature, with about 0.05 ^{o}C reproducibility and low drift over several days. The Hygrogen2 supplied the humidified gas stream at about 4 L/min, and the dew point mirror hygrometer sampled the chamber gas at 0.5 L/min. 6 platinum resistance temperature (PRT) probes (T12, MBW Calibration Ltd.) were placed in the chamber, around the carousel, and were combined with the dew point measurements from the mirror hygrometer for R.H. calculation and quantification R.H. gradients within the chamber, logged every 2 seconds via the Gecko Software provided by MBW Calibration.

5.2.3 FTIR and EDS-SEM characterisation

IR spectra were collected on materials using a Cary 640 FTIR spectrometer, with diamond attenuated total reflectance (ATR) attachment (GladiATR, Pike Technologies, USA), between 4000 and 400 cm^{-1} at 4 cm^{-1} resolution. An amount of powder was obtained from each material by use of scalpel, and then homogenised. Three scans were collected from aliquots of each material, and combined into a single spectrum. To evaluate the presence of calcite, and observe any general mineralogical trends with non-stabilisation behaviour, the peaks evaluated included the OH stretching region between 3200 and 3600 cm^{-1}, as well as the ν_3 mode at $\sim$ 1435 cm^{-1} associated with calcite-structure minerals. ATR spectra were corrected for baseline using a three-point linear function which was anchored to minima at wavenumbers of 4000, 2450 and 1300 cm^{-1}.

As a complementary technique to FTIR, energy-dispersive X-ray spectra were collected on powdered and homogenised material using a INCAx-sight EDS microanalysis system (Oxford Instruments, UK) with a resolution of 133 eV (Full Width Half Maximum) at 5.9 keV. Three replicates were performed on $\sim$ 400-500 μm diameter points on each sample (50 second acquisition time per replicate). Point areas were pre-selected by scanning electron microscope (JEOL JSM-5910). An internal copper standard was used as check the repeatability of analysis. However, no calcite quantification was performed at this stage because relative amounts of calcite are arguably sufficient to compare with non-stabilisation behaviour (which is effectively a binary phenomenon).

5.2.4 Porosity measurements

Porosity was measured by impregnation with liquid N_2 according to the method of Harry and Johnson (2004). This is a measure of *effective porosity*, i.e. the proportion of the void volume of open pores (which are connected to the surface of the material) to the total volume of the sample. This differs from the true porosity, which includes open pores, and closed pores (which are generally a function of increasing vitrification). True porosity is difficult to measure, but for low-fired relatively porous ceramics the pores are likely to be connected, and there will be minor differences between true and effective porosity. The method proceeded as follows.

A custom rig was designed which consisted of a three decimal place balance (GX series, AD Instruments Ltd., UK) on top of a scaffold, and with the sample suspended by wire from the underside of the balance. Ceramics are first dried at 105 ^{o}C for 1 h. The weight of the ceramic in air, M, was then measured. Care was taken to suspend the same just above liquid N_2 in a dewar, which cools the sample, minimising thermal shock. The dewar with liquid N_2 was then raised using a stage, and the sample immersed. The value on the balance was monitored until the constant submerged saturated weight S_1 recorded. In some cases, e.g. for highly-fired brick, this took up to half an hour. The sample was then rapidly removed from the dewar, and the weight recorded at 5 second intervals for one minute after being removed. The resultant weight loss is linear, and fitting to each curve allows extrapolation of the saturated weight in air at the instant of

removal S_2. Percentage effective porosity, P_{eff}, is then calculated as:

$$P_{\text{eff}} = \frac{S_2 - M}{S_2 - S_1} \times 100 \ . \tag{5.7}$$

It should be noted that there are other techniques to measure porosity. Although mercury intrusion porosimetry has the advantage of giving pore size and distribution information as well as effective porosity, the liquid N_2 method was used here as a first look, and is significantly cleaner, quicker and safer, posing little risk of damaging the ceramic. Harry and Johnson (2004) reported that the effective porosities determined by liquid N_2 method were generally consistent with the water-based tests, with one or two exceptions which are attributed to interaction with organics during water absorption method (where the sample is boiled). Another clear advantage is liquid N_2 does not require blotting of the ceramic surface after immersion. Since there will be additional water adhering to the surface of a ceramic in the water absorption technique, the material has to be blotted with absorbent paper, and minor differences in the timing of this blotting have a significant effect on porosity values determined by water methods.

5.2.5 Specific heat capacity measurements

The specific heat capacity c of fired-clay ceramics is not often measured. A calorimeter system was devised for the measurement of c, which consisted of 1 L milli-Q water (c = 4181 J kg^{-1} K^{-1}) in a polystyrene box, and circulated by a magnetic stirrer. Water temperature was measured with a 1000Ω PRT sensor (Correge Sensors, France), coupled to a 6 digit precision multimeter (8845A, Fluke Corporation, USA). The PRT calibration was checked by measuring the triple point of milli-Q water. The PRT was then placed inside the polystyrene box, and the temperature of the water recorded at equilibrium T_i. All ceramic samples were attached to string, and placed in an oven at 100^{o}C for a minimum of 2 hours for thermal equilibration. One by one, samples of mass m_s were rapidly transferred to the water, where they were suspended by the string without contact with the sides of the box. For each sample, the final temperature of the water T_f was recorded at stabilisation. For complete thermal transfer of heat between

the sample (denoted by subscript "s") and the water (subscript "w"), without any loss to the surroundings, we have

$$Q_s = Q_w \ , \tag{5.8}$$

$$m_s c_s (T_f - 100) = 1000 \times 4181 \times (T_f - T_i) \ , \tag{5.9}$$

and therefore c_s may be determined by rearranging the above equation. As a check on the accuracy of this method, specific heat capacities of samples of silver and brass were measured. The silver sample yielded $c = 223^{+8}_{-18}$ J kg^{-1} K^{-1}, which is slightly lower than the literature value of 233 J kg^{-1} K^{-1}. However, a sample of brass yielded $c = 379^{+11}_{-30}$ J kg^{-1} K^{-1}, which is in better agreement with the literature value of 380 J kg^{-1} K^{-1}.[5] Considering the higher thermal conductivity of silver (which means that heat is more likely to be lost to the surroundings), the former result is not unexpected. These values are reasonable, and the setup was deemed suitable for measurements of archaeological materials.

5.3 Results

5.3.1 Gravimetric experiments

Fig. 5.4 shows the mass gain behaviour of four representative samples of historical brick. Four out of eight samples exhibit what may be called "pseudo-stabilisation" behaviour. The shape of the mass gain curve for 'pseudo-stabilising" samples shows a fairly rapid gain in mass, which appears to stabilise within a couple of hours, but nevertheless continues to increase at a small but significant rate several hundred hours after reheating. Fractional mass gain, 'fmg', which is a term used by Gallet and Le Goff (2015), is reported in Table 5.1 for the period between 450 and 500 hours after reheating at 105^{o}C. Note that fmg is mathematically equivalent to y, i.e. $(m(t) - m(0))/m(0)$. The fmg of pseudo-stabilising samples is between 0.45×10^{-3} and 12×10^{-3} at between 450 and 500 hours. The non-stabilising samples all showed a similar curve shape, which indicates a relatively slower rate of early-stage mass gain, but a more marked curvature

[5] http://hyperphysics.phy-astr.gsu.edu/hbase/tables/sphtt.html#c1. Accessed 8 June 2016.

at long times. Interestingly, the fractional mass gain of the non-stabilising samples lie between 0.45×10^{-3} and 0.8×10^{-3} for the same time period, which is generally less mass gain than the pseudo-stabilising samples.

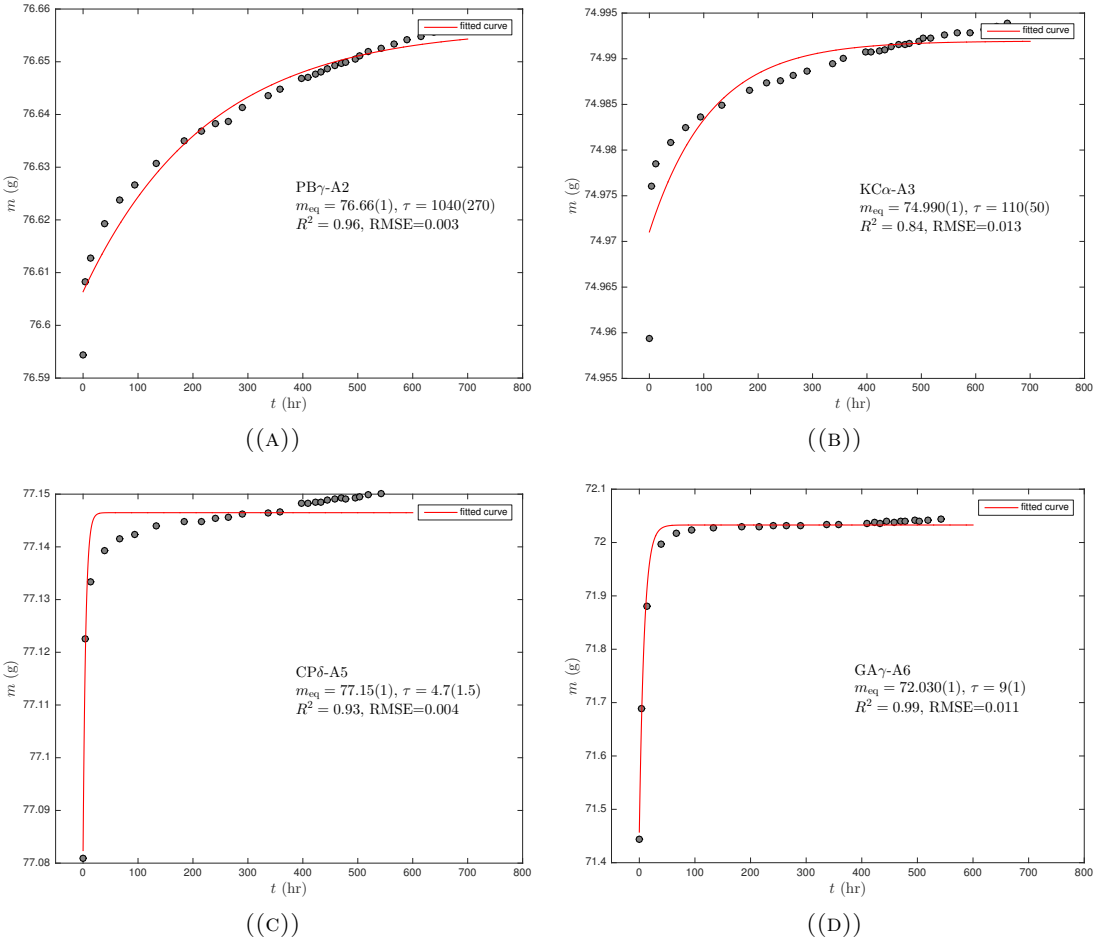

FIGURE 5.4: Fits to Lagergren rate equation (Eq. 5.1) for four representative samples of fired clay brick (A) PBγ-A2, (B) KCα-A3, (C) CPδ-A5 and (D) GAγ-A6. All of the fits are fairly poor, and tend to underestimate the late-stage mass gain. See discussion in text for further details.

Table 5.1 reports these values, along with fitted parameters (m_{eq}, τ) to the Lagergren rate equation (Eq. 5.1). Fits were performed in MATLAB by Levenberg-Marquardt method. The fitted equations are generally in poor agreement with the experimental data, and are generally overestimates of mass gain during the early part of the curve, and underestimates at later times. It seems therefore that the mass gain behaviour of all samples is inadequately described by a Lagergren rate equation. However, even though this fit is inappropriate, it is still be useful to calculate 99% mass gain from the relation $t_{99} = -\tau ln(10^{-2})$, because τ describes the curvature, which is the definitive feature of

TABLE 5.1: Fitted parameters to Lagergren rate equation (Eq. 5.1). Fitting was performed in MATLAB by the Levenberg-Marquardt method. Also shown is the fractional mass gain, fmg, between 450 and 500 hours for each sample of brick heated to 105 ^{o}C for two hours, and equilibrated at constant T and R.H.

Sample	fmg, at 450-500 hrs ($\times 10^{-3}$)	m_{eq}	τ (hrs)	t_{99} (hrs)	R^2
CPδ-A5	0.83	77.15(1)	4.7(1.5)	22(7)	0.94
PBγ-A2	0.80	76.66(1)	230(60)	1040(270)	0.96
OGα-A1	1.3	83.990(4)	9.0(6)	41(3)	0.99
GAγ-A6	0.45	72.030(2)	9(1)	40(5)	0.99
ECα-A9	3.5	83.70(1)	8(1)	40(5)	0.93
KCα-A3	0.45	74.990(1)	110(50)	520(240)	0.84
X3880-A4	12	65.330(1)	7.5(5)	34(2)	0.99
RB-A7	0.5	63.590(3)	150(50)	710(230)	0.93

non-stabilisation behaviour. t_{99} exhibits a large range from 22 ± 7 to 1040 ± 270 hours. However, apart from the lowest value for these samples, 22 ± 7 hrs from CPδ-A5, most non-stabilising samples have values of t_{99} greater than several hundred hours.

5.3.1.1 Werra ware

Mass gain curves for two samples of Werra ware, MAN037 and MAN038, which were heated at 105 ^{o}C for 3 hours, are presented in Fig. 5.5. MAN037 appears to pseudo-stabilise after 450 hours, whereas MAN038 does not pseudo-stabilise. The fractional mass gains of the non-stabilising sample and the pseudo-stabilising sample at 450-500 hours are both $\sim 1 - 2 \times 10^{-5}$, which is an order of magnitude lower than the fractional mass gain for the non-stabilising historical bricks. The fact that the fractional mass gains for these samples are both lower than those observed for historical bricks may reflect the greater resolution of the microbalance apparatus used for these measurements, which is sensitive enough to detect non-stabilisation behaviour which may previously have been masked by noise. The mass curve of MAN037 at long times shows fluctuations which are correlated with changes in R.H. of less than 1 % inside the chamber, and is greater in magnitude than the changes in mass of MAN038. This supports the previous finding for the historical bricks that 'pseudo-stabilising' samples are also more sensitive to changes in R.H., which causes larger variations in mass which may mask an underlying non-stabilising trend. Both samples had similar nominal mass, but slightly different appearances. MAN037 was prepared mostly from the interior of the ceramic, and had

a dark appearance. On the other hand, MAN038 came from the edge of the ceramic, and was a uniform red colour. ATR-FTIR spectra (not illustrated here) confirm that the dark centre has no organic component (to the limits of FTIR sensitivity), which suggests that underlying mineralogical changes caused by the original firing may play a significant role in non-stabilisation behaviour.

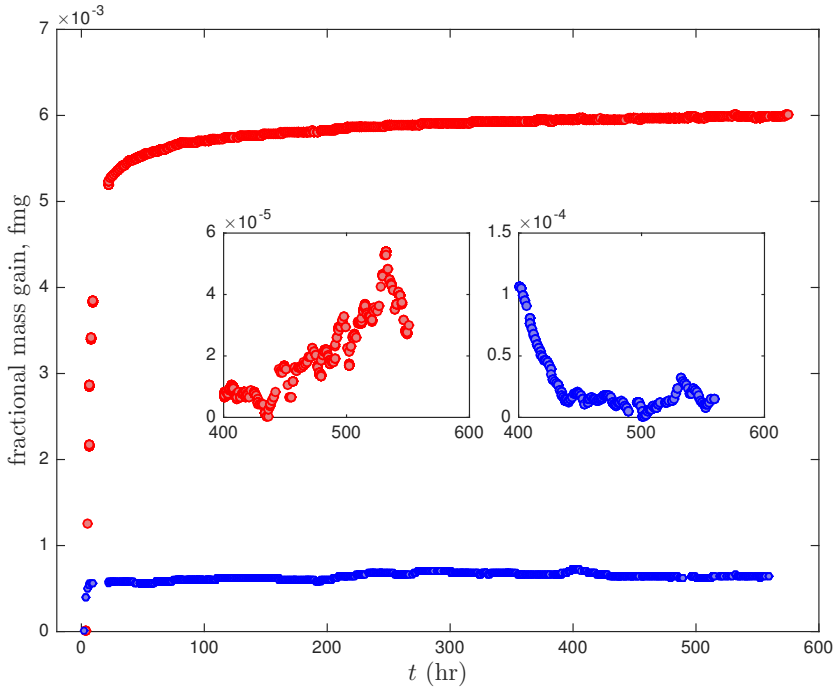

FIGURE 5.5: Mass gain curves for two fragments of Werra (MAN037 and MAN038) of similar nominal mass, heated at 105^{o}C for 3 hours, and placed in the chamber at $\sim$ 18.22 ^{o}C, 40 % RH. Red curve corresponds to MAN038, which shows higher fractional mass gain, which appears to continue after 400 hours. Blue curve shows MAN037, which has lower fractional mass gain, which is less evident after 400 hours.

5.3.1.2 Montmorillonite and kaolinite

Mass gain curves for montmorillonite and kaolinite are presented in Fig 5.6. The fractional mass gain of the montmorillonite at the 450th hour is about 0.01, which is an order of magnitude higher than the kaolinite at similar times, and comparable with the highest fmg of historical bricks. The figure shows that the kaolinite appears to pseudo-stabilise, whereas the montmorillonite exhibits a clear trend of increasing mass gain, and bears a striking similarity to Fig 5.5, with the exception that the montmorillonite shows greater sensitivity to changes in chamber R.H. The non-stabilisation of montmorillonite and the pseudo-stabilisation of kaolinite supports the hypothesis that T1 water sorption

continues over long timescales, since smectites have a greater proportion of T1 water. It also suggests that the presence of T1 water is responsible for the non-stabilisation behaviour. Little is known about the presence of T1 'chemisorbed' water in fired clays, but it seems reasonable to expect that clays with more T1 water will exhibit greater capacity for T1 water uptake upon firing, even in the face of structural changes caused by heating.

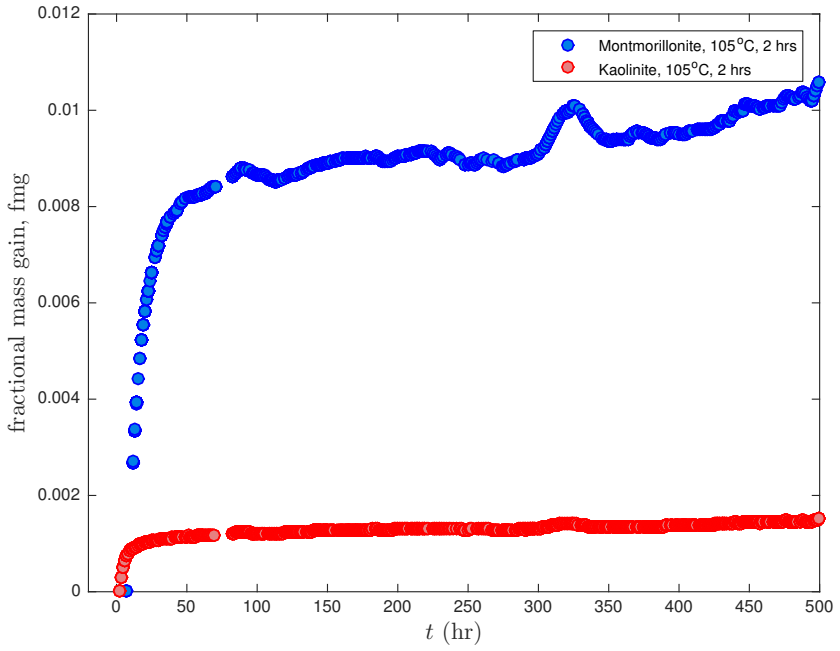

FIGURE 5.6: Mass gain curves for montmorillonite and kaolinite heated to 105^{o}C for 2 hours.

5.3.1.3 Calcite

Fig 5. 7 shows the effect of addition of calcite to the same montmorillonite clay, after heating to much higher temperatures (825^{o}C). Contrary to expectation, the two curves are very similar, and there is no difference between the mass gain characteristics of the montmorillonite sample or the sample which contained calcite. The two samples were fired at exactly the same time, and there is no obvious difference between them other than the addition of calcite. It is tempting to suggest that calcite has a negligible effect, although there are several plausible explanations for the behaviour observed with montmorillonite. There is good evidence to suggest that there is thermally-induced migration of cations into the interlayers of the montmorillonite lattice, since dehydration

and partial collapse of the structure causes charge imbalance, e.g. (Luca, 1988). In this scenario, Ca ions migrate into the interlayers after decarbonation, where they remain, and do not undergo any further chemical reaction. Consequently, there is little mass gain. For other clay minerals, the degree to which the Ca is stabilised will vary with lattice charge imbalance and the nature of interlayer spacing. For example, a sample of kaolinite with added calcite was not stable upon heating to 825 ^{o}C, and upon removal from the oven rapidly distintegrated due to hydration of CaO, which caused expansion of the material and significant cracking (lime blowing).

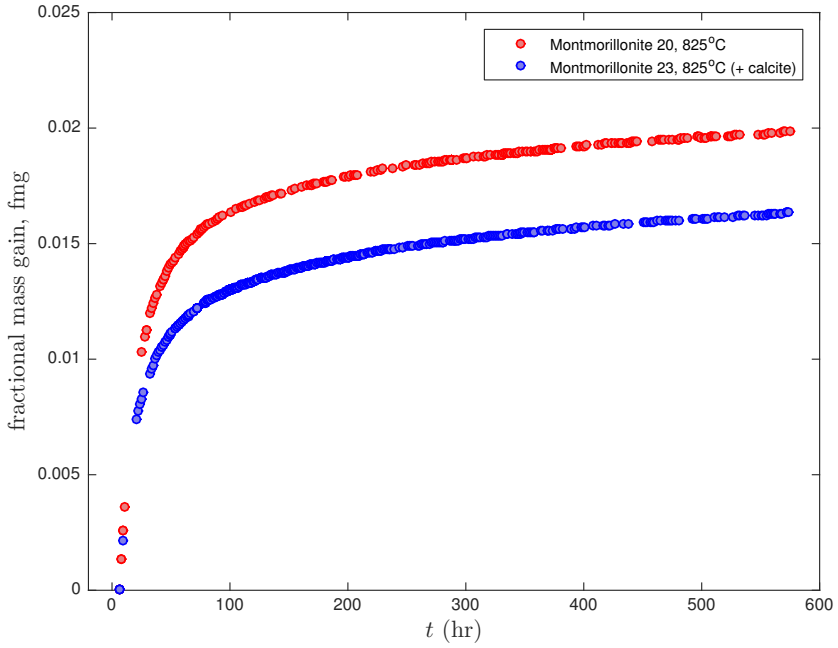

FIGURE 5.7: Mass gain curves for montmorillonite samples, initially fired at 825^{o}C for 7 hours. The blue curve indicates mass gain for the montmorillonite sample to which approximately $\sim$ 10 % calcite was added (by mass).

5.3.1.4 Terracotta samples of different thickness

The mass gain curves of terracotta samples of different thicknesses can be seen in Fig. 5.8, after initial firing at 800^{o}C, and plotted against the fourth root of time. All three samples came out of the oven at the same time. The figure shows slight differences between each curve. The thinnest piece, 4.2mm, shows a marked changed in slope at around 2 hours after firing. The 6.4 mm piece shows a slightly longer period of initial uptake, which is a trend continued by the thickest piece (9.2 mm), which has a less noticeable and slower transition to 'linearity' with the fourth root root of time. Fits

performed on this data are also shown in Fig. 5.8. The fitted model combines $t^{1/4}$-type behaviour with a Lagergren rate law (i..e Eq. 1.15, suggested by Bowen et al. (2013)):

$$m(t) = -\beta'(1 - e^{-t/\tau}) + \alpha'_4 t^{1/4} + \delta \ . \tag{5.10}$$

The fitted values of τ were 1.87 ± 0.08 for the 4.2 mm piece, 4.28 ± 0.07 for 6.4 mm and 20.0 ± 0.1 for the 9.2 mm piece. Goodness-of-fit statistics were high for all samples (R^2 >0.99), although the residuals show systematic overestimation of the mid-stage mass gain between 1.5 and 2.5 $h^{1/4}$, which was noted for the previous fits to the historical bricks. The values of τ correspond to t_{99} of 4.2 ± 0.02 h, 9.9 ± 0.2 h and 46 ± 2 h respectively. This is the first evidence for a thickness effect, given by Fick's second law (Eq. 5.3), which predicts the linear dependence of t_{99} on L^2. However, given that this model seems to overestimate mid-stage mass gain, which was also found in the case of the historical bricks, it may be argued that the fits are not a full reflection of the underlying process. In particular, there could be time-offsets and an accelerated $t^{1/4}$ or $t^{1/2}$ process during cooling of the sample which might be responsible for the discrepancy. Simulations of cooling rate effects will follow in the discussion.

In addition, Fig. 5.9 shows mass gain of two terracotta samples of the same nominal thickness (4.2 mm) and initial mass. However, the second sample was rapidly quenched in milli-Q water, and then dried under nitrogen before being placed in the chamber. It is interesting to note two features. First, the initial period of sorption seems to be absent for the 'quenched' sample. Second, the slope of the 'stage II' mass gain for this sample is around 0.000560 ± 0.000003 g $h^{1/4}$, which is an order of magnitude lower than the corresponding value for all samples which were simply removed from the oven, without quenching. One might expect the two curves to be similar, given the hypothesis that T2 water is independent of all other processes. However, this is not the case, and there are several possibilities which could explain this behaviour. First, the sites at which T2 water combines may be rapidly filled by immersion in water. Second, that there is another long-lived process of T1 sorption which is effectively stopped by submersion in water, which fills all T1 sites. And third, that there is some long-lived effect of slow cooling on an accelerated $t^{1/4}$ reaction, which contributes to a very slight curvature in

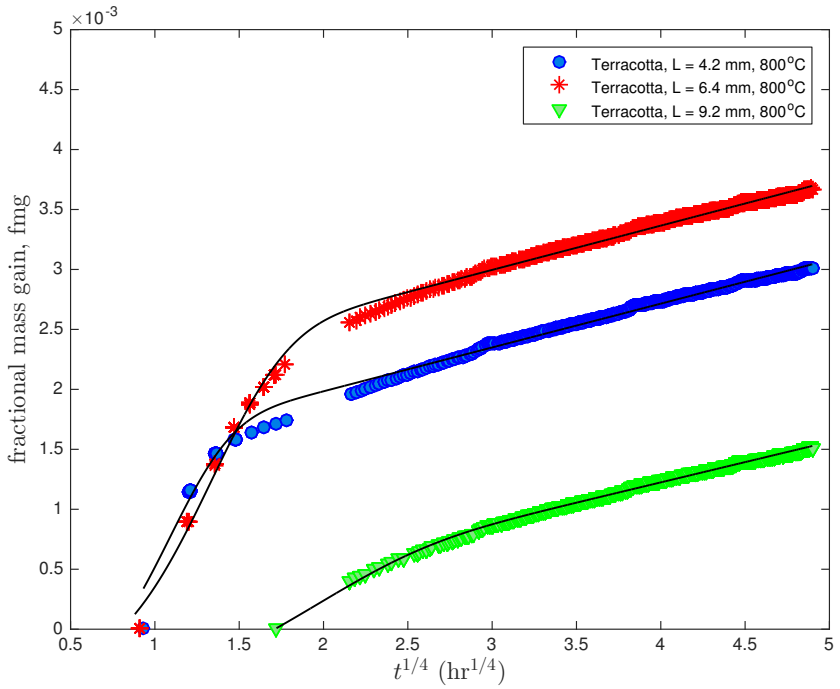

FIGURE 5.8: Mass gain curves for terracotta samples of varying thickness. Blue curve represents a 4.2 mm disk, whereas red indicates the 6.4 mm sample, and green indicates 9.2 mm. Values of β', τ, α'_4 and δ for the corresponding fits are as follows: 4.2 mm disk, $\beta' = 0.0079(4)$, $\tau = 1.87(8)$, $\alpha_4 = 0.001530(5)$, $\delta = 4.174(1)$; 6.4. mm disk, $\beta' = 0.0098(1)$, $\tau = 4.28(7)$, $\alpha'_4 = 0.00151(2)$, $\delta = 4.086(1)$; 9,2 mm disk, $\beta' = 0.0028(1)$, $\tau = 20.0(1)$, $\alpha'_4 = 0.001406(5)$, $\delta = 4.158$. The values of τ are converted into estimates of t_{99} which are 4.2 ± 0.02 h, 9.9 ± 0.2 h and 46 ± 2 h respectively.

mass gain which is not evident at current microbalance resolution.

5.3.2 Porosity and specific heat capacity

The effective porosities and specific heat capacities are presented in Table 5.2, along with the densities, which were calculated from the dry mass of the sample together with saturated mass, and the density of liquid nitrogen. This is a fairly rough estimate of density, given that the liquid nitrogen does not fill closed pores. For several samples, a reliable value of c or ρ could not be determined. This is because the sample masses were too small to obtain reliable measurements, given the sensitivity of the apparatus. P_{eff} ranges from 8.6 ± 4.4 % for the Megiddo sample, to a high of 51.1 ± 0.4 % for the montmorillonite standard. Both kaolinite and montmorillonite have higher P_{eff} than archaeological or historical materials. Most apparent porosities lie between about 25 and 32 %, and there is no clear correlation between porosity and colour or physical

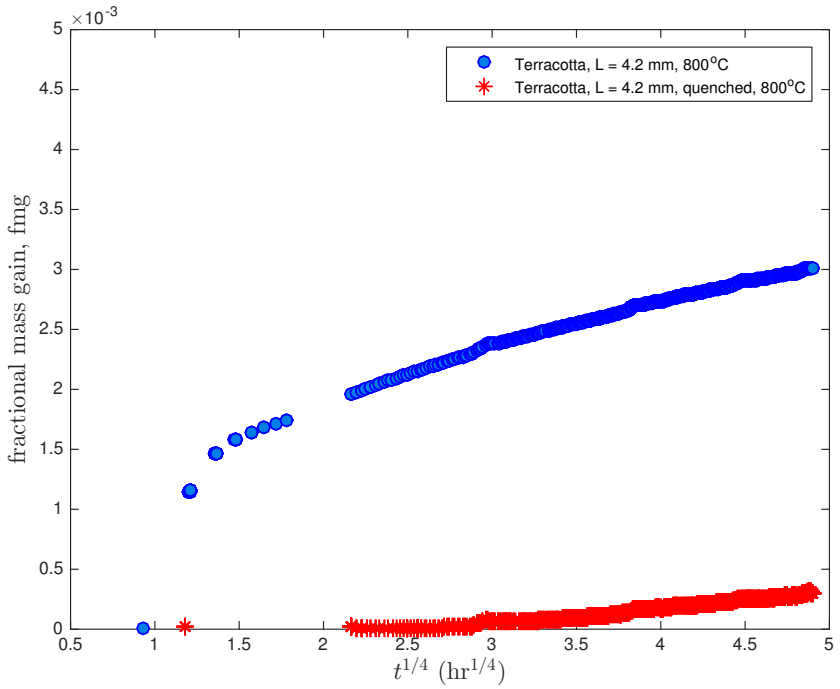

FIGURE 5.9: Mass gain curves for 4.2 mm terracotta samples of the same nominal mass. Red curve shows the effect of quenching in water, and subsequent drying under nitrogen.

appearance (red/black/etc). Samian ware ('terra sigilata') has some of the highest effective porosities for archaeological material. However, there is some variability here, since the MAN005 sample provided by Dr Moira Wilson gave a value of 45 ± 15 %, and a measurement of a second sample of gave a more precise value of 37.4 ± 0.5. The large error on the former sample is most likely the result of small sample mass (0.9 g), which is less suited to the current apparatus. Most porosity values are within the range of those obtained by Harry and Johnson (2004) for a variety of pottery wares, with the exception of the Megiddo material which is much lower at 8.6 ± 4.4 % (comparable to $\sim 11\%$ obtained for samples of modern porcelain by Harry and Johnson (2004)).

The specific heat capacities vary within a relatively narrow range, from about 844 to 922 J kg^{-1} K^{-1}, with fairly large uncertainties. There is no obvious correlation between c and effective porosity, or density. The magnitude, and asymmetry of these large uncertainties are the result of systematic effects caused by loss of heat to the air during transfer from the oven to the experimental apparatus, which results in an overestimate of T_i, and consequently an overestimate of c. Very little could be done to improve this, apart from improving the calibration of the PRT, and introducing an estimated term for

TABLE 5.2: Effective porosities P_{eff}, specific heat capacities c and densities ρ of archaeological fired-clays and fired-clay standards discussed in this text. † indicates material supplied by M. Wilson, January 2016. Several samples were too small to obtain reliable specific heat capacities, given the current experimental setup. These values are omitted. Note that densities are calculated from P_{eff} and using a value for the density of liquid nitrogen of 806.11 kg m^{-3} at 101.3 kPa.

Sample	dry mass (g)	c (J kg^{-1} K^{-1})	P_{eff} (%)	ρ (g cm^{-3})
Montmorillonite	6.9	-	51.1 $\pm$0.4	-
Kaolinite	9.8	-	41.4 $\pm$0.4	-
CPδ-A5	74.5	862^{+25}_{-68}	27.4 $\pm$0.02	1.96
PBγ-A2	74.8	866^{+25}_{-68}	32.73 $\pm$0.04	1.78
OGα-A1	69.4	922^{+26}_{-72}	28.3 $\pm$0.5	1.85
GAγ-A6	58.7	890^{+26}_{-70}	32.9 $\pm$0.4	1.70
ECα-A9	80.4	830^{+25}_{-66}	24.5 $\pm$0.1	1.85
KCα-A3	72.7	858^{+26}_{-70}	25.0 $\pm$0.1	1.93
X3880-A4	79.1	915^{+27}_{-72}	29.6 $\pm$0.1	1.81
RB-A7	61.1	844^{+25}_{-67}	33.1 $\pm$0.1	1.72
Chester Red †	2.3	-	25 $\pm$1	-
Samian (MAN005) †	0.9	-	45 $\pm$15	-
Samian (RLAHA)	12.1	-	37.4 $\pm$0.5	1.75
Megiddo †	2.5	-	8.6 $\pm$4.4	-
Werra (MAN037) †	4.2	-	31.9 $\pm$1.1	-
Werra †	0.9	-	32.0 $\pm$0.9	-
Opus spicatum (MAN088) †	0.9	-	29.5 $\pm$0.6	-
Terracotta †	4.6	-	31.2 $\pm$0.6	

the extra heat loss in Eq. 5.9. However, such an effect would cause a constant systematic offset for all samples, which means that the relative values of c can still be compared at the sample level.

5.3.3 FTIR and elemental characterisation

FTIR spectra for historical bricks are presented in Figures 5.10 - 5.18 , along with mass gain curves inset into each figure, as well as elemental compositions as determined by EDS-SEM. The most clear trend from the FTIR spectra is seen when comparing the OH stretching region of water between $\sim$ 3200 cm^{-1} and $\sim$ 3600 cm^{-1} with the mass gain curves. The samples which 'pseudo-stabilise' tend to have large peak areas in this region, whereas the samples which show a non-stabilisation behaviour have little to no water (structural or otherwise). Few samples have a $\sim$ 3620 cm^{-1} (or higher) peak associated with structural OH (or Ca-O bond). The presence of calcium is confirmed from EDS-SEM in all but two samples (OGα-A1, PBγ-A2), which is supported by peaks which

are identified from FTIR spectra. The carbonate peak at ~ 1420 cm^{-1} (Farmer, 1974) is particularly strong for GAγ-A6, which is interesting because this sample exhibits 'pseudo-equilibration'. This implies that the presence of calcium (in carbonate) may not have a significant effect on non-equilibration behaviour, and supports the previous gravimetric experiments on montmorillonite.

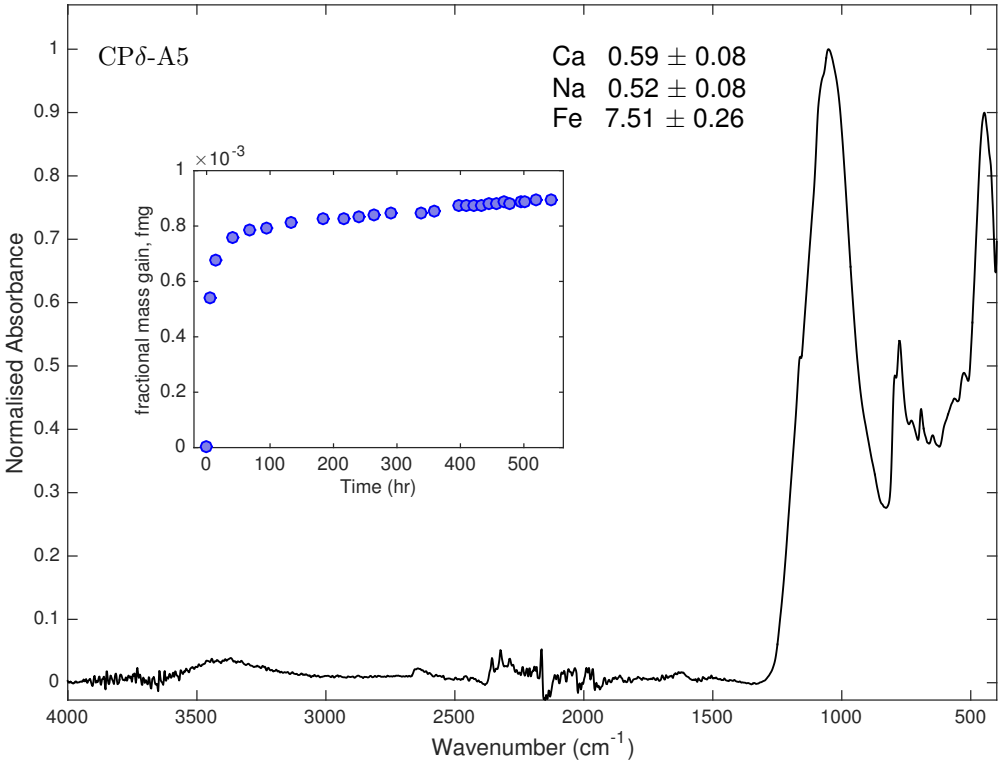

FIGURE 5.10: ATR-FTIR spectra of sample of historical clay brick CPδ-A5. Inset shows fractional mass gain, fmg, for the sample after heating to 105^{o}C for 2 hours. Also shown are selected elemental analysis determined by EDS-SEM, expressed in weight per cent (uncalibrated). Note that the term 'fmg' follows the use by Gallet and Le Goff (2015) and related papers, and is equivalent to y in the terminology of Wilson et al. (2009).

With regard to calcite, there are no correlations between the relative amount of calcite and fractional mass gain at long times, nor with t_{99}. Neither are there any obvious correlations between the non-stabilisation behaviour and P_{eff}, ρ, or the relative amount of sodium. Figure 5.19 shows the only significant relationships identified between the various parameters. Fig. 5.19 (A) shows the most prominent relationship, which is between fmg and t_{99}. High values of t_{99} are only associated with the lowest values of fractional mass gain. The result is unexpected, because non-stabilisation behaviour should show greater fractional mass gain, which is not the case here. This behaviour

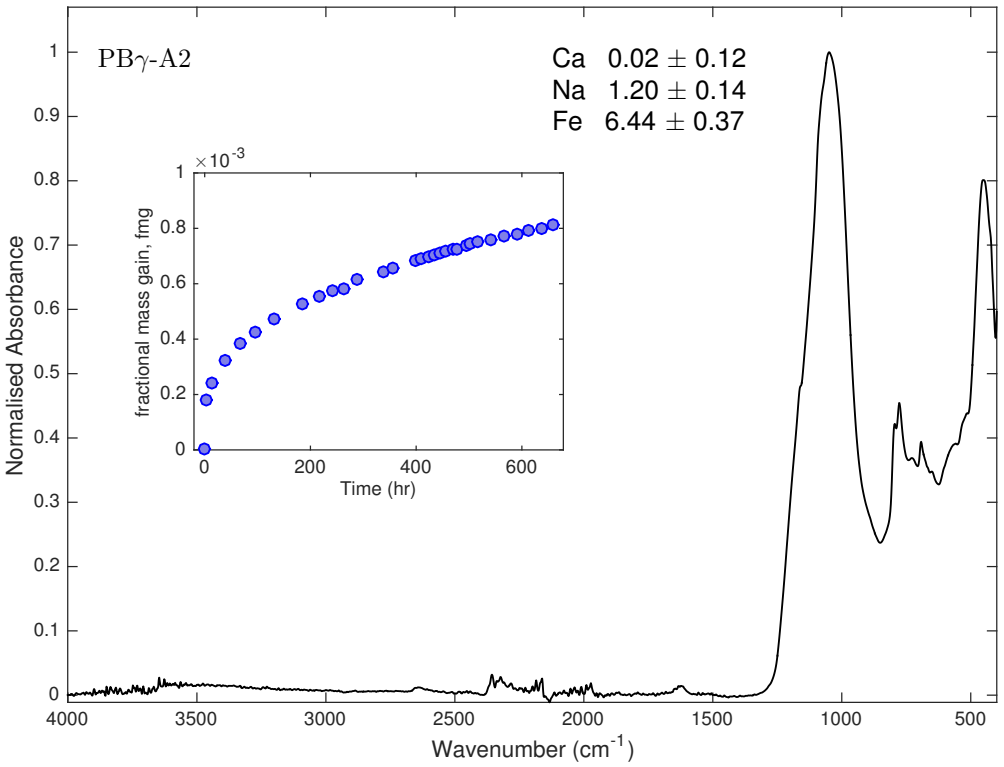

FIGURE 5.11: ATR-FTIR spectra of sample of historical clay brick PBγ-A2, with selected EDS-SEM analysis and fractional mass gain curves for the equilibrium step.

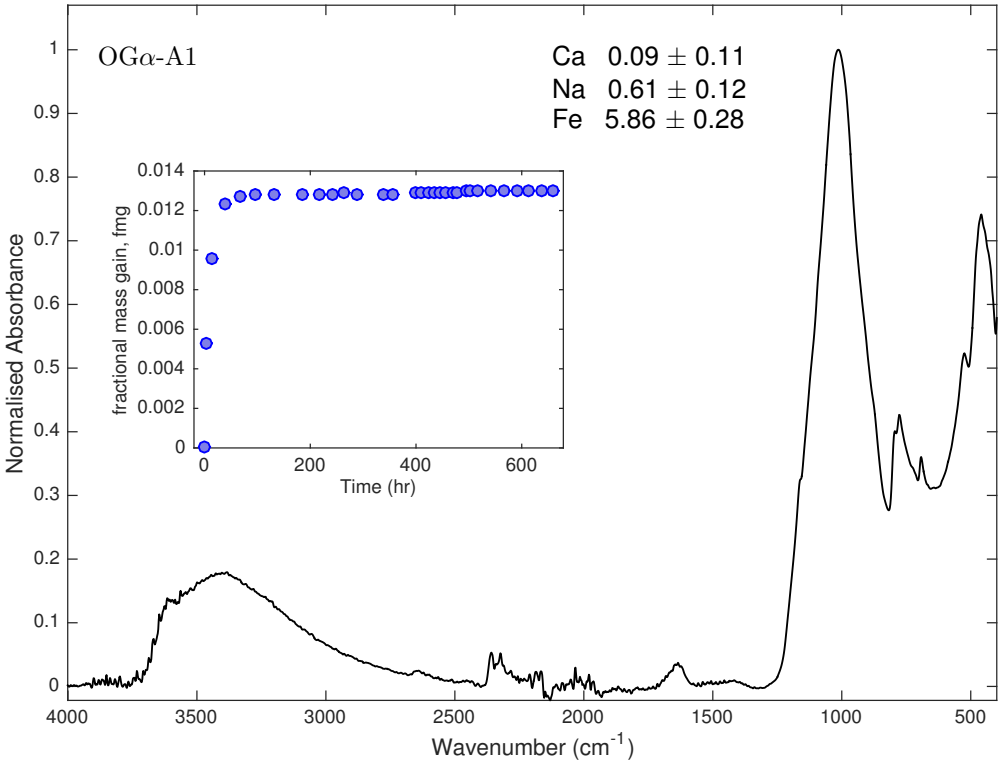

FIGURE 5.12: ATR-FTIR spectra of sample of historical clay brick OGα-A1, with selected EDS-SEM analysis and fractional mass gain curves for the equilibrium step.

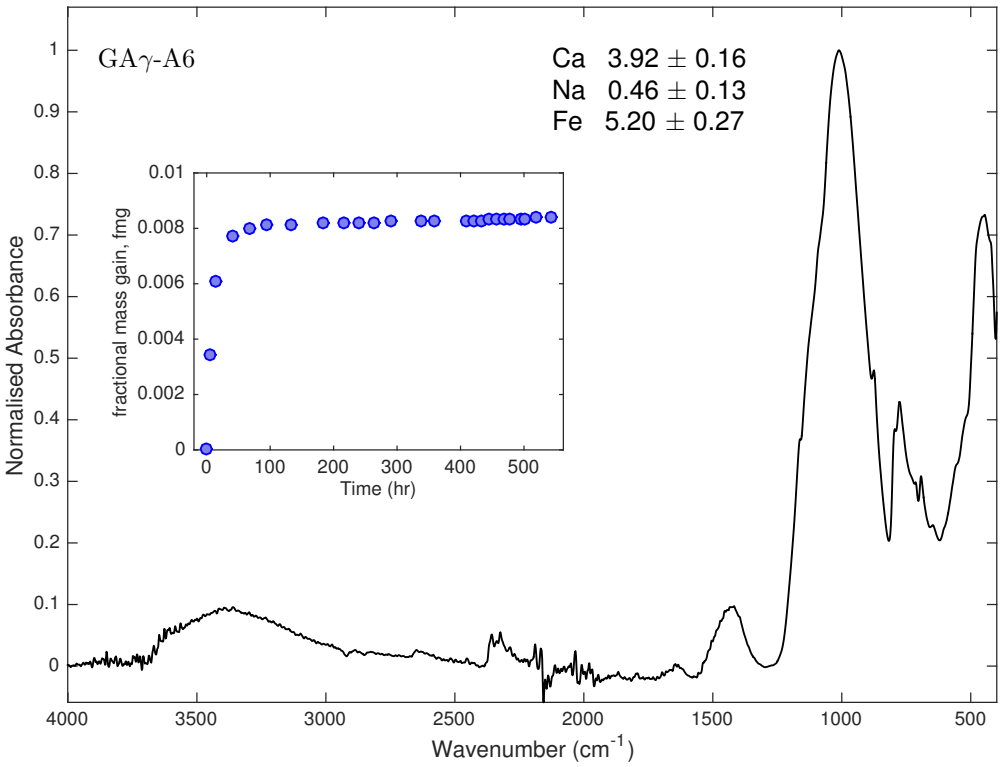

FIGURE 5.13: ATR-FTIR spectra of sample of historical clay brick GAγ-A6, with selected EDS-SEM analysis and fractional mass gain curves for the equilibrium step.

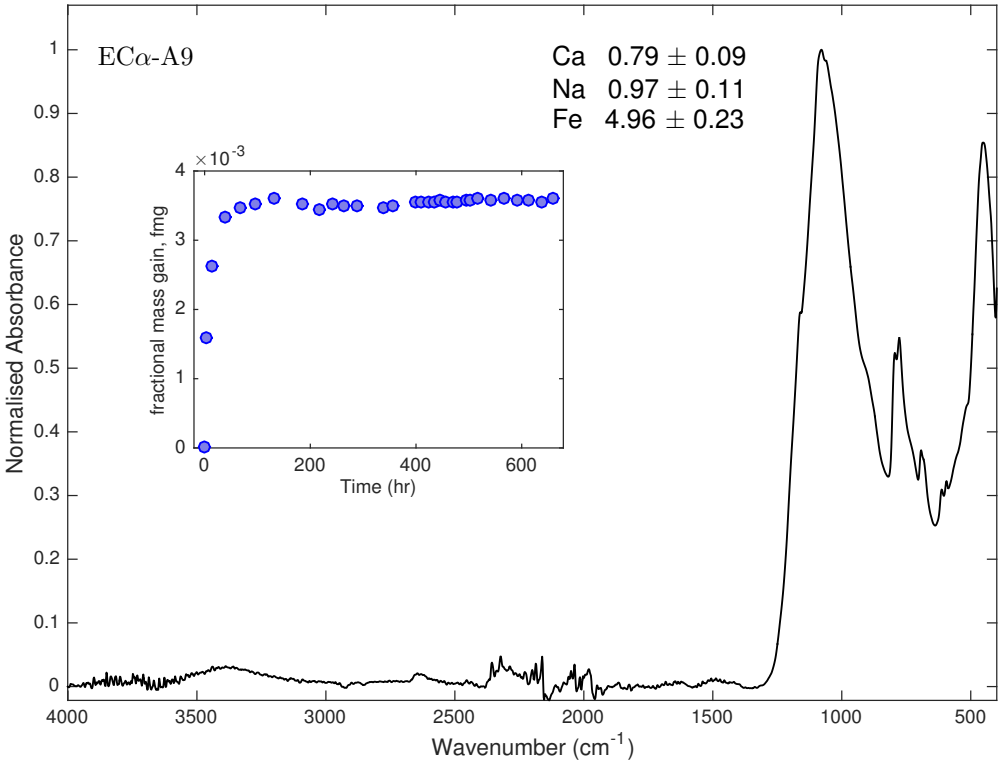

FIGURE 5.14: ATR-FTIR spectra of sample of historical clay brick ECα-A9, with selected EDS-SEM analysis and fractional mass gain curves for the equilibrium step.

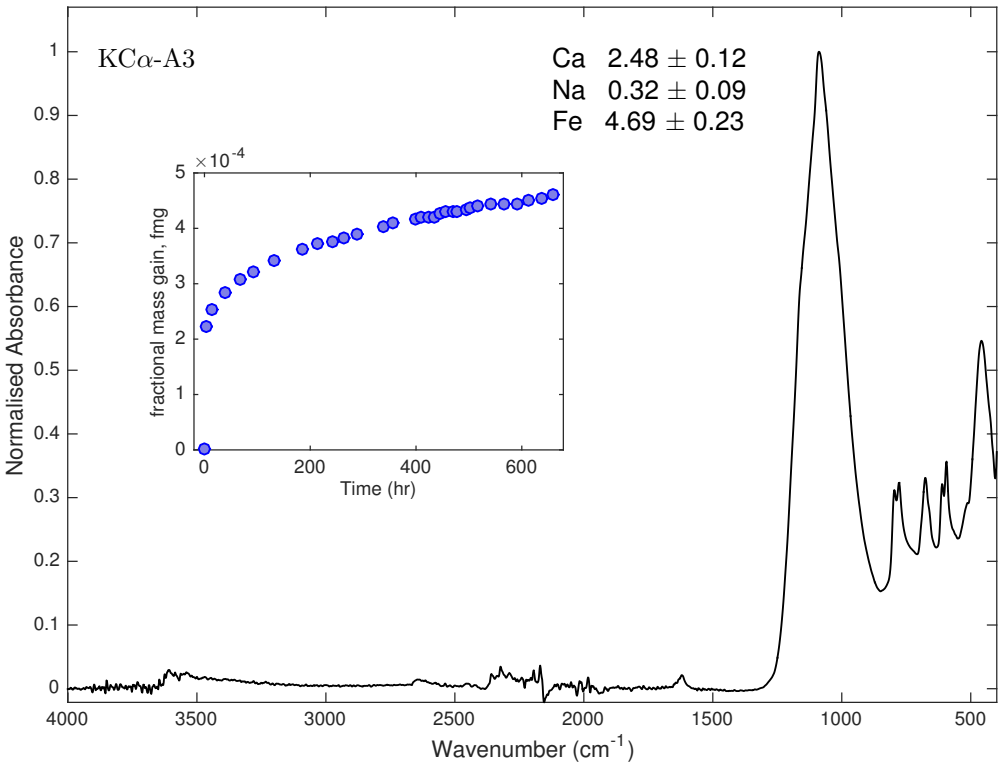

FIGURE 5.15: ATR-FTIR spectra of sample of historical clay brick KAα-A3, with selected EDS-SEM analysis and fractional mass gain curves for the equilibrium step.

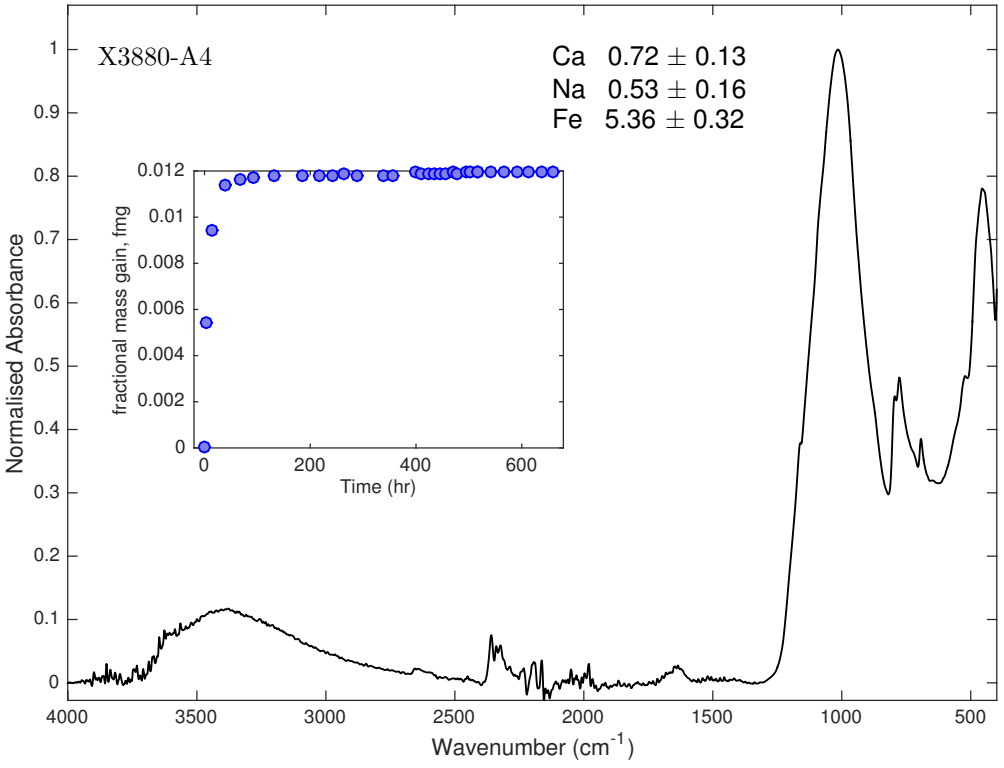

FIGURE 5.16: ATR-FTIR spectra of sample of historical clay brick X3880-A4, with selected EDS-SEM analysis and fractional mass gain curves for the equilibrium step.

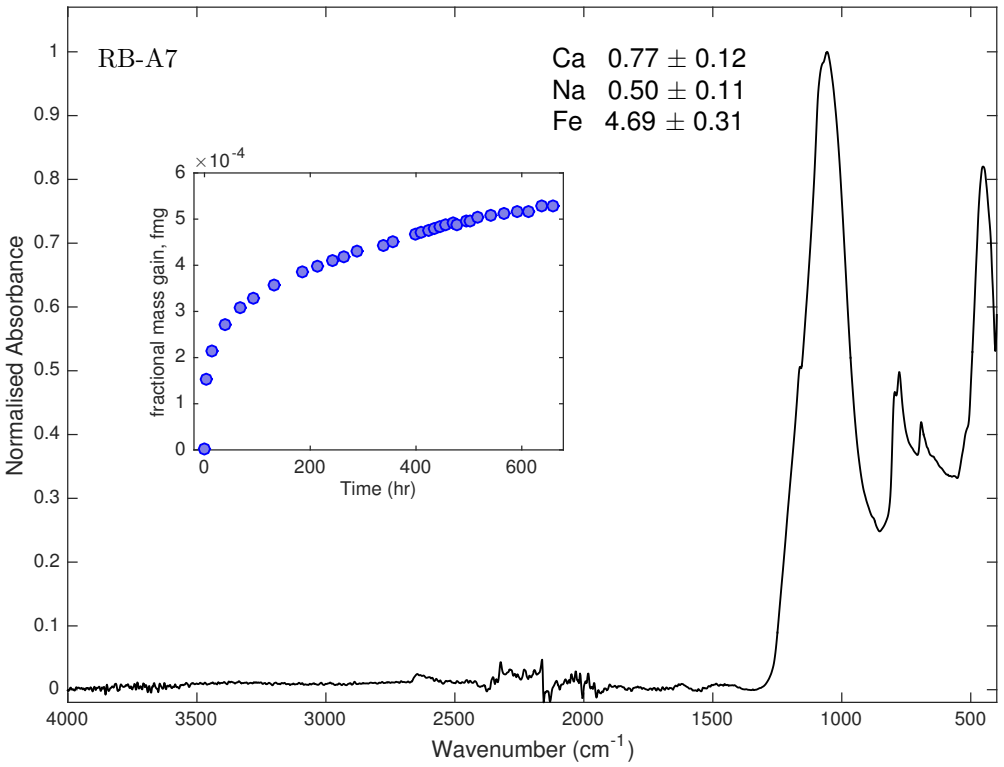

FIGURE 5.17: ATR-FTIR spectra of sample of historical clay brick RB-A7, with selected EDS-SEM analysis and fractional mass gain curves for the equilibrium step.

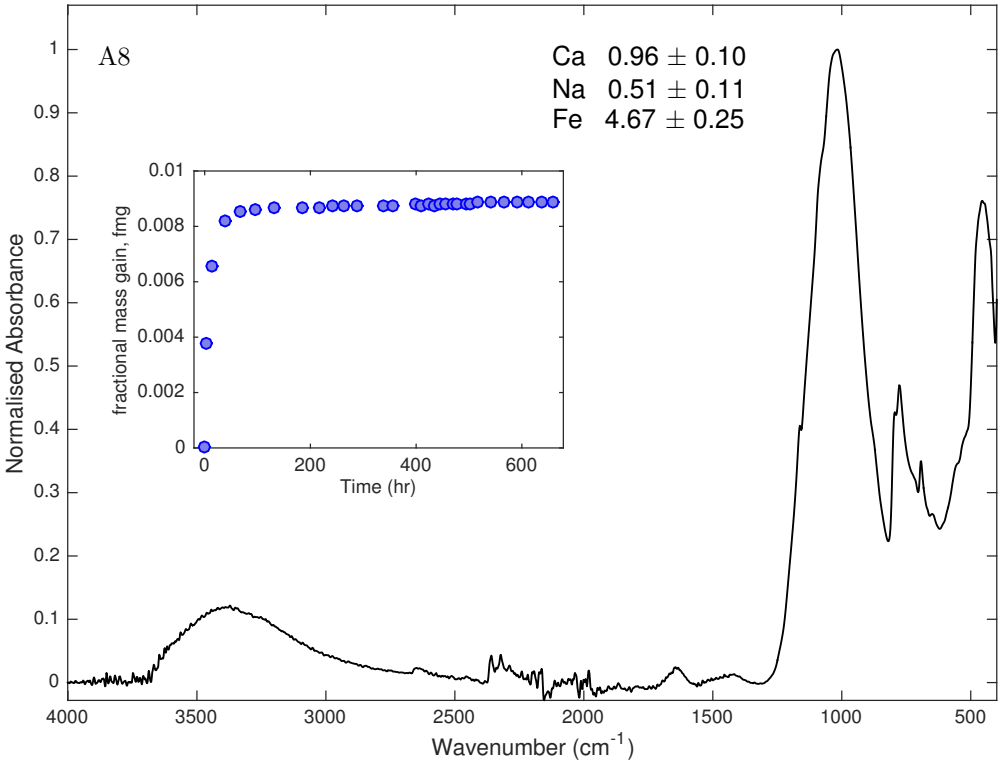

FIGURE 5.18: ATR-FTIR spectra of sample of historical clay brick A8, with selected EDS-SEM analysis and fractional mass gain curves for the equilibrium step.

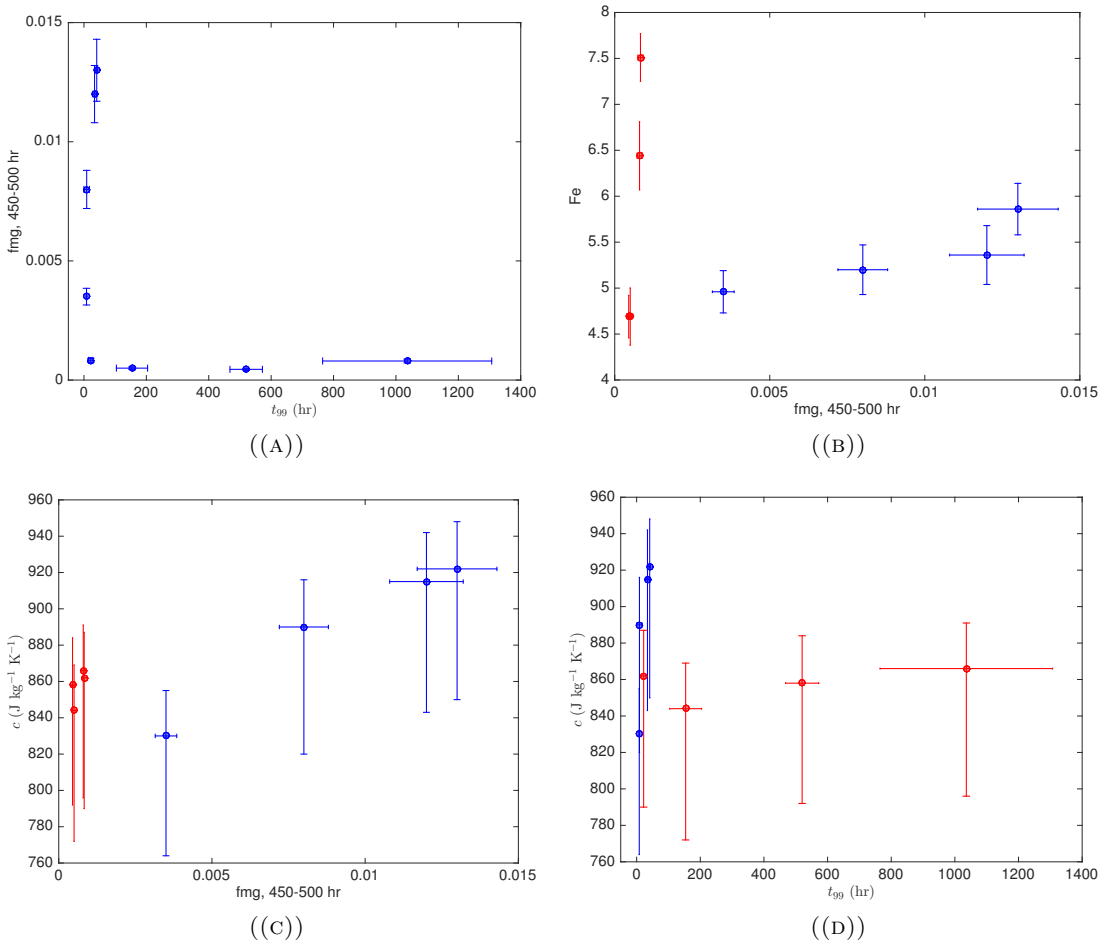

FIGURE 5.19: Plots showing relationships between various physical parameters. (A) shows fractional mass gain at 450-500 hours after reheating versus t_{99}, as determined by previous fits. This shows a quicker times to pseudo-equilibrium behaviour correspond to higher fmg. (B) shows the relationship between iron concentration (EDS-SEM) measurements to fmg. Blue data points indicate the samples which pseudo-equilibrate. (C) Similar to the previous subfigure, expect with specific heat capacity c. (D) Shows the relationship between t_{99} and c. Colour scheme as in (B) and (C).

might indicate that there is a similar mass gain relationship underlying the 'pseudo-stabilised' samples, but which is masked by the early stage of the mass gain curve, which is very rapid, and consequently very sharp (which leads to low values of t_{99} calculated from the fitted parameters).

Another relationship seems to exist between fmg and specific heat capacity, as well as fmg and t_{99} (Fig. 5.19 (C) and (D)). High values of fmg are associated with increasing values of c (particularly for those samples which 'pseudo-equilibrate'), although the effect is not evident for all samples, and might be poorly constrained by the large uncertainties on these measurements. It is not known why this should be the case, but specific heat

capacity will clearly depend on the elemental composition, as well as the presence of any vitreous phases.

The only element which corresponds (weakly) to fmg is iron (Fig. 5.19 (B)). High relative amounts of iron are associated with very low fmg, and non-stabilisation behaviour, although the effect is not evident in all samples. For example, although samples ECα-A9 and KCα-A3 have similar relative amounts of iron ($\sim$ 4.8-4.9), they have very different values of t_{99} (8.2 and 520 hrs respectively).

5.4 Discussion and findings

What are the most likely causes of non-stabilisation of m_2? The various explanations will now be evaluated in light of these new results.

5.4.1 Physical effects

Although a significant phenomenon, it seems unlikely that hydration of T0 water is the most significant cause of long-term instability in most samples. One reason is that a Lagergren-type rate law is not an appropriate fit to the mass gain curves, and there is clearly some other behaviour which is not accurately described by a Bowen et al. (2013) model. However, the evidence presented for terracotta indicates that sample thickness does seem to play a role in the rapidity of stage II onset. t_{99} ranged from 4.3 h and 46 h for identical samples of thicknesses between 4.2 and 9.2 mm. If this relationship is then extrapolated to the maximum thickness of the historical bricks (35 mm), then one obtains a t_{99} of 1810 hours, which is the same order of magnitude observed independently for some of the bricks (PBγ-A2). This might suggest that, for some samples at least, uptake of T0 water may be a cause of long-term instability. However, it does not explain the variability between sample to sample, as the historical bricks were cut into similar dimensions, and about half showed pseudo-stabilisation.

5.4.2 Thermal effects

Thermal effects on early-stage mass gain involve the rate of cooling of each sample, which is predicted to depend on parameters such as porosity, specific heat capacity, and density. Because these parameters will change from sample to sample, the rate will be different, and therefore it may take longer for some samples to reach isothermal mass gain. Since there is not much dependence between fractional mass gain (450-500 h) and porosity, specific heat capacity, or density of the historical bricks, this might suggest that thermal effects are insignificant at very large times. One important thing to consider is that non-stabilisation is usually a very small effect - of the order of 10^{-3} to 10^{-5} for fractional mass gain between the 450^{th} and 500^{th} hour of measurement. An estimate can be made of the likely magnitude of mass gain due to an accelerated rehydroxylation reaction several hundred hours after removal from an oven, and compared with the observed magnitude of non-stabilisation. Consider the exponential relation given by Eq. 5.5, which is an approximation for the temperature change in a sphere which cools by convection.[6] If this assumption is reasonable in the case of archaeological ceramics, then the time constant Λ in Eq. 5.5 is approximately equal to $d\rho c/6H$, where d is the sample diameter, and H is the heat-transfer coefficient. H can be estimated from its relationship with Nusselt number, Nu. For heat transfer at the boundary surface of a sphere undergoing forced convection, $\mathrm{Nu} = Hd/\lambda_{\mathrm{N_2}} \approx 2$ (Nield and Bejan, 2006), where the thermal conductivity of nitrogen is $\lambda_{\mathrm{N_2}} = 0.026$ W m^{-1} K^{-1}. For a sample of diameter 35 mm, we have $H \approx 1.5$ W m^{-2} K^{-1}, and for samples which decrease to 10mm we have $H \approx 5$ W m^{-2} K^{-1}. 1.5 W m^{-2} K^{-1} is perhaps unreasonably low, because the Nusselt number will also increase with sample dimensions, but is included here as an extremely conservative estimate, which in turn places an extremely conservative upper bound on the magnitude of accelerated rehydroxylation mass gain after heating, since Λ will be very high.

A simulation of the effect can be found in Fig. 5.20, which shows two numerical results obtained for two different scenarios. Code can be found in Appendix C. Both theoretical

[6] Here I am grateful to Prof. Christopher Hall for outlining this approach in personal communication, 3 March 2016. See also derivation of differential equation describing rehydroxylation kinetics in Hall et al. (2013).

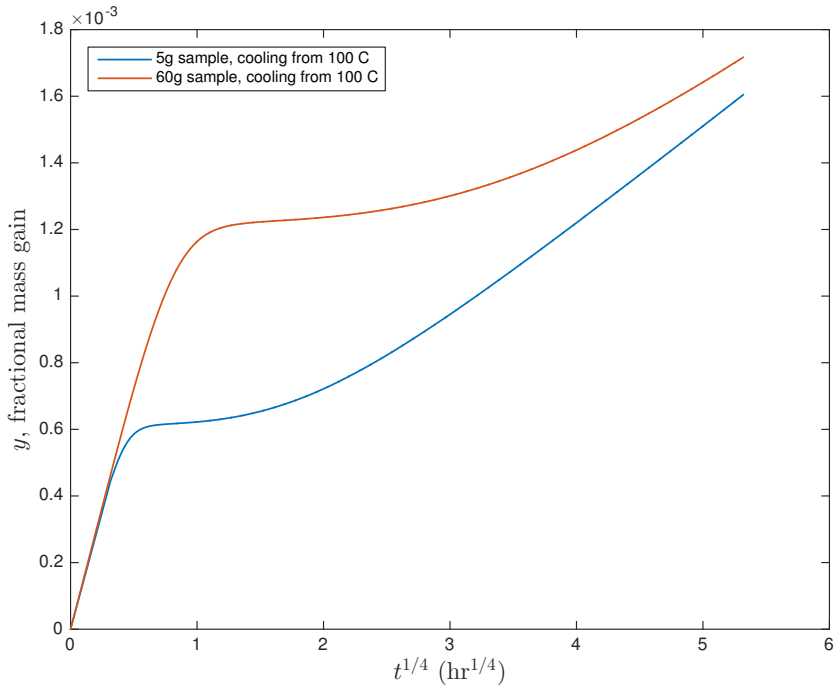

FIGURE 5.20: Numerical simulation of an accelerated rehydroxylation reaction following cooling from 100^{o}C to 18^{o}C, assuming rehydroxylation begins at 100^{o}C, and follows $t^{1/4}$ kinetics. Blue curve shows 5g sample with parameters $H = 5$ W m^{-2} K^{-1}, $\rho = 1.7$ g cm^{-3} , $c = 777$ J kg^{-1} K^{-1} and $d = 0.01$ m. Red curve shows 5g sample with extremely conservative parameters $H = 1.5$ W m^{-2} K^{-1}, $\rho = 1.96$ g cm^{-3} , $c = 948$ J kg^{-1} K^{-1} and $d = 0.035$ m.

samples have the same rehydroxylation rate constant, $\alpha = 0.0003$ h$^{-1/4}$ at 18 ^{o}C, but the larger sample has conservative values of H, ρ, c. For this sample (blue curve) the values of ρ and c are set as the maximum ranges of the measured values for historical bricks, along with $d = 35$ mm. A noticeable deviation from linearity is observed for $t > 600$ h, which is also noted when H is adjusted to a larger value of 5 W m^{-2} K^{-1}. On the other hand, the red curve shows a smaller sample (5 g) with the lowest values of c and ρ noted for historical bricks. For this sample, there is little deviation from linearity with $t^{1/4}$ at large times. Therefore it is noted that accelerated mass gain due to a faster rehydroxylation reaction following cooling cannot be ruled out for some ceramics, specifically following dehydroxylation at $> 500^o$C (assumed in the above simulation). The effect would also be stronger for samples which begin to rehydroxylate at temperatures higher than 100 ^{o}C, which delays linearity of stage II, and may complicate fitting to determine α_{m}. However, in this Chapter we are not strictly concerned with the initial dehydroxylation (only the non-stabilisation upon reheating to 105^{o}C at long times). The implication that an accelerated rehydroxylation reaction may cause lengthy times until isothermal

mass gain (and therefore estimation of α_{m} will be examined further in Chapter 7.

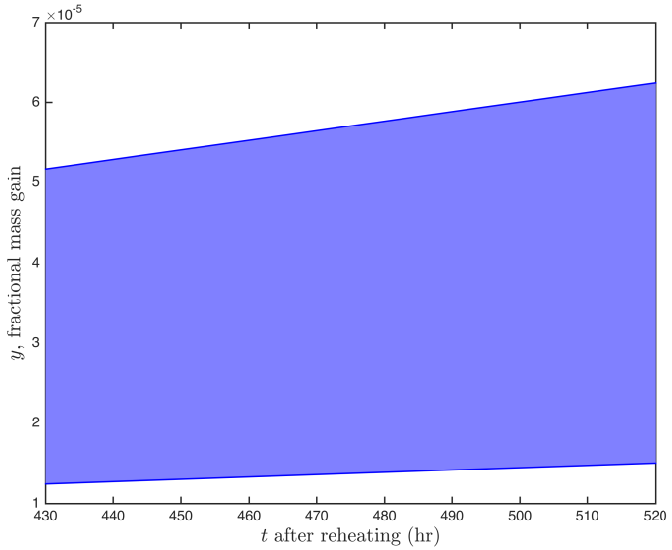

FIGURE 5.21: Range of fractional mass gain associated with rehydroxylation reaction following cooling from 100^{o}C to 18^{o}C, and assuming heating occurs 2 years after initial firing. The parameters are a 60 g sample with $H = 5$ W m^{-2} K^{-1}, $\rho = 1.96$ g cm^{-3} , $c = 948$ J kg^{-1} K^{-1} and $d = 0.035$ m, which are conservative values. The top bound indicates a simulation for a high rate constant ($\alpha = 0.00075$ h$^{-1/4}$), and the lower bound represents a low rate constant ($\alpha = 0.00018$ h$^{-1/4}$).

In modelling the non-stabilisation of m_2 we need to consider the fact that an archaeological or historical sample is fired many years before the m_2 step. When first analysed in the laboratory, fractional mass gain will obviously be much smaller because of the effect of the power law at large times. Fig. 5.21 shows the effect on late stage mass gain. Here, simulations proceeded as follows. First, a temperature profile was constructed. A 60 g sample ($H = 5$ W m^{-2} K^{-1}, $\rho = 1.96$ g cm^{-3} , $c = 948$ J kg^{-1} K^{-1} and $d = 0.035$ m) was assumed to begin rehydroxylation at some point during cooling from high temperatures. It seems plausible that $t = 0$ corresponds to 100 ^{o}C. The sample achieves thermal equilibrium with the chamber (18 ^{o}C) according to Eq. 5.5 after many hours. Then, at $t = 17520$ h (approximately 2 years), when y is small, the sample is heated to 100^{o}C, and allowed to cool to 18 ^{o}C again. Fig. 5.21 shows the effect between $t = 17520$ h and $t = 18320$ h (i.e. 800 hours after reheating). The area on the graph corresponds to fractional mass gain between two extreme values of α, 0.00018 h$^{-1/4}$ and 0.00075 h$^{-1/4}$. This area is the likely region of fractional mass gain for a large range of samples, with the most conservative estimates of H, ρ, c and d. Between the 450^{th} and 500^{th} hour after reheating, the curve shows a range of fractional mass gains between 10^{-5} and 10^{-6},

which is approaching the detection limit for a conventional microbalance. This range is smaller than the expected magnitude of the observed non-stabilisation behaviour at 10^{-3} to 10^{-5} (compare, for example, Fig. 5.15). Therefore it seems unlikely that acceleration of rehydroxylation during reheating to 105 ^{o}C is responsible for non-stabilisation. The finding is reinforced by the data for historical bricks, which showed no obvious correlation between non-stabilisation behaviour and c or ρ.

It is briefly noted that the simulated fractional mass gains which immediately follow reheating to 100 ^{o}C are much lower than the initial behaviour noted for historical bricks, which gained up to 1% of their nominal mass in the first few hours. This behaviour is more adequately described by a Fickian-type diffusion regime, because of the magnitude of the mass gain, as in light of the evidence presented here for dependence on sample dimension.

5.4.3 Chemical effects: hydration of carbonate and other species

Contrary to the suggestions of previous authors (Wilson et al., 2013), FTIR spectra suggest that the hydration/recarbonation of lime is not responsible for the non-stabilisation behaviour. This is supported by the gravimetric experiment on montmorillonite clay to which calcite was added before firing. No correlation was also observed between non-stabilisation and the relative amounts of Ca determined by EDS, which support the FTIR spectra, and the gravimetric results independently. The agreement between FTIR and EDS also suggests that powdering and homogenising samples is a valid approach for comparing relative amounts of Ca.

Cultrone et al. (2004) considered that the primary influence on the porosity of bricks was the presence of carbonates, which they found promoted the formation of fissures and pore sizes under 1 μm in diameter when fired between 800 and 1000 ^{o}C. These authors obtained porosity and pore size distribution measurements by mercury intrusion porosimetry, in combination with SEM image analysis. They also monitored the uptake of water after heating to 110 ^{o}C. One sample of brick clay contained significant carbonates (calcite and dolomite with a micritic texture), and another sample had no

carbonates, but a higher proportion of clay minerals and quartz. Upon firing and subsequent reheating, the calcite-containing bricks in Cultrone et al. (2004) lost water much more slowly than the calcareous bricks (compare 'G' and 'V' samples in Fig. 3a/b of that paper), and fractional mass gain upon uptake of water was also slower. They contend that the pore size distribution (and fissures) is a more important predictor of slow uptake than effective porosity. The latter decreases with firing temperature, along with pore size, but there is an increase in pore connectivity which ultimately leads to more and slower uptake of water than the non-calcareous samples (which have low porosity, low pore connectivity). No obvious correlation between residual Ca and effective porosity is evident in the historical bricks in the present study, and pore size distribution measurements are needed to further evaluate this hypothesis.

Another possible cause of non-stabilisation might be the vitreous components of highly fired ceramics, which may react with moisture to form hydrous minerals under environmental conditions (Hamilton and Hall, 2012). The effect was noted in an early study by Schurecht and Pole (1929), who found that a mixture of pure clay and feldspar exhibited little moisture expansion after firing. In contrast, the addition of silica temper resulted in a significant increase in moisture expansion. Several authors (Cultrone et al., 2004; Hamilton and Hall, 2012; Shoval et al., 1991) have also found that calcium silicates may form at higher temperatures ($> 1000\ ^{o}$C), as well as other mineral phases such as mullite (particularly in 2:1 clays) and haematite. The formation of these phases coincides with irreversible changes in the original clay minerals, which decrease the extent of reversible dehydroxylation (decreasing meta-stability), as indicated by FTIR spectra in the study of Shoval et al. (1991). If high temperature phases cause long-term fractional mass gain, then one might expect that lower OH peaks in FTIR spectra coincide with non-stabilisation behaviour, since the absence of OH peaks may be regarded as an indication of irreversible changes in highly-fired material. Superficially, this appears to be the case in the data presented here. Meta-clays tend to survive to higher temperatures in the absence of lime, which has been pointed out by Hamilton and Hall (2012). Therefore, some highly-fired materials may still present with strong OH peaks, if the amount of CaO in the ceramic matrix is low. The corollary is that high-fired low CaO ceramics should not show non-stabilisation. In the present study, there does not seem to be such a

correlation. However, without an accurate estimate of firing temperature this hypothesis is difficult to evaluate in more detail.

With regard to rehydroxylation, Burakov and Nachasova (2013) suggested that the formation of iron hydroxides (from haematite/magnetite) is a significant source of extra mass gain. The relationship noted between iron and fractional mass gain (Fig. 5.19 (B)) shows that the two samples with the highest amount of iron show visible non-stabilisation behaviour (but small fractional mass gain). However, two samples with the lowest amounts of iron also did not stabilise, which means that the effect is not consistent.

5.4.4 The model of Gallet and Le Goff (2015)

Perhaps a more compelling factor influencing non-stabilisation is underlying clay mineralogy. The difference in fractional mass gain (and t_{99}) between montmorillonite and kaolinite is clear. This shows that montmorillonite is much less stable, which may be an indication that uptake of T1 water is responsible for non-stabilisation. The finding is expected, since T1 water is lost fairly continuously up to $\sim 300\ ^{o}$C. These samples were fired at 825 ^{o}C, which is low enough to ensure meta-stability, without much vitrification.

In the Gallet and Le Goff (2015) model, it was proposed that three processes are at play. T0 water obeys a Lagergren-type relation, whereas T1 water uptake is associated with a normal diffusion regime ($t^{1/2}$), and rehydroxylation is associated with some form of subdiffusion ($t^{1/4}$ or similar). By heating to 105^{o}C, all three forms of water are removed, to varying degrees. Upon subsequent removal from the oven, the degree to which one process dominates over the other corresponded to the diversity and size distribution of available cracks/interlayer spaces, as well as the availability after each heating of vacant sites in the clay mineral matrix. In terms of mass gain, this means that observed time dependence is therefore neither $t^{1/2}$ or $t^{1/4}$, but some combination of the two (with the addition of a T0 Lagergren component). Therefore, in smectites one might expect there to be a greater proportion of T1 sites, and consequently a greater fractional mass gain associated with a long-lived $t^{1/2}$ regime. This is in agreement with the data presented here. Although a Lagergren-type equation is a good fit to the data ($R^2 > 0.99$), fits to a

Lagergren plus $t^{1/2}$ relationship (not shown) are generally in slightly better agreement, with lower residuals. However, contrary to Gallet and Le Goff (2015), FTIR spectra show that samples with small T1 OH peaks are associated with non-stabilisation, and long t_{99}. On the other hand, the fact that greater fractional mass gain is present in pseudo-stabilised samples might indicate that the same process is at play, but is simply over more quickly.

The experiment on quenched terracotta also implies that much of the initial mass gain behaviour after reheating at 500 ^{o}C is associated with long-lived uptake of T1 water, since quenching samples should help to saturate this component quicker than hydrating in air. It is briefly noted that this might be an option for a future dating methodology.

One intriguing finding is that the structural hydroxyl peak at $\sim$ 3620 cm^{-1} is not very visible on any of the FTIR spectra in this work. The IR spectroscopic study of Clegg et al. (2012) has been regarded as evidence for the association of a $t^{1/4}$ regime with structural OH. However, closer inspection of the data in Clegg et al. (2012) suggests that these spectra predominantly show growth in the broad shoulder associated T1 water, which continues over the duration of measurement (1 month). The thermo-gravimetric analysis of Shoval and Paz (2013) also seem to provide good support for a long-lived temporal dependence for T1 water, since the masses lost upon heating to 350^{o}C are broadly correlated with the age of the ceramic (see Fig. 2 of that paper). Therefore, it seems that another argument can be made that mass gain is mostly characterised by T1 water, with relatively little T2 component. This supports the model of Gallet and Le Goff (2015). More FTIR data from pure clays, heated at different temperatures, is needed to assess this hypothesis properly.

5.5 Summary

This chapter examined the non-stabilisation of mass after heating to 105^{o}C or higher, which is currently required to estimate m_2 in the rehydroxylation dating methodology of Wilson et al. (2012). Based on mass gain experiments on a range of bricks and archaeological materials, a pattern is noted whereby low fractional mass gain is associated

with clear non-stabilisation behaviour. However, even in the most well-behaved samples, which generally display high fractional mass gains, it seems that there is some degree mass gain between 450 and 500 h after reheating at 105^{o}C. The amount of calcite, in itself, is not a good predictor of non-stabilisation, and neither is the amount of iron. Experiments on calcareous montmorillonite showed little effect on the rate of uptake following heating to 500 ^{o}C, which effectively rules out any uptake due to hydration of lime at lower temperatures. However, this is only the case in montmorillonite, and other clay minerals may behave differently when fired. This finding suggests that acid pretreatment might not be necessary in samples with high smectite/2:1 clay mineral content.

The experiments showed that there is little obvious correlation between non-stabilisation and physical parameters such as porosity, specific heat capacity or density. However, the strongest effect is that of sample dimension (thickness), which is found to cause long-times to stage II data following higher temperature heating ($<$ 500 ^{o}C). These times are roughly proportional to the thickness squared, which suggests long-lived contributions from Fickian diffusion. In some cases, thicker samples also may lead to acceleration of the rehydroxylation reaction after reheating to 500 ^{o}C. However, on the basis of numerical simulations, an accelerated effect of of mass gain due to increased rehydroxylation during slow cooling seems unlikely to produce the magnitude of fractional mass gain observed in several samples of historical bricks and archaeological ceramics when reheating to 100 ^{o}C after several years. It is briefly noted that in the case of heating to 500^{o}C, the effect of sample dimension creates the need for a trade off between sample size and precision. Thicker samples will need more time for uptake of T0 water, as well as isothermal T2 mass gain. Thinner samples would avoid long initial times for stabilisation, but at the expense of providing less precision in α_{m}.

Another plausible explanation is that non-stabilisation might be caused by the vitreous components of highly fired ceramics, which react with moisture to form hydrous minerals under environmental conditions. Here the crucial factors are the amount and type of temper, in combination with firing temperature.

For some samples, FTIR spectra indicate that uptake of T1 might be a cause of long-term instability, but this behaviour is hardly clear, and in many cases the opposite relationship is observed. Clay minerals with high original T1 water content, such as montmorillonite, display higher fractional mass gains, and greater sensitivity to R.H.. More spectroscopic data from montmorillonite and kaolinite is perhaps needed to properly evaluate this hypothesis, as it is currently impossible to properly distinguish between thermal effects and the effects of long-term T0/T1 uptake. For future experiments, FTIR experiments on pure clays, as well as further mineralogical characterisation and the measurement of pore size distribution would greatly help to elucidate the various contributions to anomalous mass gain.

Chapter 6

Results of dating experiments on samples of known age

This Chapter will present rehydroxylation age determinations for a variety of clay standards, as well as one subsample of Werra earthenware from Enkhuizen, Netherlands. Other subsamples of Werra have already been dated in other laboratories (Wilson et al., 2012; Nümrich et al., 2015), and the test should provide a good comparison of instrumental precision. Clay standards were chosen for a number of reasons. First, RHX age determinations of precision < 10 % should be possible on these materials, given well designed experiments. This was shown in Chapter 2 (see Fig. 2.5 A). Second, various compounds can be added to these relatively pure clays in order to evaluate the practical effects of RHX interferents (discussed in Chapter 3/4) to be evaluated. Evaluating the effects of chemical pretreatment on archaeological samples (e.g. Nümrich et al. (2015)) is inherently problematic, since there will be considerable variation in the quantity of interferent from subsample to subsample. Using the same clay mineral standard can therefore provide a useful measure of the efficiency of a pretreatment protocol, as well as the extent to which chemical pretreatment effects structural OH. Third, the samples can be fired under the same controlled conditions, and stored at different temperatures, which can be recorded over their history. Accurate effective lifetime temperatures can therefore be estimated, with greater precision than environmental samples. Third, by using different clay mineral groups (i.e. kaolinite and montmorillonite) it is possible

to evaluate if there is any mineralogical correlation with RHX age determination, or if there is variation in the $t^{1/4}$ power which might be explained by the microstructure of the individual meta-clay.

6.1 Materials and Methods

The materials here comprised four samples of montmorillonite K-10 and four samples of kaolinite (Fisher Scientific, U.K.), with negligible Ca and organic content, which were formed into 10g samples with the addition of milli-Q water, as in the previous Chapter. The samples were designated 'M' or 'K' for brevity. One sample, M23, was montmorillonite to which calcite was added (previously presented in Chapter 5). All clay samples were fired at 825 ^{o}C on 31 January 2015, for 7 hours, and removed from the oven at 550 ^{o}C. Half the samples were placed in a sealed incubator at 22.6 $\pm$ 0.1 ^{o}C, whilst the other half were placed in a similar incubator at 18.1 $\pm$ 0.2 ^{o}C. In principle, having two samples (two clays) with two different activation energies should allow for the calculation of lifetime temperature (as suggested by Moinester et al. (2014)), which can be compared with the known values. Two samples of kaolin, K1 and K2, and one sample of montmorillonite, M20 were stored in the 18.1 ^{o}C incubator. Two samples of montmorillonite, M21 and M23, and one sample of kaolinite, K7 were stored at 22.6 ^{o}C. In order to test the effect of chemical pretreatments, before the gravimetric experiment, M21 was treated with 0.1M HCl for 10 minutes, followed by three rinses of milli-Q water. Nümrich et al. (2015) recommended 1M HCl at 60^{o}C for 30 minutes. However, 0.1M was chosen on the basis of the FTIR spectra in Chapter 4, which show clear effects in these materials at stronger concentrations. Any increase in T1 water (as evident in Fig. 4.3) due to this pretreatment should result in a significantly older age determination (relative to M20, which is the control). Nümrich et al. (2015) found that an acid plus oxidation treatment was the most effective at removing organic interferents. Therefore, to test the effect of oxidation, a similar procedure was carried out on K1. After treatment with 0.1M HCl at room temperature, and subsequent rinses with milli-Q, the sample was treated with 30 % H_2O_2 for 12 hours. This sample was then be compared with K7 and K2.

In addition, the efficiency of organic extraction with supercritical CO_2 was evaluated by three samples of terracotta, fired under the same conditions as above. Olive oil was added to one sample, whereupon all samples were treated at 150^{o}C for 2 hours to simulate thermal lipid degradation. Two of the samples were then treated with supercritical CO_2. A third sample acted as control. Any change to structural OH due to this treatment, as well as incomplete organic removal, should be reflected in additional mass loss, and consequently RHX age determination.

FIGURE 6.1: $\sim$ 10 g Kaolin and montmorillonite clay standards fired at 825^{o}C for 7 hours. The samples are stamped with a reference number to aid identification.

6.2 Dating methodology

The dating methodology follows that of Wilson et al. (2012), outlined in Chapter 1. However, there are three modifications. First, the m_2 estimation step was conducted by filling the chamber with N_2 at near-zero R.H., then allowing samples to equilibrate at the same R.H. and temperature used in the subsequent RHX step. This avoids the issues of non-stabilisation by heating to 105^{o}C, which were covered in the previous chapter, and allows the (Fickian) diffusion characteristics of each sample to be evaluated (to obtain

a rough estimate of t_{99}, which informs the range over which subsequent fitting of α_{m} is performed, under the assumption that there is no T1 component). Second, after the 500^{o}C step, samples of kaolinite, montmorillonite and terracotta were kept out of the oven, and were placed in the carousel along with their reheated partner samples. This procedure was followed by Nümrich et al. (2015), who used the variation in the masses of partner samples to with relative humidity to construct a first order correction for the heated samples. Although the present apparatus does have humidity control, this procedure was followed here to attempt to minimise small non-linearities in stage II data which are the result of < 0.5 % variations in relative humidity. Third, in the original method samples were reheated to complete (or near-complete) dehydroxylation. Since the original firing time is known for the clay standard samples in the present experiment (7h, 825^{o}C), reheating at the same temperature for the same period of time should be sufficient. However, dehydroxylation generally takes place at lower temperatures and times upon subsequent refiring. Like Wilson et al. (2012), the samples are reheated at 500^{o}C, but for 3 hours. This time and temperature was chosen to avoid further progressive dehydroxylation (and therefore reduction in the number of reactive sites in the meta-clay). It was thought better to err on the side of incomplete dehydroxylation, as any changes due to pretreatment in fired clay standards should still cause a relative changes in t_{a}, regardless of offset in true age.

In addition, an attempt was made at estimation of activation energy, ELT and α_{e}, which are required to correct an RHX age determination in the current methodology (Hall et al., 2013; Wilson et al., 2012). Here, temperature data from each incubator (logged at 30 minute intervals) were used to construct a continuous function via piecewise linear interpolation in MATLAB. Initial cooling rate was estimated as in Chapter 5, and combined with the interpolated function (which is most valid for long times after firing). α_e was computed from the combined time series using the numerical routine from the previous chapter (found in Appendix C) as the fourth power mean of $\alpha(t)$ over the temperature time series:

$$\alpha_{\mathrm{e}} = \left\langle \alpha(t)^4 \right\rangle^{1/4} . \tag{6.1}$$

6.2.1 Corrections for reference mass

The new apparatus for gravimetric measurements offers the opportunity to place a reference mass in the carousel, which allows corrections to be made for instrument drift. The reference mass is a stainless steel 10 g calibration weight, which is measured once per complete cycle (80 minutes). The instrument thus becomes a *mass comparator*, which should offer several advantages over a conventional setup. As seen in Fig. 6.2, the reference mass varies throughout the experiment (having a total range of about 50 μg). The variations exhibit no obvious correlation with temperature or relative humidity.

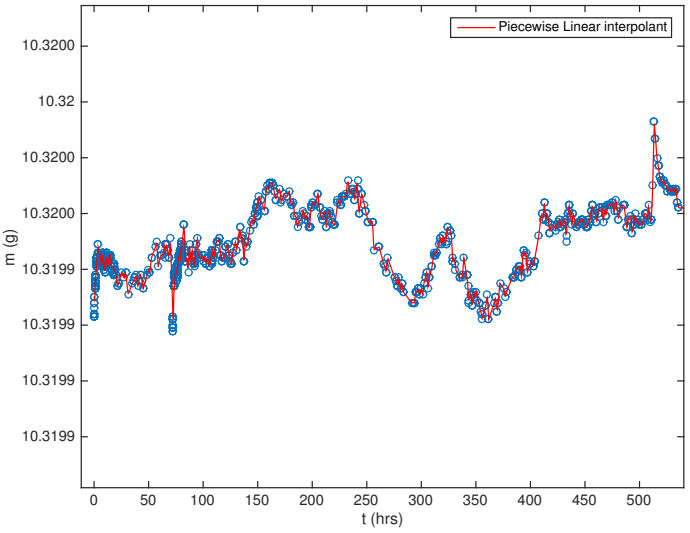

FIGURE 6.2: Correction function created by piecewise linear interpolation of calibration mass values over the course of an RHX experiment. The blue data show raw data of a 10 g calibration weight plus $\sim$ 0.3 g sample holder. The drift in calibration mass is of the order of 50 μg over 500 hours, and is independent of changes in chamber relative humidity, pressure, temperature or flow rate. The difference between interpolated values and the nominal mass are subtracted from all mass gain data.)

Ideally, the reference mass would be measured between each sample, but because the carousel is designed to rotate slowly and continuously, with continuous power from the DC motor, it has to be measured once per complete rotation. To have more frequent measurements of the calibration weight would require a more complicated mechanism with variable power output, therefore causing greater fluctuations in chamber temperature.

To get around this limitation, a piecewise linear interpolant was constructed from the reference mass time series. The reference mass was then interpolated at the time of each sample mass measurement, and the deviation from nominal mass subtracted from the sample mass. The maximum difference between successive reference mass measurements is 5 μg (per 80 minutes). The procedure is therefore essential for accurate sample mass estimation at large times when rehydroxylation is very slow, and greatly improves the smoothness of the mass gain curves.

6.2.2 Chamber stability

The chamber conditions for a typical run are presented in Fig. 6.3, along with a mass gain curve for MAN037 after reheating to 105^{o}C. The temperature in the chamber between 400 and 500 hours is 17.411 $\pm$ 0.003 ^{o}C, where the uncertainty is taken as the standard deviation of the six temperature measurements taken throughout the chamber. In Fig. 6.3 the total range between maximum and minimum temperature is shown ($\sim$ 0.15 ^{o}C).

Likewise, the mean relative humidity of the chamber was 39.11 $\pm$ 0.08 %, along with the total range of variation in RH, which is 0.3 %. On the second run, the chamber temperature was calculated as 18.438 $\pm$ 0.006 ^{o}C, and an RH of 49.24 $\pm$ 0.08 %, with slighter larger total ranges (0.2 ^{o}C for temperature and 0.4 % for RH).

6.2.3 Corrections for relative humidity

In addition to corrections for reference mass, a similar procedure was performed to correct for fluctuations in R.H. A piecewise linear interpolant function was obtained on non-reheated partner samples, after initial diffusion was judged to be complete. A simple first order correction was then constructed using the partner sample mass, together with RH data. If the mean mass is represented by m_{c}, and the RH is represented by RH_{c}, then we have:

$$m_{\mathrm{c}} = A(RH_{\mathrm{c}} - RH(t)) + m(t) \ . \tag{6.2}$$

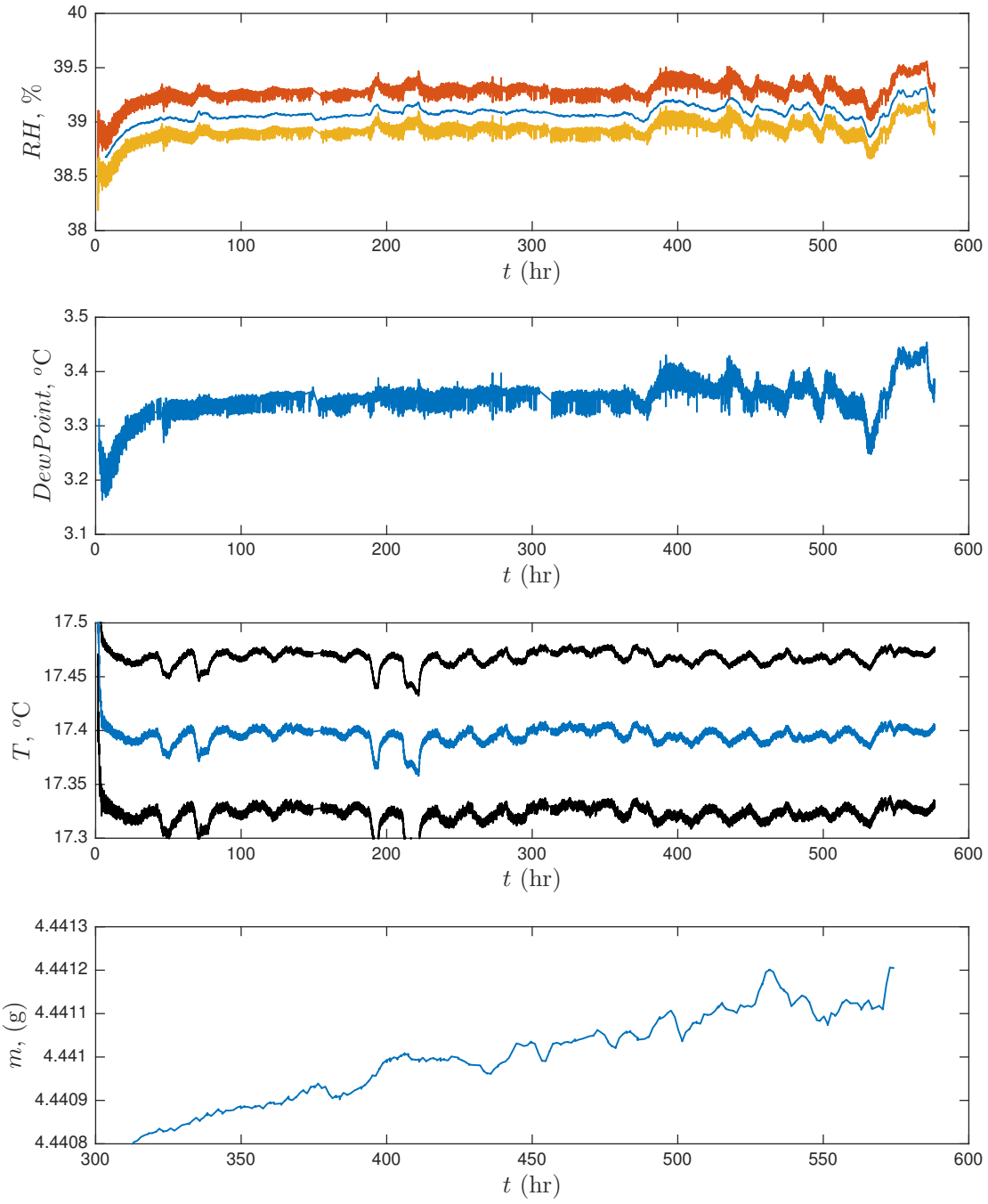

FIGURE 6.3: Chamber conditions for 550 hours during the run of the 21 Feb 2016. Top shows mean RH (blue curve) and range of RH computed from temperature range and dew point. The second graph shows dew point, and the third graph shows mean chamber temperature (blue), plus the temperature range inside the chamber (black). The bottom graph shows mass gain data for sample MAN037, which was reheated at 105^{o}C for 3 hours, showing non-stabilisation. Fluctuations in mass gain on the scale of a few hours are most correlated with changes in RH, but with a time lag, and the effect is not uniform throughout the mass gain curve.

Once the proportionality A is determined (by linear least squares fit), then it is possible to obtain the 'corrected mass' by the above equation, by substituting RH and m

measured at some time t.

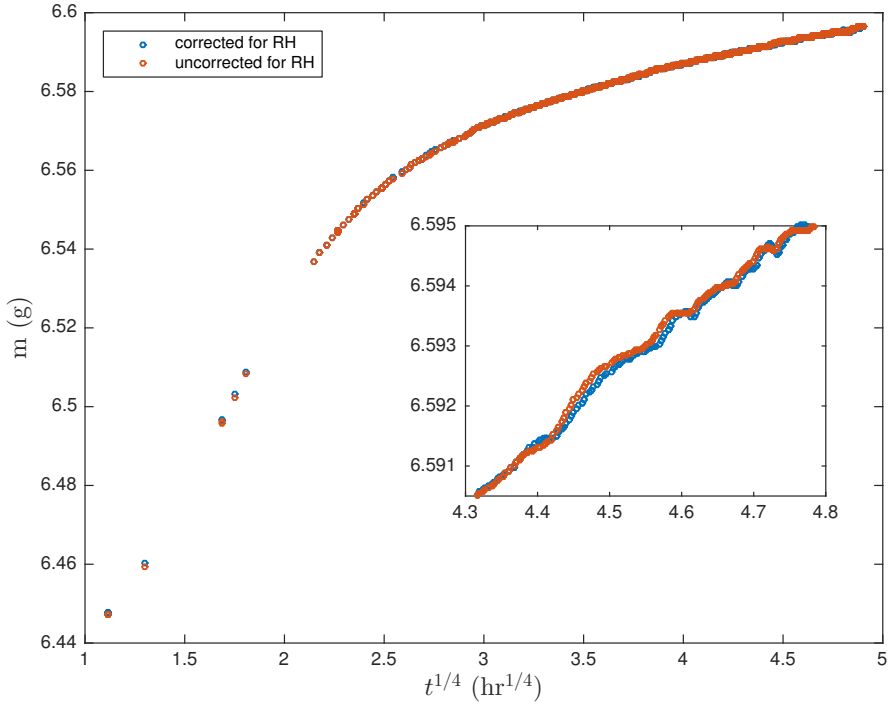

FIGURE 6.4: RH corrections for sample M21, with chamber conditions of T = 17.411 ± 0.003 ^{o}C and RH = 39.11 ± 0.08 %. Red curve shows data corrected for reference mass fluctuations, but not for RH. Blue curve shows first-order correction for RH (as suggested by Nümrich et al. (2015)), which was constructed by monitoring the mass of a paired sample which was not reheated at 500^oC.

The effect of this procedure can be seen in Fig. 6.4 for a sample of montmorillonite, which is the material most sensitive to changes in RH. It reduces the amplitude of the variations, but only slightly. This may be the result of the amount of time it takes for RH effects to be expressed as mass gain/loss in the sample, which is ultimately a function of the (Fickian) diffusion characteristics of the material. There might also be hysteresis in this behaviour. However, the procedure still reduces the overall scatter, and therefore we retain this correction for all data.

6.3 Results

The results of fitting to the stage II data, along with the m_2 estimation step, are presented in Table 6.1, along with the time range over which the appropriate fits were performed. Linear least squares fitting was performed in MATLAB, and the ranges adjusted manually until minimal scatter in the residuals was observed.

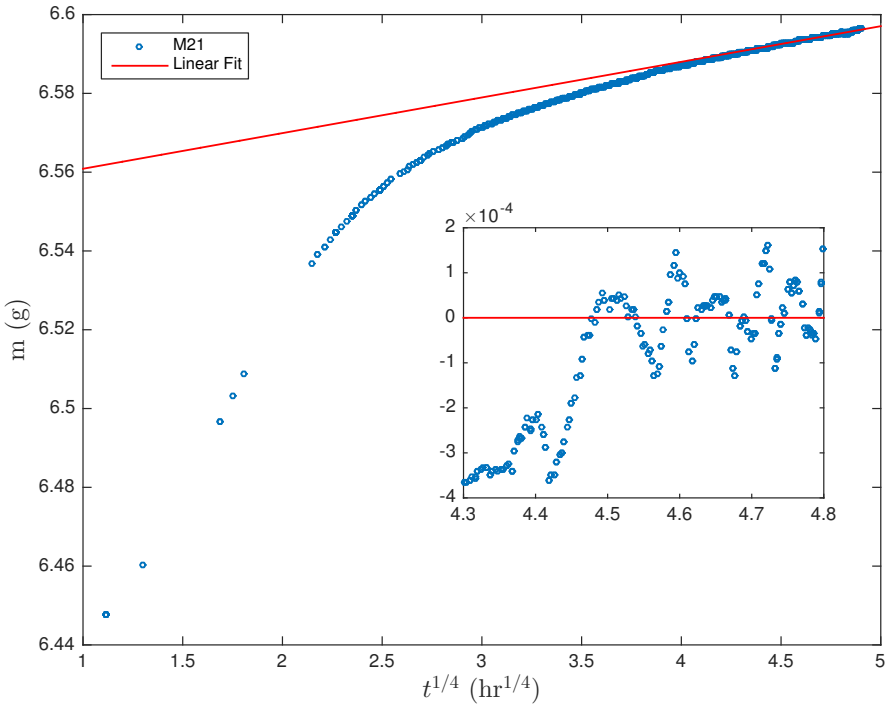

FIGURE 6.5: RHX fits for sample M21, with chamber conditions of T = 17.411 ± 0.003 ^{o}C and RH = 39.11 ± 0.08 %. Residuals are shown in the inset. Fitted parameters are α_{m} = 0.0093(1) g h$^{1/4}$, m_4 = 6.5505(5) g. The time selected for fitting was from 406 to 576 hours (4.48 to 4.90 h$^{1/4}$).

Figure 6.5 shows a typical fit to stage II data. The data are generally of a higher quality than has been previously obtained by this author (Hare, 2012), or Nümrich et al. (2015) or Bowen et al. (2013), and are comparable to the data obtained by Le Goff and Gallet (2014a), Le Goff and Gallet (2014b) and Gallet and Le Goff (2015), and in some cases Wilson et al. (2012). In some cases there are noticeable trends in the residuals; although in amplitude they are evenly scattered around 0, they exhibit an oscillation which is consistent with temperature fluctuations in the chamber. In most cases $R^2 > 0.99$.

Generally speaking, the stage II fits to the run at higher temperature (18.428 ^{o}C) are poorer (in the case of K2, R^2 = 0.5), and there was more scatter in this data than the former run at 17.411 ^{o}C. The reason for this is the greater instability in T and RH during this run, which are correlated with the scatter. RH became progressively unstable as the experiment progressed, most probably due to the desiccant cell of the humidity supply, which was running low.

With regard to trends, the measured rehydroxylation rate constants α_m of the three montmorillonite standards (M20, M23 and M21) were significantly higher than all other

samples, showing a range of between 9.8 ± 0.4 and 18.6 ± 2 mg $h^{-1/4}$. Kaolinite (K7, K2 and K1) on the other hand showed a range between 2.4 ± 0.1 and 4.91 ± 0.04, for higher values of m_4. Since the nominal masses of kaolinite samples were higher, this corresponds (roughly) to α in a range between 0.00028 and 0.0003 $h^{-1/4}$, which is within the range of α of materials from other studies. The acid treated kaolinite K1 had the highest α of the kaolinites at 0.0003 $h^{-1/4}$. The range of α for the montmorillonite samples is 0.0015 to 0.0016 $h^{-1/4}$, an order of magnitude higher than the kaolinite. The acid treated sample M21 had the lowest value of $\alpha = 0.0015$ $h^{-1/4}$. This is the higher than any value of α yet reported in all studies. The fact that the rate constant is higher for montmorillonite is also consistent with the finding in the previous chapter that montmorillonite had the highest fractional mass gain.

For all samples, there is a small but consistent decrease in the value of m_4 fitted between the run at 17.411 ^{o}C and 18.438 ^{o}C, ranging from about 2 mg to 30 mg depending on sample, which is higher than any drift due to reference mass. This may be due to the fact that the relative humidity was different in the second run. We use the value of m_4 deduced from the first run for two reasons. First, the T and TH of this run was the same as the T and RH of the equilibrium step, which is an important condition for the approximation $y_a \approx (m_2 - m_4)/m_4$. Second, the quality of data on this run is generally a bit better than the second run. Note that α_m should be the same at a range of humidities. The alternative explanation for the fact that m_4 is lower on the second run is that there was further progressive dehydroxylation caused by successive reheatings.

The uncorrected (t_a) and corrected ($t_{a,ELT}$) rehydroxylation age determinations are presented in Table 6.2, along with the calculated values of activation energy and α(ELT). E_a is very low for all samples, having a range of 21 ± 1 kJ mol^{-1} to 40.5 ± 15 kJ mol^{-1} for montmonillonite, and 4.9 ± 1 to 68 ± 1 kJ mol^{-1} for kaolinite. This is lower than the known ranges for archaeological materials, and the values here are clearly underestimates. It is likely that this results from the fact that only two temperatures were chosen for measurement of α_m, and the choice of temperatures is only ~ 1 ^{o}C apart. Ideally, E_a should be calculated from the slope of a graph of $\ln(\alpha_m)$ versus $1/T$, for at least

TABLE 6.1: Fitted values for samples following the equilibrium step (m_2), and two rehydroxylation setps at 500^{o}C. T_1 corresponds to 290.561 ± 0.003 K, and T_2 corresponds to 291.589 ± 0.006 K. 'T' indicates a sample of terracotta, 'M' montmorillonite and 'K' kaolinite. $\alpha_{\rm m}$ is reported here in mg h$^{-1/4}$. Also reported are the times over which the fitted data were performed (for the determination of $\alpha_{\rm m}(T_1)$). In most cases, similar times were taken for fits to the corresponding dataset for the T_2 run.

Sample	m_2 (g)	m_4 (g)	$\alpha_{\rm m}(T_1)$	$\alpha_{\rm m}(T_2)$	Fit times (h)
T (no SFE)	5.878670(2)	5.8560(1)	2.22(2)	-	311→550
T (SFE)	5.584799(2)	5.5440(1)	1.82(7)	-	410→550
T(lipid, SFE)	5.463321(2)	5.4490(1)	1.60(2)	5.4490(1)	326→487
MAN037	4.45139(1)	4.4390(2)	0.483(7)	2.16(9)	410→502
K7	9.776654(20)	9.7471(1)	2.741(2)	3.2(1)	326→570
K2	8.793538(5)	8.7541(6)	2.4(1)	2.59(7)	349→498
K1 (acid + ox.)	9.627719(2)	9.5620(5)	2.845(7)	4.91(4)	231→569
M20	6.424399(5)	6.238(2)	9.8(4)	18(3)	547→574
M23 (calcite)	6.063458(2)	5.939(5)	9.2(1)	17.5(2)	330→518
M21 (acid)	6.718930(5)	6.5505(5)	9.3(1)	18.6(2)	406→501

three temperatures, differing from one another by at least 5^{o}C. In the present case, the small temperature difference was a conservative choice because the new apparatus was not fully tested for month-long experiments at relatively lower or higher temperatures. However, the apparatus should be capable of reaching well below 5 ^{o}C, and about 30 ^{o}C, given the limit of 15 W per Peltier element. The present experiment was also limited in time, and therefore another rate measurement was not possible. This represents a limitation of the current analysis, but should be easily improved upon in future.

TABLE 6.2: Uncorrected and corrected rehydroxylation age determinations for clay samples and Werra ware, along with $y_{\rm a}$ and activation energy. 'T' indicates a sample of terracotta, 'M' montmorillonite and 'K' kaolinite. $t_{\rm a}$ is calculated at 17.411 ^{o}C, and is shown in years before reheating on the 21 Feb 2016, with measurement uncertainty at 1σ. $t_{\rm a,ELT}$ refers to the RHX age determination corrected to ELT, given the activation energy determined from each sample. Calculations based on alternative activation energies are given in the text.

Sample	$y_{\rm a}$ $\times 10^{-3}$	$\alpha(ELT)$ (h$^{-1/4}$)	$E_{\rm a}$ (kJ mol^{-1})	known age (a)	$t_{\rm a}$ (a)	$t_{\rm a,ELT}$ (a)
T (SFE)	3.9	-	-	0.3	1.23 ± 1	-
T (lipid, SFE)	7.4	-	-	0.3	29 ± 1	-
T (no SFE)	2.6	-	-	0.3	0.73 ± 0.01	-
MAN037	2.8	0.000084	49 ± 3	411	49 ± 4	134 ± 23
K7	3.0	0.00028	4.9 ± 1	1.1	1.56 ± 0.04	1.51 ± 0.04
K2	4.5	0.00029	23 ± 2	1.1	8 ± 2	8 ± 2
K1 (acid + ox.)	3.0	0.0003	68 ± 1	1.1	32.5 ± 0.3	30.1 ± 0.3
M20	29.8	0.0016	40.5 ± 15	1.1	14.8 ± 2.5	14 ± 2
M23 (calcite)	21.2	0.0016	21 ± 1	1.1	3.8 ± 0.6	3.3 ± 0.2
M21 (acid)	25.7	0.0015	22 ± 1	1.1	12.2 ± 0.6	9.5 ± 0.5

With regard to 'archaeological mass' y_a, montmorillonite showed the highest fractional mass gains, between 21.2 and 25.7 $\times 10^{-3}$. The acid treated sample M21 had a value of 25.7, which is slightly lower than the control sample M20 (29.8), but not as low as the calcareous sample M23 (21.2). However, it is difficult to compare raw y_a values as M21 and M23 were stored at different lifetime temperatures from M20. Likewise, the range of y_a of kaolinite is 3.0 to 4.5, but comparison is difficult. MAN037 had one of the lowest values of y_a of 2.8.

The estimated ELTs of montmorillonite were between 18.12 ^{o}C and 22.61 ^{o}C using the values of E_a presented in Table 6.2. ELTs are therefore close but not identical to the original temperatures, indicating that initial cooling effects make a small but significant contribution at the early stages of rehydroxylation. However, the values of E_a are quite low in this instance, and temperature effects will be stronger for higher E_a. For kaolinite, ELT ranges between 22.60 ^{o}C and 18.11 ^{o}C. The ELT of the Werra (MAN037) is not calculated directly, but was taken from Wilson et al. (2012) as 10.5 ^{o}C. Although E_a is different for Wilson et al. (2012), 10.5 ^{o}C is deemed sufficiently close to the true value for this sample.

6.4 Pretreatment effect on rehydroxylation age determinations

6.4.1 Uncorrected RHX age determinations

The uncorrected age determinations for all clay standard samples were calculated from $\alpha_m(T_1)$, and are mostly < 10 a, which is consistent with the recent firing (1.1 a). Note that uncertainties in RHX age determinations are calculated from Eq. 2.20, and are always reported at 1σ. Sample K1, which is the sample treated with HCl and H_2O_2, had the 'oldest' age of 32.5 ± 0.3 a. Likewise, sample M21 had a larger age of 12.2 ± 0.6. However, this age is similar to that obtained for the control sample M20 ($t_a = 14.8 \pm 2.5$ a), but the two samples have different temperature histories, which makes comparison

problematic. A greater age is expected for acid-treated samples, due to increased uptake of T1 water upon treatment with acid (as shown by FTIR in Chapter 4).

Since the three terracotta samples had the same lifetime temperature history, it is possible to compare t_a. The SFE-treated sample showed an age determination of $t_a = 1.23 \pm 1$ a, which is indistinguishable from the non-SFE treated sample ($t_a = 0.73 \pm 0.01$ a), which suggests that SFE does not affect structural OH. However, the lipid-containing sample which was treated with SFE gave an age of ($t_a = 29 \pm 1$ a), which is consistent with a small amount of extra mass loss due to organic burn off at 500^oC. Clearly, the SFE was not completely effective in removing the organic carbon. However, the RHX age determination is much more reasonable than that expected from significant lipid contamination, where the contribution to the overall mass of the sample could be as high as several percent, making RHX age determinations off by several thousand years. In any case, 30 years is the minimum age uncertainty for samples of archaeological age, which means that the residual effect of contamination following SFE is insignificant in comparison to the ceramic age. On this basis, SFE is therefore a promising candidate for minimally-destructive removal of significant quantities of lipids. However, much replication work remains to be done to investigate this further.

The uncorrected age of the Werra (MAN037) is the oldest at 49 ± 4 a, but is still significantly younger than the known age (411 a). However, this is not corrected for ELT.

6.4.2 Corrected RHX age determinations

The RHX age determinations, corrected for ELT using the values of E_a presented here, are found in the last column of Table 6.2. The effect of correction is to bring RHX age determination closer to the known age (1.1 a), but generally only by between 0.5 and 3 years. This is partly a consequence of small activation energy, which creates a very weak temperature dependence. Similarly, there are differences between acid treated samples and the control samples for kaolinite and montmorillonite, but it is difficult to properly asses these differences with more accurate activation energies, and/or replicate samples.

6.4.3 Calculations based on alternative E_a

Stevenson and Gurnick (2016) recently report activation energies for kaolinite and montmorillonite, fired at a range of temperatures between 600 ^{o}C and 900 ^{o}C. These values were determined by FTIR spectroscopic analysis, and are perhaps more reasonable values than presented here, because they are within the range of activation energies previously reported for fired clay ceramics. If we use their value for kaolinite fired at 800^{o}C, which is 76.7 kJ mol^{-1}, then we obtain corrected ages of 0.89 $\pm$ 0.02 a, 7.24 $\pm$ 1.8 and 29.64 $\pm$ 0.27 for K7, K2 and K1 respectively. This shows the similar relative changes as the previous activation energies, but futher adjust the dates younger (i.e. towards the known age). This is further evidence for inaccurate determination of activation energies in the previous section.

If the same procedure is performed for montmorillonite (E_a = 96.059 kJ mol^{-1} at a firing temperature of 900 ^{o}C), then we obtain $t_{a,ELT}$ = 13 $\pm$ 2 a, 5.8 $\pm$ 0.3 a and 1.48 $\pm$ 0.07 a for M20, M21 and M23 respectively. These are closer to the known values, but little inferences can be made with regard to relative differences, and the effect of acid.

With regard to MAN07, with an activation energy of 82.7 kJ mol^{-1} and at an ELT of 10.5 ^{o}C Wilson et al. (2012), $t_{a,ELT}$ = 169 $\pm$ 30 a. This is closer to the known age (411 a), but is still significantly younger. There are a number of possible explanations. It seems unlikely that this is an organic contamination issue (as found by Nümrich et al. (2015)), because the effect of organic contamination would be to give older dates, not younger. Another explanation is a error in fitting the slope to the stage II gradient, although for this sample there are not expected to be significant cooling rate effects which cause non-linearity in stage II data, given the dimensions and other physical parameters of this sample. A more plausible explanation is the limited reheating times (3 h). Dehydroxylation may take longer for this sample. Another possible explanation is a long-lived T1 uptake, which contributes to a $t^{1/2}$ regime which partly masks $t^{1/4}$-type behaviour, or that the power is not 1/4, but rather some value $1/N$, with $2 < N < 4$.

6.4.4 Same Age Samples (SAS) determination of ELT

Because two samples of two different materials (montmorillonite and kaolinite) were fired at the same time, and therefore should have the same lifetime temperature and age t_{a}, it should be possible to determine the effective lifetime temperature via the method proposed by Moinester et al. (2014), and under several assumptions. Further details can be found in Appendix A, but here the effective lifetime temperature is estimated by the following equation which follows Moinester et al. (2014):

$$T_{\mathrm{e}} = \frac{E_{\mathrm{a}'} - E_{\mathrm{a}}}{4\mathbf{R}ln\left(\frac{\alpha_{\mathrm{m}'}}{\alpha_{\mathrm{m}}}\right) + 4\mathbf{R}ln\left(\frac{m_2 - m_4}{m_2' - m_4'}\right) + \frac{E_{\mathrm{a}'}}{T_{\mathrm{m}}} - \frac{E_{\mathrm{a}}}{T_{\mathrm{m}}}} \ , \tag{6.3}$$

Where $E_{\mathrm{a}'}$ and E_{a} represent the activation energies of kaolinite and montmorillonite, and likewise $\alpha_{\mathrm{m}'}$ and α_{m} are the measured stage II rehydroxylation gradients at temperature T_{m}, and m_2', m_4' and m_2, m_4 correspond to the masses measured for the two materials. For the combination of M23 and T7 (which were kept at 22.6^{o}C), by 'same age samples' (SAS) method we obtain $T_{\mathrm{e}} = 61.85$ ^{o}C. And for the combination of M21 and K7, also stored at the same temperature, we obtain $T_{\mathrm{e}} = 132$ ^{o}C. These two temperatures are clearly much higher than the ELT. For the combination of M20 and K2 (kept at 18.1^{o}C), SAS yields $T_{\mathrm{e}} = 45$ ^{o}C, and for another combination of M20 and K1 (also kept at 18.1^{o}C) we obtain $T_{\mathrm{e}} = 38$ ^{o}C. Both of these values are lower than those obtained from the samples stored at 22.6^{o}C, but the two values are clearly not in agreement with each other. The relative difference between ELT obtained by SAS for the two different groups is intriguing, although there are clearly systematic errors in either the model or the measurements which a responsible for the significant offsets. It is briefly noted that a higher ELT would improve the accuracy of all of the dates presented here.

The SAS estimate of ELT is calculated under the assumption that only $t^{1/4}$ kinetics are present, and there is no T1 water. The fact that ELT estimated by SAS does not agree with the expected ELT is not surprising, given the lack of consistent dating results presented in the previous section, and may be an indication that there is some other extra mass loss due to T1 water, or alternatively that the process is not $t^{1/4}$. Another important assumption of using the above equation is that both samples have similar

ELT. This is unlikely to be the case if rehydroxylation starts at different temperatures upon initial cooling from firing. In other words, if rehydroxylation of montmorillonite starts at 150 ^{o}C and the rehydroxylation of kaolinite starts at 100^{o}C, then the difference between the ELT of the montmorillonite and the kaolinite is estimated to be $\sim$ 7 ^{o}C, using typical parameters for the rehydroxylation rate simulations presented previously. If rehydroxylation in montmorillonite starts at a higher temperature, 200 ^{o}C, then we have a difference in ELT of $\sim$ 27 ^{o}C. Such a difference in ELT between the two samples would make use of the SAS method impossible. The implication is that samples need to have similar ELT (and therefore mineralogy) for SAS to work.

6.4.5 Implications for pretreatment

What are the implications of the dating results for pretreatment methods? For the terracotta samples, the interpretation seems clear. The added lipid comprised $\sim$ 4 % of the mass of the ceramic. Therefore, for a sample without pretreatment, the extra burn off at 500 ^{o}C would be similar to the maximum y_{a}, which would give an age determination of several thousand years at the measured α. The fact that the maximum age is $\sim$ 30 years means that this pretreatment has removed most of the lipid. The fact that the sample is older than the assigned age could be a small residual organic burn off, and possibly also some accompanying rehydroxylation (which is difficult to tell). It seems unlikely that the method causes dehydroxylation.

For the montmorillonite and kaolinite samples, the interpretation is less clear. However, it seems that there is little difference between the calcareous montmorillonite and the control sample, which means that it is unlikely that calcite is either a category A contaminant or a category B contaminant. Then again, it might be both category A and category B. In this scenario the extra mass lost upon reheating (category A) is approximately cancelled out by the increased rate gain upon rehydration (category B), yielding the same age determination. However, it has previously been shown that there is little difference between the stage II rates for both calcareous montmorillonite and the control sample, which suggests that the presence of calcite is not a significant effect in general.

There are small differences in the RHX age determinations of the the acid-treated samples, but the differences are small and hard to interpret. Like the terracotta, all age determinations for the fired clay standards are less than a few decades, which might indicate that the effects caused by chemical pretreatment are not strong, although the scenario of both category A and category B contaminants (as above) cannot be ruled out. The weak effect of acid pretreatment contradicts the finding of Chapter 4 that acid causes the uptake of T1 water and attacks clay mineral structure, but it may be that the concentration and acid used in the dating experiment (0.1M HCl) is sufficiently low as to not cause de/rehydroxylation. Further FTIR data on the samples and chemical pretreatments on much older materials would both be needed to provide clarity on this issue.

6.5 Summary

In this Chapter I presented gravimetric RHX data which attempted to replicate the method of Wilson et al. (2012), with minor modifications. The experimental apparatus shows acceptable performance, particularly for a chamber of this size. Particularly good control of temperature was achieved. However, variations in RH cause significant variation in mass gain curves, which are only partially remedied by the current correction strategy, which is based on Nümrich et al. (2015). More subtle and effective correction strategies are perhaps possible.

RHX age determinations for several samples of fired clay standards were presented which show variable results, but which are generally plausible given the known age. However, a more nuanced interpretation of the differences between pretreatment regimes, particularly treatment with 0.1M HCl, is problematic, given the inconsistent behaviour of samples, and the lack of replicates. The RHX age determination on the sample of archaeological Werra ware did not agree with the known age, which has several possible explanations.

Corrections for lifetime temperature effects improve the accuracy of RHX dating, but only slightly. Activation energy should be determined by measurements of α_{m} at a

minimum of three temperatures, with $\sim$ 5 ^{o}C differences between temperature. This should be within the capabilities of the current instrument.

The calculated ELTs, as determined by same age samples (SAS) method, are inconclusive. However, the relative difference between ELTs of both sets of samples kept under different conditions is promising, and deserves a fuller investigation and more replication. However, there are strong theoretical considerations which suggest that ELT may not be the same for different clay minerals, which means that the SAS method may be invalid in its current form.

On the basis of experiments with terracotta, SFE shows promise as a potential pretreatment method for degraded lipids, which is expected to be a common organic interferent in archaeological pottery. The residual effect of contamination following SFE is insignificant in comparison to the minimum level of combined measurement uncertainty associated with RHX age determinations on old ceramics. However, further replication on archaeological samples of greater age is necessary to determine the true effectiveness of this promising pretreatment strategy.

Chapter 7

Implications for the power law

7.1 Overview[1]

Several authors have suggested that long-term mass and strain data are best fit by a $t^{1/N}$ power law model with N closer to 3 or 2 (Le Goff and Gallet, 2014c; Bowen et al., 2013) as opposed to $N = 4$ obtained for datasets by Wilson et al. (2003) and Hall et al. (2011). Subsequently, Gallet and Le Goff (2015) have suggested that the mass gain behaviour reflects the sum of two long-lived temporal regimes: a slow progressive $t^{1/4}$ rehydroxylation, and an ordinary $t^{1/2}$ diffusion process. The purpose of this chapter is to investigate the value of the power $1/N$ of the time dependence of mass gain, and the relationship between different models and diffusion phenomena.

No clear consensus has emerged as to the value of the power, or its variability with different fired-clay ceramics, as well as the relationship between the power and diffusion mechanisms. Wilson et al. (2003) and Savage et al. (2008) linked the $t^{1/4}$ behaviour to theoretical models of single-file diffusion (e.g. Levitt (1973)), which have predicted that the mean square displacement $\langle x^2 \rangle_{sf}$ of a diffusing particle is proportional to $t^{1/2}$. Savage et al. (2008) suggested that this leads to $t^{1/4}$ kinetics because the distance travelled by the queue of molecules is proportional to the amount of reaction, and therefore mass gain/expansion. In this scenario, it is also not clear where such single-file diffusion should

[1]Some of the ideas presented here are briefly discussed the recent paper Hare (2016), but in this chapter a more detailed analysis will be provided.

occur. The possibilities include (a) the collapsed interlayer spaces, and (b) through the 6-ring of the silica tetrahedral layer to inner structural OH sites (suggested by Mazzucato et al. (1999) for mica). However, these hypotheses are difficult to evaluate because there is currently a lack of spatial/structural evidence for meta-clay structure, and there is also disagreement over the value of the $1/N$ power as determined from mass gain and expansion experiments.

A key question is therefore the level of uncertainty associated with $1/N$. One challenge is that goodness-of-fit statistics tend to be high for several values of N. Another challenge is that fits are sensitive to the choice of m_4 and t_0, the time offset (e.g. Barrett (2013). In Chapter 5 it was also first identified that a temperature-accelerated rehydroxylation reaction may cause lengthy times until stage II (isothermal) mass gain. A crucial parameter seems to be the temperature at which rehydroxylation begins after cooling from 500 ^{o}C. If this temperature is high, 'linearity' of stage II will be delayed for some samples, and therefore it is difficult to know where the 'true' $1/N$ behaviour begins. Another important set of parameters are H, ρ, c, and sample dimensions, which delay stage II by increasing the length of time taken for T0 uptake.

Here several fitting strategies to help determine the value of the power are proposed. Mass gain data from clay standard samples of montmorillonite and kaolinite are used. The experimental procedure with these samples has already been presented (Chapter 7). In addition, simulated datasets are obtained by a numerical method, and compared with the fitting techniques.

7.2 Comparison of models of Bowen et al. (2013) and Gallet and Le Goff (2015)

It will first be useful to evaluate the models of Bowen et al. (2013) and Gallet and Le Goff (2015), which assume a known value of N. The Bowen et al. (2013) model is represented by the following equation

$$m(t) = -\beta'\left(1 - e^{-\tau' t}\right) + \alpha_4' t^{1/4} + \delta \ , \tag{7.1}$$

where the first term is the Lagergren behaviour of T0 water, and the second term is the Wilson et al. (2012) model for T2 water. On the other hand, Gallet and Le Goff (2015) suggest a model in which there are terms for T0, T1 and T2 water:

$$y(t) = -\beta e^{-t/\tau} + \mu + \alpha_4 t^{1/4} + \alpha_2 t^{1/2} \ , \tag{7.2}$$

where α_4 is analogous to α of Wilson et al. (2009) for T2 water, and α_2 is the mass gain rate for a normal diffusion regime corresponding to chemisorbed T1 water.

In Fig. 7.1 both models are fitted to the data for montmorillonite M20 and kaolinite K2, utilising the Levenberg-Marquardt (L-M) alogrithm in MATLAB. Both samples are free of calcite and chemical pretreatment. In both cases $R^2 > 0.99$. However, the Gallet and Le Goff (2015) model is a better fit for both M20 (root mean square error, RMSE $= 2.4 \times 10^{-4}$) and K2 (RMSE $= 4.1 \times 10^{-5}$) than the model of Bowen et al. (2013) (RMSE $= 8.3 \times 10^{-4}$, 9×10^{-4} respectively). In addition, there are fewer trends which are visible in the residuals (black points, Fig. 7.1 A and B). Since the mass gain data were obtained over ~ 600 h, this suggests that there is a long term T1 component which needs to be considered in models of rehydroxylation, as well as in the dating method.

However, it should be noted that neither of these models properly incorporate the effect of accelerated kinetics following initial cooling. Previous simulations have suggested that if there is only a $t^{1/4}$ regime, then in some cases it may take several hundred hours to reach constant α_m, for materials of these dimensions. The transient stage I phase may look identical to a long-lived $t^{1/2}$ behaviour, which introduces a complexity in correct interpretation of the present fits. Furthermore, the fitted values of $\alpha_4' = 0.0126(2)$ g $h^{-1/4}$ and $\alpha_4 = 0.0392(6)$ g $h^{-1/4}$ (e.g. for K2) are significantly different from the value of α_m presented for the same sample in Chapter 6 ($0.0024(1) g h^{-1/4}$), which was fitted over 'stage II', assuming only $t^{1/4}$ kinetics. The fitted values of M20, $\alpha_4' = 0.00511(1)$ g $h^{-1/4}$ and $\alpha_4 = 0.0071(1)$ g $h^{-1/4}$ are in slightly better agreement with the value reported in Chapter 6 ($0.0098(4)$ g $h^{-1/4}$). One possible reason for the better agreement is that there should be a greater number of sites available for a T1 component based on the chemical structure of montmorillonite, which means that the Gallet and Le Goff (2015) model is a more appropriate fit because it incorporates a T1 $t^{1/2}$ regime.

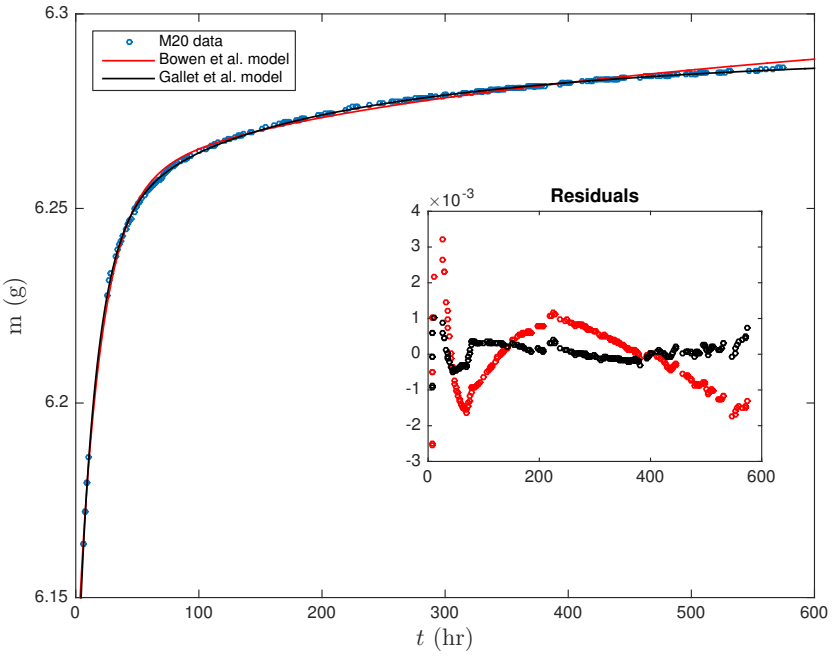

((A))

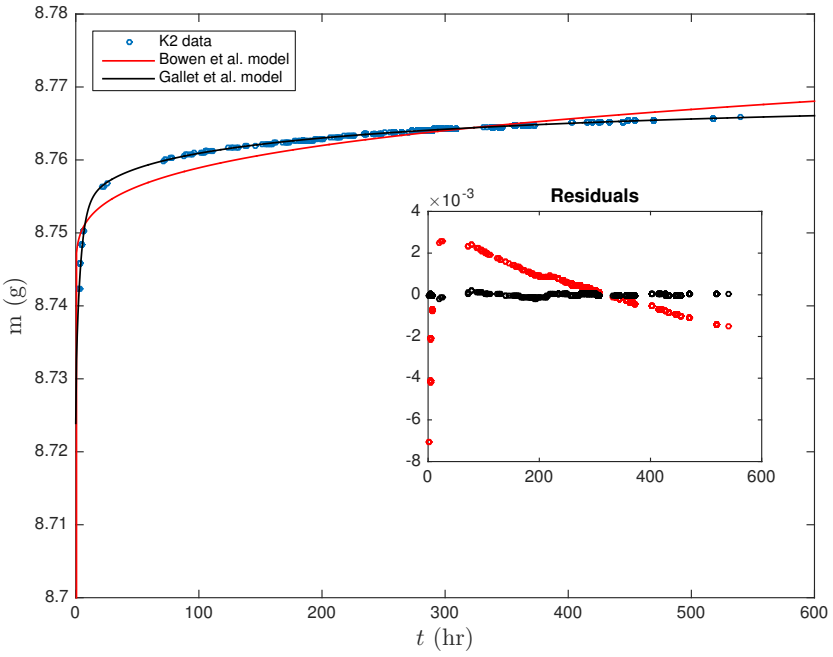

((B))

FIGURE 7.1: Fits to the models of Bowen et al. (2013) (red line) and Gallet and Le Goff (2015), showing residual plots. (A) shows sample montmorillonite 20 (M20). Fitted parameters for the Bowen et al. (2013) model are: $\beta' = -0.113(1)$, $\tau' = 0.053(1)$ h^{-1}, $\alpha'_4 = 0.0126(2)$ g h$^{-1/4}$, $\delta = 6.113(2)$ g. Fitted parameters for the Gallet and Le Goff (2015) model are $\beta = 0.098(1)$, $\tau = 14.7(2)$ h, $\mu = 6.174(2)$ g, $\alpha_4 = 0.0392(6)$ g h$^{-1/4}$, $\alpha_2 = -0.0033(1)$ g h$^{-1/2}$. (B) shows sample kaolinite 2 (K2). Fitted parameters for the Bowen et al. (2013) model are: $\beta' = -0.4(1)$, $\tau' = 100(10)$ h^{-1}, $\alpha'_4 = 0.00511(1)$ g h$^{-1/4}$, $\delta = 8$ g. Fitted parameters for the Gallet and Le Goff (2015) model are $\beta = 0.0197(2)$, $\tau = 3.83(4)$ h, $\mu = 8.74(2)$ g, $\alpha_4 = 0.0071(1)$ g h$^{-1/4}$, $\alpha_2 = -0.00052(1)$ g h$^{-1/2}$.

However, in most cases the uncertainties in α_4 and α_2 are too large to use the fitted models for accurate dating. In addition, the models do not allow for a fit to a different power $1/N$.

7.3 The value of N

7.3.1 Modified models of Bowen et al. (2013) and Gallet and Le Goff (2015)

If Eq. 7.1 and 7.2 are amended to incorporate a variable power $t^{1/N}$ in place of $t^{1/4}$, it is possible to obtain fits to the mass gain data from M20 and K2. The fits are displayed in Fig. 7.2, along with the fitted parameters. Once again, all fits give $R^2 > 0.99$. Similarly, the model of Gallet and Le Goff (2015) displays a better agreement with the data, with smaller residuals than the Bowen et al. (2013) model for sample M20. However, the magnitude of the residuals for sample K2 are roughly the same for both models, with similar RMSE (4.6×10^{-5} for Eq. 7.1 and 4.7×10^{-5} for Eq. 7.2). Fitted values of α_4 and α_4' are generally two orders of magnitude higher than those obtained for the $t^{1/4}$ fits (previous section), with significantly higher uncertainties ($\sim$ 70% to 200%). Similarly, the fitted values of N display high uncertainties. For M20, the modified Gallet and Le Goff (2015) model gives $N = 18(19)$, whereas the modified Bowen et al. (2013) model gives $N = 13 \pm 7$. For K2, the fitted values are $N = 1.7 \pm 0.2$ and $N = 1900 \pm 2000$ respectively.

Clearly, the fits are poorly constrained. Only the modified Gallet and Le Goff (2015) model for K2 provides reasonable uncertainty. Here, the value of 1.7 ± 0.2 seems to rule out a $t^{1/4}$ type behaviour. This value is more consistent with the usual $t^{1/2}$ regime. In both cases, RMSE is lowest for a modified Gallet and Le Goff (2015) model (RMSE = 1.9×10^{-4}), followed by a modified Bowen et al. (2013) model (RMSE = 5.8×10^{-4}), and lastly a modified model of Wilson et al. (2013), which has a variable power but no T0 or T1 terms (RMSE = 6.5×10^{-4}). On the basis of this fitting procedure and the available evidence it seems likely that the $t^{1/N}$ power law model has N closer to 2. As

before, the large uncertainties on the fitted parameters preclude the use of these models for dating.

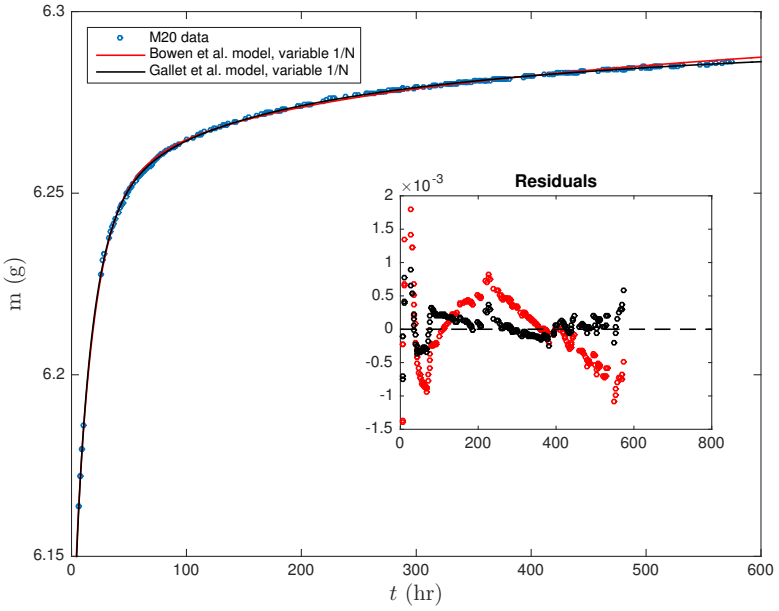

((A))

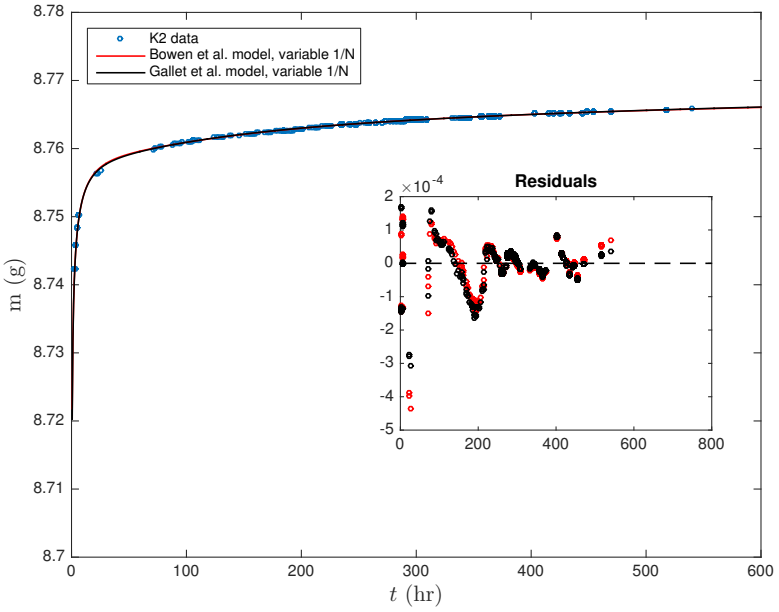

((B))

FIGURE 7.2: Fits to the models of Bowen et al. (2013) (red line) and Gallet and Le Goff (2015), showing residual plots. (A) shows sample montmorillonite 20 (M20). Fitted parameters for the Bowen et al. (2013) model are: $\beta' = -0.103(3)$, $\tau' = 0.06(1)$ h^{-1}, $\alpha'_4 = 0.10(8)$ g h$^{-1/4}$, $\delta = 6.02(8)$ g, $N = 13(7)$. Fitted parameters for the Gallet and Le Goff (2015) model are $\beta = 0.089(4)$, $\tau = 14.9(2)$ h, $\mu = 5.9(4)$ g, $\alpha_4 = 0.3(3)$ g h$^{-1/4}$, $\alpha_2 = -0.0011(4)$ g h$^{-1/2}$, $N = 18(19)$. (B) shows sample kaolinite 2 (K2). Fitted parameters for the Bowen et al. (2013) model are: $\beta' = -0.0173(2)$, $\tau' = 0.269(5)$ h^{-1}, $\alpha'_4 = 7 \pm 60$ g h$^{-1/4}$, $\delta = 3 \pm 60$ g, $N = 1900 \pm 2000$. Fitted parameters for the Gallet and Le Goff (2015) model are $\beta = 0.0197(2)$, $\tau = 3.83(4)$ h, $\mu = 8.74(2)$ g, $\alpha_4 = 0.0071(1)$ g h$^{-1/4}$, $\alpha_2 = -0.00052(1)$ g h$^{-1/2}$, $N = 1.7 \pm 0.2$.

7.3.2 Fitting to simulated datasets

One possible complication is the effect of cooling rate on an accelerated $t^{1/4}$ regime, which creates a similar mass gain behaviour to a combined $t^{1/2} + t^{1/4}$ model. The effect is expected to be greater for samples with large dimensions, as previously discussed in Chapter 5. To investigate this further, two simulated datasets were created using the numerical simulation presented in Section 5.4.2. The parameters for the first dataset represent a fairly rapid cooling; $H = 5$ W m^{-2} K^{-1}, $\rho = 1.7$ g cm^{-3}, $c = 777$ J kg^{-1} K^{-1}, $d = 0.01$ m. The second has conservative parameters which represent a fast cooling: $H = 1.5$ W m^{-2} K^{-1}, $\rho = 1.96$ g cm^{-3}, $c = 948$ J kg^{-1} K^{-1}, $d = 0.035$ m. Both datasets use the same choice of $\alpha = 0.0003$ h$^{-1/4}$, and assume that rehydroxylation begins at 100 ^{o}C, and samples cool to 18 ^{o}C. Temperature fluctuations of the order of 0.1 ^{o}C are added to the dataset as noise, drawn from a normal distribution by Markov chain Monte Carlo (MCMC) method using the Metropolis-Hastings algorithm, since the variation in temperature under isothermal conditions can be reasonably well approximated as a Markov chain (Dunn and Shultis, 2012). An amplitude of 0.1 ^{o}C was chosen as a conservative estimate of typical chamber instability.

When fitting is performed, the Bowen et al. (2013) model (Eq. 7.1) displays a higher goodness-of-fit (RMSE = 3.3×10^{-5} for slow cooling, RMSE = 2.7×10^{-5} for fast cooling) than the Gallet and Le Goff (2015) model (Eq. 7.2) for fast cooling (RMSE = 1.7×10^{-5}). The highest goodness-of-fit is for the Gallet and Le Goff (2015) model applied to the slow cooling dataset (RMSE = 8.2×10^{-6}), which underlines the difficulty in distinguishing between thermal effects and T1 water uptake, particularly in large, slow cooling samples. Note that these simulated models all show a high degree of goodness-of-fit, and RMSE is better for these datasets than for similar models applied to the M20 and K2 datasets.

If the cooling rate effect delays the onset of stage II, then it seems more appropriate to choose a portion of the dataset over which the Wilson et al. (2013) model can be fitted, under 'isothermal' conditions. As an alternative fitting strategy, a script was therefore written to perform successive fitting on log-linearised data, to determine the optimal range for stage II fitting. The advantage is that for each successive fit, the

program performs a Shapiro-Wilk test on the residuals, to determine normality. The disadvantage is that a smaller data range is selected. The script also performs successive Hartigan's dip tests, which check that the distribution of residuals is unimodal. When both the Shapiro-Wilk and Hartigan's dip tests are satisfied, then the value of α_m is automatically reported. The script can be found in Appendix C, and more details can be found there.

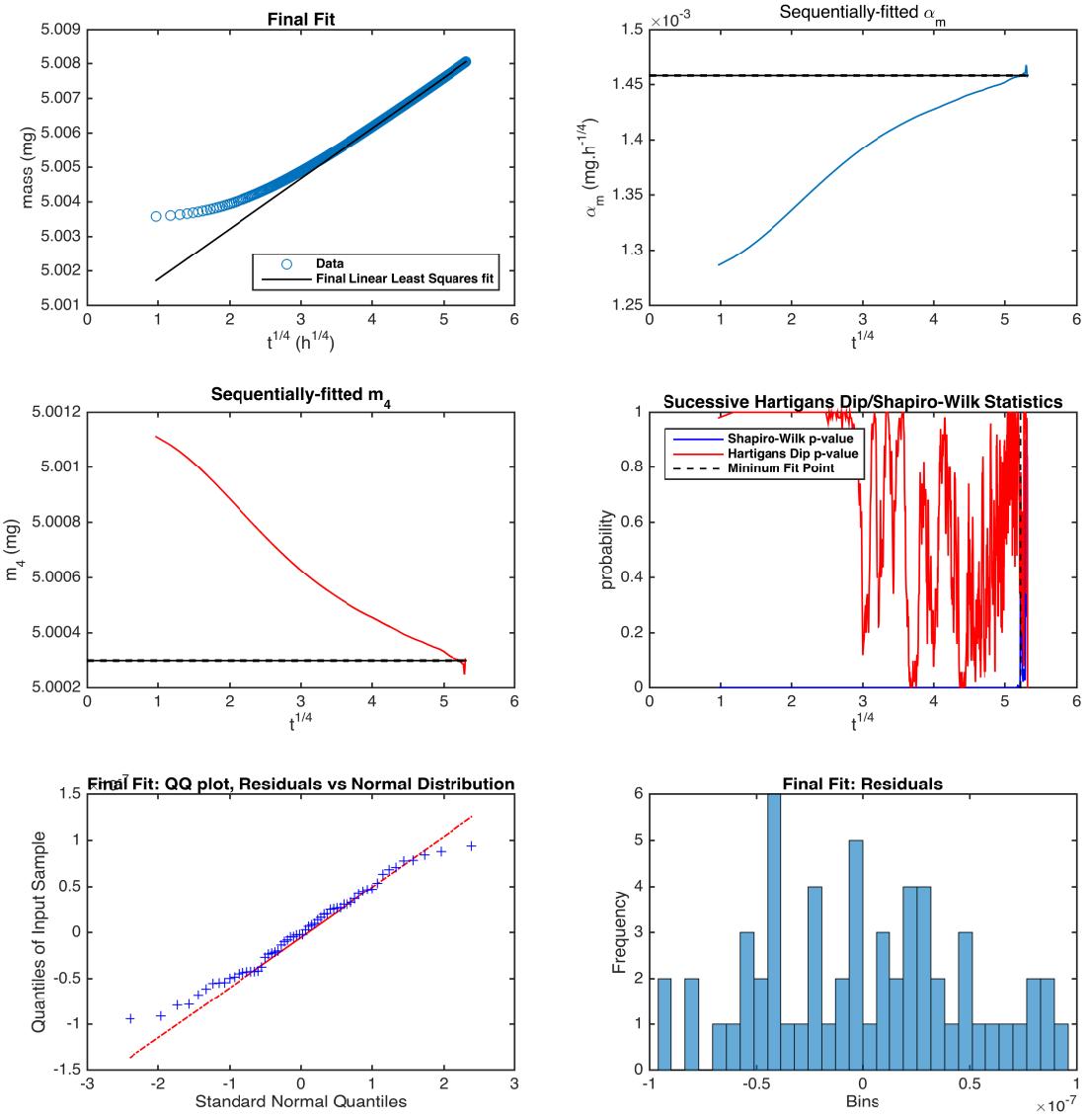

FIGURE 7.3: Sequential fitting of α_{m} (top right) and m_4 (middle left) to simulated dataset with relatively fast cooling. Also shown are successive Hartigan's dip (red curve, middle right) and Shapiro-Wilk (blue curve, middle right) statistics for successive fits, and a quantile-quantile (QQ) plot of residuals to the final fit (bottom left), also shown as a histogram (bottom right). The final fit was performed from 740.9 hours to end of dataset at 799.9 hours, and fitted values are $\alpha_{\mathrm{m}} = 1.4580 \pm 0.0001$ mg $\mathrm{h}^{-1/4}$ and $m_4 = 5.000301(2)$.

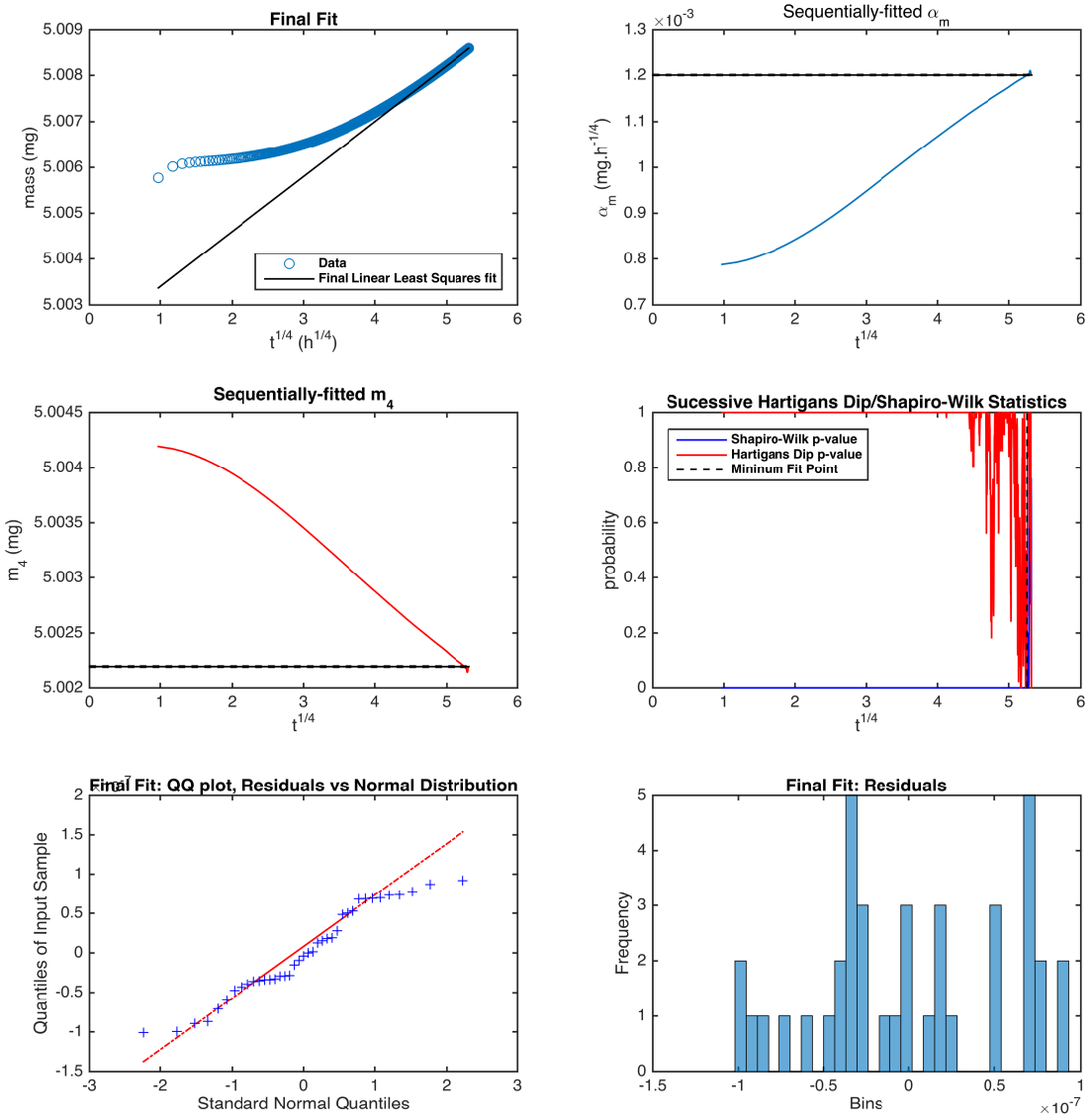

FIGURE 7.4: Sequential fitting of α_{m} (top right) and m_4 (middle left) to simulated dataset with relatively fast cooling. Also shown are successive Hartigan's dip (red curve, middle right) and Shapiro-Wilk (blue curve, middle right) statistics for successive fits, and a quantile-quantile (QQ) plot of residuals to the final fit (bottom left), also shown as a histogram (bottom right). The final fit was performed from 761.9 hours to 799.9 hours, and fitted values are $\alpha_{\mathrm{m}} = 1.2010 \pm 0.0001$ mg $\mathrm{h}^{-1/4}$ and $m_4 = 5.002199(2)$.

This script was used to determine optimal fitting conditions for the two simulated datasets. Shapiro-Wilk and Hartigan's dip tests are passed at 761.90 h (slow cooling) and 740.90 h (fast cooling), which suggests that the cooling rate effect is a significant source of error in assigning correct stage II fits for both datasets. The fitted value of α_{m} for the slow cooling dataset is 1.2010 ± 0.0001 mg $\mathrm{h}^{-1/4}$, and the value is 1.4580 ± 0.0001 mg $\mathrm{h}^{-1/4}$ for the fast cooling dataset. Both values are significantly different from the known values (1.5 mg $\mathrm{h}^{-1/4}$), which suggests that there is a small but significant

curvature in the plots which is not noticeable in residuals. In Fig. 7.3 and Fig 7.4 the sequentially fitted values of α_{m} and m_4 are plotted. It seems from this plot that neither properly stabilise, even though the residuals appear normal, and both Shapiro-Wilk and Hartigan's dip tests are passed at the 0.05 significance level.

The disagreement between fitted values of α_{m} and α_{m} and their known values suggests that the cooling rate effect is a significant source of error in assigning correct stage II fits for all samples. The conditions for the passing the Shapiro-Wilk and Hartigan's dip tests might be tightened, but this would exclude all datapoints in the range of $\sim$ 800 h. On the basis of this result, it might be concluded that reliable fitting of α_{m} is highly problematic, since the fast and slow cooling datasets encompass the range of behaviour thought to exist in fired clays, and the typical maximum measurement time for an RHX experiment is of the order of 700-800 hours. At longer times the mass gain due to RHX is so slow as to be below practical detection limits.

7.3.3 An alternative method for determining N

Assuming that the Wilson et al. (2013) model holds for some power $1/N$, we have

$$\frac{m(t) - m_4}{m_4} = \alpha(T)t^{1/N} \ . \tag{7.3}$$

Differentiating both sides gives

$$\frac{dm}{dt} = \frac{d}{dt} m_4 \alpha(T) t^{1/N} + m_4 \ . \tag{7.4}$$

If an approximation to the gradient, $\Delta m/\Delta t$, is obtained from each successive datapoint, then we can write

$$ln(\Delta m/\Delta t) = (1/N - 1)ln(t) + z \ , \tag{7.5}$$

where z is a constant if $\alpha(T)$ is also constant (i.e. isothermal conditions). Therefore, the gradient of the plot of $ln(t)$ versus $ln(\Delta m/\Delta t)$ should allow the determination of N, independent of any knowledge of m_4. The method clearly depends on appropriate

spacing of mass measurements, which impact the accuracy of $\Delta m/\Delta t$. However, this approach requires neither m_4 nor any knowledge of the time offset t_0.

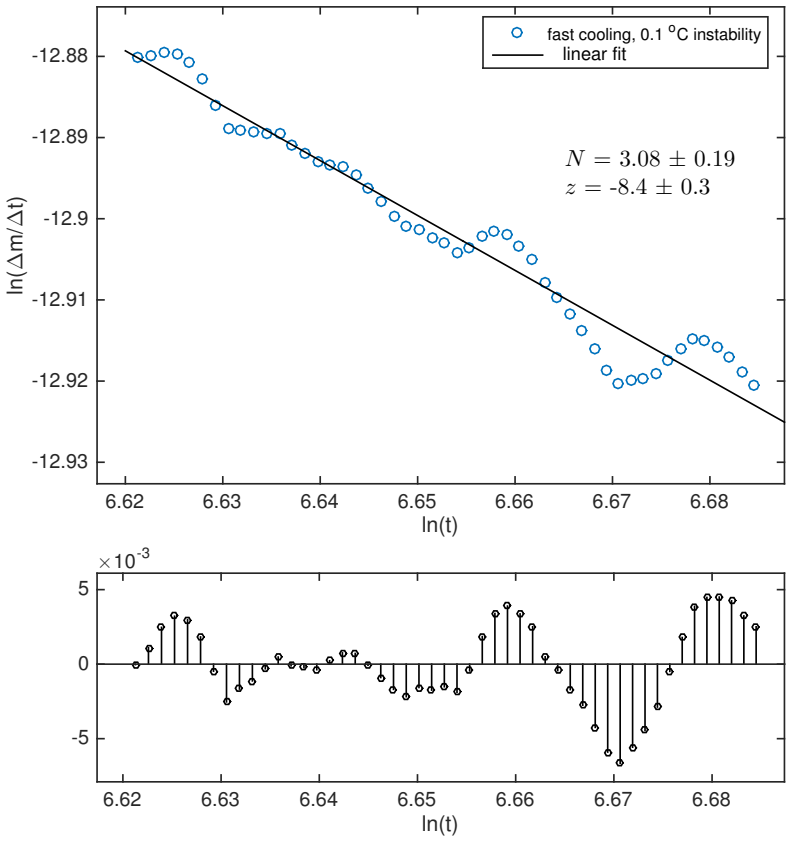

FIGURE 7.5: Alternative method of determining N. Top graph shows a linear fit, using Eq. 7.5, for a simulated dataset with relatively fast cooling. Bottom graph shows the residuals. Parameters of the simulation are given in the text. Temperature fluctuations have amplitude 0.1 ^{o}C, and are generated by Metropolis-Hastings algorithm. Automatic fitting is performed between 740.9 h and the end of the dataset at 799.90 h, when the residuals are found to be normally distributed (Shaprio-Wilk test, $p > 0.7$ at a significance level of 0.5), and unimodal.

A fit of Eq. 7.5 is presented in Fig. 7.5 using the fast cooling dataset presented in Section 7.3.2. As before, the optimum range is selected by the automated fitting procedure. The fit yields a value of $N = 3.08 \pm 0.19$, which is not consistent with the known value of 4. This supports the finding that it is not possible to obtain a reliable N from fits to the Wilson et al. (2013) model with a variable power over common dataset lengths. Recall that the previous fitting to this dataset showed a value of α_{m} which was also significantly different from the known value.

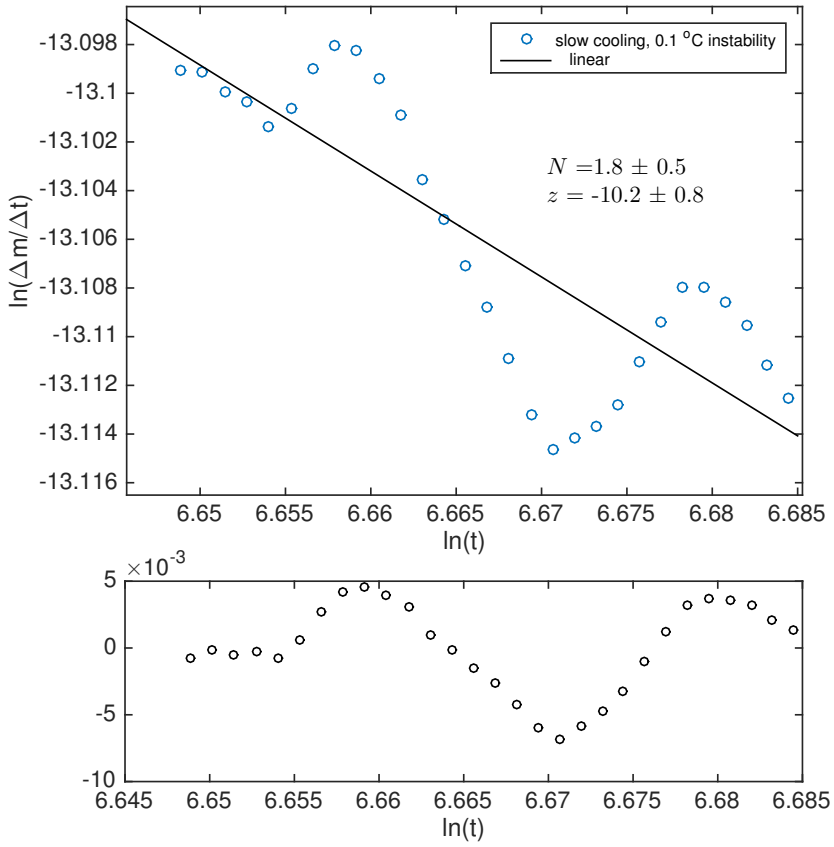

FIGURE 7.6: Fit to Eq. 7.5 for a simulated dataset with relatively slow cooling. Bottom graph shows the residuals. Parameters of the simulation are given in the text. Temperature fluctuations have amplitude 0.1 ^{o}C. Automatic fitting is performed between 761.9 h and the end of the dataset at 799.90 h, when the residuals are found to be normally distributed (Shaprio-Wilk test, $p > 0.7$ at a significance level of 0.5).

When the procedure is also performed on the slow cooling dataset (Fig. 7.6), a similar picture emerges. Here $N = 1.8 \pm 0.5$, which means that the dataset looks most like a $t^{1/2}$ relationship over this range, rather than the known $t^{1/4}$ relationship. Fig. 7.7 shows the procedure applied to sample M20. Here the fit is very poor ($R^2 = 0.3$), although the residuals are fairly normal. The fitted value of N is 5 ± 7, which means that neither $t^{1/2}$ nor $t^{1/4}$ behaviour can be ruled out, and the method is not as useful as a standard non-linear fit to a Gallet and Le Goff (2015) model with variable N, and appropriately chosen start points for a Levenberg-Marquardt algorithm. A similar fit to the sample K2 showed a value of $N = -0.64 \pm 7$, and $R^2 = 0.01$, which is not a useful result.

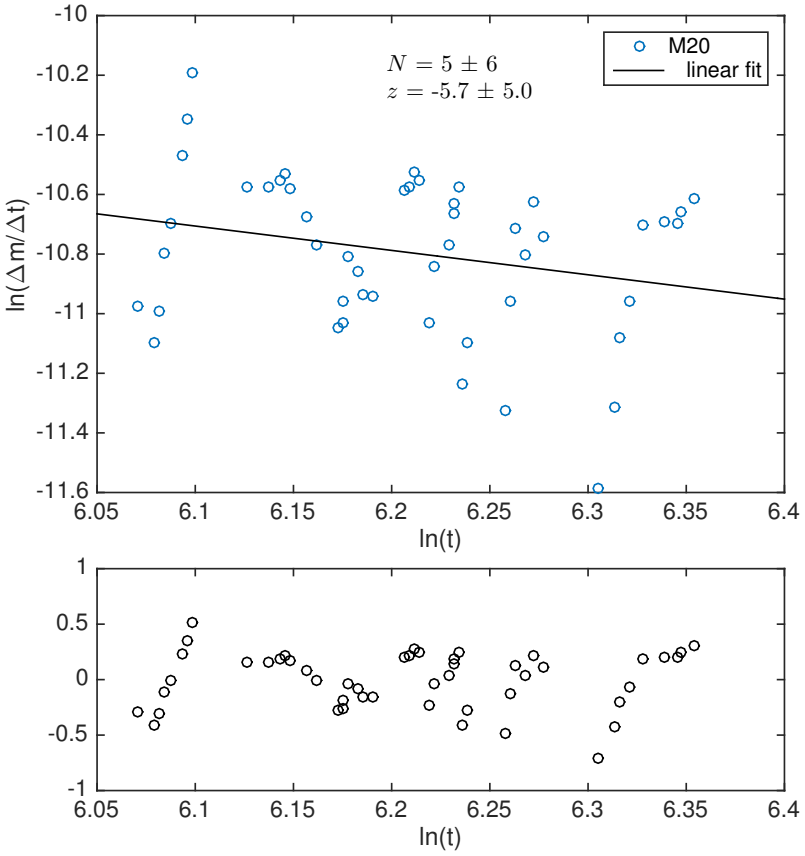

FIGURE 7.7: Fit to Eq. 7.5 for sample M20. Bottom graph shows the residuals. Automatic fitting is performed between 547 h and the end of the dataset at 574 h, when the residuals are found to be normally distributed (Shaprio-Wilk test, $p > 0.7$ at a significance level of 0.5).

7.4 Discussion

Obtaining the value of the power through fitting is clearly a complex and sensitive procedure. In the standard approach by Levenberg-Marquardt algorithm, fitted values of N are highly sensitive to the initial choice of m_2 and t_0. However, results for N can be obtained for a variety of models if the entire range of the dataset is considered and care is taken to minimise RMSE or other goodness-of-fit statistics. In the alternative log-gradient method, the fitting is less dependent on m_4 and the time offset, but the statistics are not good enough to decide upon any single value of N, if the dataset is limited to a range over which the residuals are normally distributed.

On the basis of the available evidence, it is not possible to exclude the possibility of

a $t^{1/4}$ regime for most datasets considered in this analysis. It is possible to exclude a $t^{1/4}$ regime in only one case (sample K2, $N = 1.7 \pm 0.2$, with a modified Gallet and Le Goff (2015) model over the entire range). On the other hand, a lower value of N is precisely the behaviour that would be expected given a $t^{1/4}$ regime, accelerated after reheating (as shown by simulated datasets). Note that the value of N for sample K2 falls within the range for the alternative fitting method on slow ($N = 1.8 \pm 0.5$) and fast ($N = 3.08 \pm 0.19$) cooling regimes.

7.4.1 Relationship to diffusion mechanisms

It is difficult to draw any firm conclusions as to the presence of anomalous diffusion in fired clays given the uncertainty in the power $1/N$. In most mass gain experiments it is not possible to exclude the possibility of a single-file diffusion regime, as first suggested by Wilson et al. (2003) and Savage et al. (2008). With regard to kaolinite, which is a possible exception, an ordinary Fickian diffusion regime ($t^{1/2}$) is consistent with the spectra reported in Chapter 4, which also showed no significant growth in the T2 water band after firing. This might suggest that kaolinite shows only T1 water uptake, which is associated with a long-lived $t^{1/2}$ process. However, FTIR lacks the quantitative sensitivity of microgravimetric measurements, which means T2 uptake (corresponding to a $t^{1/4}$ regime) may still be present below the detection limit. It is not possible to make any conclusions with regard to montmorillonite, other than that the model of Gallet and Le Goff (2015) provides the best fit (RMSE) to the entire dataset (although this might reflect accelerated $t^{1/4}$ after reheating).

The study of Mazzucato et al. (1999) examined the dehydroxylation of muscovite mica. They suggest that the rate limiting step of dehydroxylation reaction kinetics is mono-dimensional diffusion through the 6-ring of the silica tetrahedral layer to inner structural OH sites in the aluminium layer. They found that the time dependence goes as $t^{1/N}$, with the power ranging from 0.262(6) to 0.325(5).

If a similar sub-diffusion process is linked to rehydroxylation in muscovite mica (i.e diffusion through the 6-ring of the silica tetrahedral layer), then one implication is that a $t^{1/4}$ regime should not occur in 1:1 clay minerals such as kaolinite, where the aluminium

layer is more easily accessible to diffusing molecules, which do not have to pass through the silica tetrahedra 6-ring. In this case $t^{1/2}$ behaviour should be apparent. It would be interesting to perform similar XRPD measurements on kaolinite (both dehydroxylation and rehydroxylation) to evaluate this hypothesis. Additionally, small sample sizes would avoid the issue of a delayed 'stage II' due to accelerated reaction kinetics after reheating.

7.4.2 Theoretical considerations for single-file diffusion

Conventionally, single-file diffusion should occur within channels where the particle diameter d_P is bigger than half the channel diameter d_T (Kärger et al., 2012). For a single particle in such a system of infinite length, theory (Levitt, 1973; Hahn et al., 1996; Kukla et al., 1996) gives the time dependence as:

$$\langle x^2 \rangle_{sf} = 2Ft^{1/2} \ , \tag{7.6}$$

where F is the single-file mobility, which is related to the diffusion coefficient of a single particle D_1, and the mean free path, l, between two adjacent particles in the file:

$$F = l\sqrt{\frac{D_1}{\pi}} \ . \tag{7.7}$$

In the scenario of Wilson et al. (2003) and Savage et al. (2008), molecules diffuse along pathways sufficiently small enough that they cannot pass one another, and that when the leading H_2O molecule encounters a site of rehydroxylation, it is removed from the queue. The entire file then advances a set distance until the next reaction site, which leads to a $t^{1/4}$ regime because the root mean square distance travelled by the queue of molecules is proportional to the number of reactions (which therefore leads to mass gain).

Two observations can be made with regard to the conventional theory of single-file diffusion and the Wilson et al. (2003) model. First, there is currently no microstructural evidence for such pathways in fired clays, but even if there were, there would be deviations from single-file diffusion, and therefore $t^{1/4}$ behaviour. The reason is that the 1/4 power only holds in an infinite single-file system (Levitt, 1973), and the pathways

in clay minerals would clearly be finite. Second, it is easy to imagine scenarios where $d_P < 1/2d_T$, which means that two diffusing H_2O molecules can pass one another. In this case there will also be deviations from the $t^{1/4}$ behaviour (Hahn and Kärger, 1998).

This single-file picture is slightly different from the scenario of Mazzucato et al. (1999), because here the distance through the six-ring will be a few Ångström, and therefore there is no file. In this case, the time dependence is related to the probability that an H_2O molecule encounters a site through the six-ring channel, and the single-file mobility F is no longer relevant.

7.4.3 Implications for archaeological dating

What are the implications for RHX dating if the power is not 1/4? Consider the RHX age determination in Table 4.2 for sample MAN037. With $t^{1/4}$ the age is 49 ± 4 a. If the calculation is performed with $t^{1/3}$, the age determination is younger by an order of magnitude. With a $t^{1/2}$ relationship the RHX age determination is still younger. This effect is expected to scale with the age of the ceramic, so for very old materials one might see differences of several hundred years. Clearly, the power needs to be well-characterised for accurate dates.

Additionally, accurate dating is not possible at current levels of microbalance resolution, and if the power law is different for each sample. Notably, there will be a extra uncertainty term to add to the uncertainty budget, associated with N. Given the uncertainties of N presented in this Chapter, the contribution of this uncertainty is likely to make gravimetric RHX dating impossible via a modified Wilson et al. (2012) model with a variable power. Likewise, the models which describe the concurrent processes of T0 and T1 mass gain (Eq. 7.1 and Eq. 7.2) are arguably too complex to be used in any inversion to determine a date, because the uncertainties in α_4 and α_2 are very high. RHX dating by gravimetric analysis is therefore only possible if T1 water is found to be short-lived (hours/days), and the power is known to high accuracy. If T1 water follows a long-lived $t^{1/2}$ process, and T2 water follows a $t^{1/4}$ process, then a gravimetric method of RHX might work better if the amounts of T0/T1/T2 water (plus the separate rate

constants) can be determined independently by thermo-gravimetric analysis, or it is possible to measure the archaeological mass after heating to 300 ^{o}C to drive off T0 and T1 water, as suggested recently by Zhao et al. (2015). On the other hand, IR spectroscopy might offer an advantage over conventional RHX dating by mass gain. Although these methods might be less precise, they should be able to separate the contributions of T1 water and structural OH (T2). However, much work remains to be done so that the diffusion processes are accurately characterised and understood.

Chapter 8

Conclusions

This thesis evaluated several different aspects of rehydroxylation dating. The aim was to better understand the disagreement between current studies, and some of the underlying models of rehydroxylation in fired clays. An overview of the history of research into long-term chemical change in fired clays was presented in Chapter 1. This Chapter also identified the different models which have been proposed to explain mass gain and expansive strain data, and several key questions.

Chapter 2 investigated the uncertainty budget for rehydroxylation dating. The analytical expressions show that previous studies (e.g. Wilson et al. (2012)) have underestimated the uncertainties associated with rehydroxylation age determinations. The finding is supported by MC simulations. One significant contribution to combined measurement uncertainty is from sample mass/microbalance resolution (which contributes to uncertainty in α_{m}). The range of relative uncertainties varies across four orders of magnitude in current published studies. It can be concluded that most studies of rehydroxylation dating are therefore inappropriate tests of the dating method. This effect is primarily the result of a mismatch between balance resolution and sample size. For measurement precision under 1% the ratio of microbalance resolution to sample mass should be of the order of 10^{-6} or less. For typical values of α_{m} reported by authors we can expect a minimum relative error of $\sim 0.5\%$, which translates to an increase of 10 years in error every 2000 years or so. The second significant contribution to combined measurement uncertainty is from the effective lifetime temperature. Analytical expressions suggest

that the uncertainty in effective lifetime temperature should contribute to uncertainty of between 1 and 3 % of the age of the ceramic, across a range of E_a and given an uncertainty in ELT of 0.3 ^{o}C. This might be higher for certain scenarios, for instance if an object is moved to a very different geographical area over a significant portion of its lifetime, or if the object is used for cooking. This makes RHX dating of such artefacts problematic, as the combined uncertainty would be much higher.

An expression for the age limits of the technique was presented which depends on E_a, ELT, and y_{max}. However, this expression assumes a Wilson et al. (2012) model, with only one long-term $t^{1/4}$ regime, where y_{max} is related to the number of free sites available in the meta-clay structure (in a scenario originally suggested by Shoval et al. (1991)). The expression predicts that the RHX age determination will be a minimum age in some cases (high ELT, low y_{max} or α). In addition, it seems unlikely that highly-fired materials such as porcelain are suitable for RHX, because α is too low for precise measurements with current microbalances. The theoretical framework suggests that a Wilson et al. (2012)-type RHX method is only appropriate to some low-fired earthenwares and historical bricks. However, given well-designed experiments, and appropriate samples, a combined measurement uncertainty of $\sim$ 4 % should be possible, if the underlying model is correct. It can be noted that although this new framework for combined uncertainty is an improvement, future developments could mean that the uncertainty is much higher. In particular, covariance has not yet been properly evaluated. However, a complete treatment of uncertainties is a significant statistical task, which should only be approached once discrepancies in the $t^{1/4}$ model are resolved.

Later chapters focused on systematic effects, including issues of organic contamination and calcite contamination, as well as disagreement with the $t^{1/4}$ model and underlying relationships to diffusion. In Chapter 3, an overview and discussion of possible contaminants was presented. Calcite has been considered problematic for rehydroxylation dating (since it should be both a 'category A' and 'category B' contaminant). It is expected to form CaO upon heating, which subsequently combines with water (and CO_2). The recombination with water was thought to cause a prolonged stage I, and an erroneously high α_m which leads to young ages. Additionally, the reheating of carbonate at 500^{o}C

was thought to cause some mass loss. However, this investigation shows that there is no significant difference in the RHX ages of recently-fired calcareous montmorillonite when compared to non-calcareous montmorillonite, which suggests that the effect is small (at least for this clay mineral). Other clay minerals and archaeological pottery may behave differently.

In all samples, treatment with 0.5M HCl at 70 ^{o}C for 30 minutes removed significant amounts of calcite. This treatment follows the recommendation of Nümrich et al. (2015). However, such treatment may not be necessary given the dating results. In addition, ATR-FTIR spectra indicate that there is a small amount of rehydroxylation under these pretreatment conditions, both T1 and T2 water. If an acid wash is somehow necessary, treatment with 0.1M HCl at room temperature produced no clear difference in RHX age determinations of kaolinite and montmorillonite. With regard to removal of organics, and lipids in particular, chloroform/methanol solvent extraction with ultrasonication is not as efficient as SFE. However, FTIR results of SFE performed on samples of archaeological pottery give slightly inconsistent results, which may be because these materials show high variability in lipid quantity and preservation. Preliminary results suggest some rehydroxylation occurred during SFE, which is supported by RHX age determinations on terracotta, presented in Chapter 6.

Chapter 5 examined the question of non-stabilisation of m_2 mass after reheating to 105^{o}C. There are few clear correlations between non-stabilisation and physical parameters such as porosity, specific heat capacity or density. The strongest effect is that of sample dimension (thickness), which is found to cause long times to pseudo-equilibration behaviour following reheating to 105 ^{o}C. This time is roughly proportional to the thickness squared, which suggests long-lived contributions from Fickian diffusion. Another plausible explanation is that non-stabilisation might be caused by the vitreous components of highly fired ceramics, which react with moisture to form hydrous minerals under environmental conditions. Acceleration of the underlying rehydroxylation reaction is unlikely to cause the magnitude of mass gain observed after reheating to these temperatures, as determined by simulations (and assuming the correct model is indeed $t^{1/4}$). Also, acceleration of the rehydroxylation reaction after reheating to 500 ^{o}C, as

well as the upper temperature at which rehydroxylation begins, were identified as highly significant causes of prolonged stage I mass gain (in many cases greater than 500 h). The effect is strongest for samples with highest ρ, c, and sample dimensions (as well as low H). The effect of sample dimension poses a fundamental challenge for gravimetric rehydroxylation dating. There is an obvious trade off to be made between sample size and microbalance precision. Thicker samples will need more time for uptake of T0 water, as well as isothermal T2 mass gain. Thinner samples would avoid long initial times for stabilisation, but at the expense of providing less precision in α_{m}.

With the aid of the simulations presented in Chapter 2, a new multi-sample apparatus for the gravimetric analysis of rehydroxylation in fired clays under controlled conditions was designed and constructed. Clay mineral standards were prepared to compare the effect of pretreatment, and to investigate differences in mass gain behaviour between different meta-clays. Simulations suggested that RHX age determinations on these fired materials would be possible for relatively recent firing (1.1 a). RHX age determinations for several samples of fired clay standards were presented which show variable results, but which are generally plausible given the known age. However, comparison of pretreatment regimes is slightly problematic, given the inconsistent behaviour of samples, and the lack of replicates. Corrections for lifetime temperature effects improve the accuracy of RHX dating, but only slightly. For future known-age tests of this method, activation energy should be determined by measurements xsof α_m at at least three different temperatures. With regard to the SAS method proposed by Moinester et al. (2014), the expression for ELT does not seem to give accurate results, although the activation energies of kaolinite and montmorillonite may not be well-known, which hinders a proper evaluation of the SAS method. The relative difference between ELTs of samples kept under different lifetime conditions is intriguing. However, there are theoretical reasons to expect that SAS will not work for samples which begin rehydroxylation at different upper temperatures, because ELT will be very different for the two samples.

Chapter 7 evaluated evidence for the variability of the proposed $t^{1/N}$ power law. There are essentially three factors which complicate the accurate determination of N. First, the multi-parameter models suggested by Gallet and Le Goff (2015) and Bowen et al.

(2013) are prone to overfitting, and in most cases the uncertainty associated with N is too high to draw any firm conclusions. On the basis of the available evidence, it is not possible to exclude the possibility of a $t^{1/4}$ regime for most datasets considered in this analysis. The exception is kaolinite, which appears to exhibit little to no $t^{1/4}$ behaviour, and no uptake of T2 water (on the bases of FTIR spectra). Second, m_4 and t_0 are not generally known, and non-linear fitting algorithms are highly sensitive to the choice of initial parameters. Third, and most significantly, slow cooling causes long times to 'stage II' behaviour. When samples cool from high temperatures, the accelerated effect on $t^{1/4}$ kinetics produces a mass gain behaviour which is very similar to a combination of $t^{1/2}$ and $t^{1/4}$ processes. Consequently, it is impossible to decide between the models of Gallet and Le Goff (2015), Bowen et al. (2013) and Wilson et al. (2012), even though goodness-of-fit statistics are highest for a Gallet and Le Goff (2015) model with long-lived T1 and T2 regimes.

However, there is strong independent evidence for a long lived T1 component. The IR spectroscopic study of Clegg et al. (2012) was thought to show $t^{1/4}$ behaviour in a peak associated with structural hydroxyl. However, closer inspection of this data suggests that there is also growth in the broad shoulder of T1 water, which continues over the duration of measurement (1 month). The thermo-gravimetric analysis of Shoval and Paz (2013) seems to also provide support for a long-lived temporal dependence for weakly-bound water. Additionally, the experiments on quenching terracotta may be interpreted as indicating that mass gain data reflect both T1 and T2 components, because quenching fills up sites which are available to T1 water, and then only T2 uptake is measured (and α_{m} is much lower).

8.1 Future directions

If T1 water is long-lived, then clearly a gravimetric method of RHX dating cannot work in its current form, and alternatives need to be considered. One alternative is isolating the contributions (and time dependencies) of T0, T1, and T2 water by some stepwise heating method. Such a method would be very time consuming, and there would still

be issues of resolution and cooling rate (in mass gain experiments). Several practical steps may lead to greater precision in gravimetric RHX dating; most notably reducing the ratio of microbalance resolution to sample mass to less than parts-per-million (ppm) level. However, independent of any problems associated with long-lived T1 water, the systematic effects of cooling rate and non-stabilisation mean that accurate estimation of the ceramic age is highly problematic. However, if precision is not the objective, RHX might still be used as a reasonably rough method of testing the authenticity of fired-clay objects, as the amount of RHX water does seem to increase with time.

An alternative method would be IR spectroscopy, which would offer the obvious advantage of being able to target T1 and T2 water specifically, but at the cost of precision. RHX dating by IR spectroscopy should be investigated, because it would also avoid cooling rate effects (i.e. sample dimensions would be much smaller).

With regard to pretreatment, IR would also offer the advantage that pretreatment methods would be less necessary. If gravimetric RHX is pursued, pretreatment is mandatory for organics. More work is required to asses the effect of SFE pretreatment on structural OH, if gravimetric RHX dating is pursued. In addition to clay standards, known-age archaeological material should be pretreated, to further assess the effect on RHX age determination of samples of much greater age. As to the SAS method, the relative difference between ELTs of both sets of samples kept under different conditions is promising, and deserves a fuller investigation and more replication. The SAS method is also possible to evaluate by IR spectroscopy of thin clay films.

Perhaps the most interesting question is how processes of diffusive transport might give rise to such behaviour in fired clays. The possibility of correlating the time dependence of rehydroxylation with a particular mechanism of anomalous diffusion is very interesting, although currently beyond the scope of this work. A better understanding of the relationship between rehydroxylation and meta-clay microstrucure is perhaps the key to future development of a robust dating tool for archaeological ceramics. It should also assist in establishing a new framework for understanding the long-term chemical changes of fired clays, with wider implications for geology, construction and material science.

Appendix A

Same Age Samples measurement protocol (Moinester et al., 2014)

A brief outline of the same age samples (SAS) method is presented in this Appendix, along with a derivation of Eq. 6.3 which is presented in Chapter 7, which is also presented in Moinester et al. (2014).

Let us assume that rehydroxylation kinetics are described by the equation

$$y_{\mathrm{a}} = \alpha(T) t^{1/4} \ . \tag{A.1}$$

If $y_{\mathrm{a}} = (m_2 - m_4)/m_4$, then we have

$$m(t) = m_4 + \alpha(T) t^{1/4} \tag{A.2}$$

We also have the Arrhenius dependence of the rate constant

$$\alpha(T) = A exp(-E_{\mathrm{a}}/4RT) \ . \tag{A.3}$$

Now, assume that two samples, with rate constants denoted by α' and α and masses likewise denoted by m_4' and m_4, etc. are both fired at the same time. For one sample,

we have that

$$\alpha_{\mathrm{m}}(T_m)/\alpha_{\mathrm{m}}(T_e) = exp\big[E_{\mathrm{a}}(1/T_{\mathrm{e}} - 1/T_1)/4\mathbf{R}\big] \ , \tag{A.4}$$

and a similar equation can be derived the the second sample. Inserting Eq. A.4 into Eq. A.2 and rearranging yields a pair of equations for the samples:

$$t_{\mathrm{a}} = (m_2 - m_4)^4 exp\big[E_{\mathrm{a}}(1/T_{\mathrm{e}} - 1/T_{\mathrm{m}})/\mathbf{R}\big]\alpha_{\mathrm{m}}(T_{\mathrm{m}})^4 \ , \tag{A.5}$$

$$t'_{\mathrm{a}} = (m'_2 - m'_4)^4 exp\big[E'_{\mathrm{a}}(1/T'_{\mathrm{e}} - 1/T_{\mathrm{m}})/\mathbf{R}\big]\alpha_{\mathrm{m}}(T_{\mathrm{m}})^4 \ . \tag{A.6}$$

Now, we make the assumption that that the ELT of the two samples is similar, so $T_{\mathrm{e}} \approx T'_{\mathrm{e}}$. We also assume that there is a small but significant difference in activation energy between the two samples. Since $t'_{\mathrm{a}} = t_{\mathrm{a}}$, we can equate A.5 to A.6, and rearrange the expression to solve for T_{e} as follows:

$$T_{\mathrm{e}} = \frac{E_{\mathrm{a}'} - E_{\mathrm{a}}}{4\mathbf{R}ln\big(\frac{\alpha_{\mathrm{m}'}}{\alpha_{\mathrm{m}}}\big) + 4\mathbf{R}ln\big(\frac{m_2 - m_4}{m'_2 - m'_4}\big) + \frac{E_{\mathrm{a}'}}{T_{\mathrm{m}}} - \frac{E_{\mathrm{a}}}{T_{\mathrm{m}}}} \ . \tag{A.7}$$

This equation should allow for the determination of ELT by measurement of α_m at two temperatures; the second is needed to determine the activation energy, and once the activation energies are determined for both samples then they can be substituted back into Eq. A.7, along with rehydroxylation rate constants for a particular measurement temperature T_{m}.

Appendix B

Mineralogical characterisation: raw data

Table B.1: EDS-SEM data for archaeological fired-clay bricks discussed in this text. All values are wt %, uncalibrated.

Sample	K	Fe	Na	Mg	Ti	Ca
CPδ-A5	1.91 ± 0.09	7.51 ± 0.26	0.52 ± 0.08	0.42 ± 0.07	0.48 ± 0.10	0.59 ± 0.08
PBγ-A2	-	6.44 ± 0.37	1.20 ± 0.14	1.13 ± 0.12	0.52 ± 0.16	0.02 ± 0.12
OGα-A1	1.86 ± 0.12	5.86 ± 0.28	0.61 ± 0.12	0.53 ± 0.10	0.49 ± 0.13	0.09 ± 0.11
GAγ-A6	2.10 ± 0.13	5.20 ± 0.27	0.46 ± 0.13	0.66 ± 0.11	-	3.92 ± 0.16
ECα-A9	1.53 ± 0.10	4.96 ± 0.23	0.97 ± 0.11	0.54 ± 0.09	0.57 ± 0.11	0.79 ± 0.09
KCα-A3	2.44 ± 0.12	4.69 ± 0.23	0.32 ± 0.09	0.56 ± 0.09	0.42 ± 0.10	2.48 ± 0.12
X3880-A4	1.61 ± 0.15	5.36 ± 0.32	0.53 ± 0.16	0.54 ± 0.13	-	0.72 ± 0.13
RB-A7	2.07 ± 0.13	4.69 ± 0.31	0.50 ± 0.11	0.57 ± 0.10	1.16 ± 0.15	0.77 ± 0.12
A8	1.94 ± 0.12	4.67 ± 0.25	0.51 ± 0.11	0.56 ± 0.09	0.50 ± 0.11	0.96 ± 0.10

Appendix C

MATLAB/python Code

```
%% OPTIMISATION OF LINEAR FIT TO TWO-STAGE RHX DATA.
%-------------------------------------------------------------------------
% Procedure follows standard least-squares fitting, performed sequentially
% for decreasing range of t^{1/4} up till the final mass values, with an
% optimisation algorithm based on successive Shapiro-Wilk Tests and
% Hartigan's Dip Tests to optimise the normality and unimodality of the
% residuals.
% Shapiro-Wilk tests utilise the function swtest written by A. BenSada,
% available at http://uk.mathworks.com/matlabcentral/fileexchange/13964-
% shapiro-wilk-and-shapiro-francia-normality-tests/content/swtest.m
% Hartigan's Dip test utilises the function HartigansDipTest, written by
% F. Mechler, and originally based on a FORTRAN subroutine in
% APPL. STATIST. (1985) Vol. 34. No.3 pg 322-325. HartigansDipTest is
% available for download from http://www.nicprice.net/diptest/
%-------------------------------------------------------------------------

%% Specify start parameters, file to be read.

%clear all

%number of bootstrapped samples for Hartigan's Dip Test. 100 recommended.
nboot=100;

minskew=0.2;
minp=0.7;

%extra number of datapoints after minimum criteria met.
extra=3;
```

```
load MAN072_PROPOSED_ROUND_ROBIN_DATA.txt
t=MAN072_PROPOSED_ROUND_ROBIN_DATA(:,1);
tttq=MAN072_PROPOSED_ROUND_ROBIN_DATA(:,2);
mass=MAN072_PROPOSED_ROUND_ROBIN_DATA(:,4);
%t=montacid_t./(3600);
%tttq=t.^(0.25);
%mass=montacid_m.*1000;
%% Linear Least-Squares Fitting to linearised data

pf=zeros(length(mass),2,'double');
new=zeros(length(mass),1,'double');
new2=zeros(length(mass),1,'double');
new3=zeros(length(mass),1,'double');
dipp=zeros(length(mass),1,'double');
p_valuep=zeros(length(mass),1,'double');
xloww=zeros(length(mass),1,'double');
xupp=zeros(length(mass),1,'double');

for i=1:length(mass)-2
    pf(i,:)=polyfit(tttq(i:length(tttq),1),mass(i:length(mass),1),1);
    yfit(i,:) =  pf(i,1).* tttq' + pf(i,2);
    yresid(i,:) = mass' - yfit(i,:);
    SSresid(i,:) = sum(yresid(i,:).^2);
    SStotal(i,:) = ...
        (length(mass(i:length(mass),1)-1)).*var(mass(i:length(mass),1));
    rsq(i,:) = 1 - SSresid(i,1)./SStotal(i,1);
    % Shapiro-Wilk.
    [new(i,:), new2(i,:), new3(i,:)] = swtest(yresid(i,i:length(mass)));
    % Skewness
    skewnesss(i,1)=skewness(yresid(i,i:length(mass)),0);
    [dipp(i,1), p_valuep(i,1)] = ...
        HartigansDipSignifTest(yresid(i,i:length(mass)),nboot);
end

%Cumulative sums of new2, p_valuep and skewness
new2_cusum = cumsum(new2(end:-1:1))./((1:length(new2))');
new2_cusum = new2_cusum(end:-1:1);
p_valuep_cusum = cumsum(p_valuep(end:-1:1))./((1:length(p_valuep))');
p_valuep_cusum = p_valuep_cusum(end:-1:1);
skewness_cusum = cumsum(skewnesss(end:-1:1))./((1:length(skewnesss))');
skewness_cusum = skewness_cusum(end:-1:1);

p_valuep=p_valuep(1:length(p_valuep)-2,:);
new2=new2(1:length(new2)-2,:);
```

```
new=new(1:length(new)-2,:);

%% Optimisation of all three  statistics.
%ind = min(find(p_valuep>minp & new2>minp & skewnesss<minskew & ...
%    skewnesss>-minskew & new<1))...
%    + extra;
%% uncomment the following to leave out Hartigan's dip...
ind = min(find( skewnesss<minskew & ...
    skewnesss>-minskew & new<1))...
    + extra;

FormatSpec='Final fit performed from %3.2f hours (datapoint %4.0f) ...
    to end of dataset at %3.2f hours (datapoint %4.0f).\n';
fprintf(FormatSpec,t(ind), ind, t(length(t)), length(t))

cf = fit(tttq(ind:length(tttq)),mass(ind:length(mass)),'poly1');
cf_coeff = coeffvalues(cf);
cf_confint = confint(cf);
a = cf_coeff(1);
b = cf_coeff(2);
a_uncert = (cf_confint(2,1) - cf_confint(1,1))/2;
b_uncert = (cf_confint(2,2) - cf_confint(1,2))/2;

FormatSpec2='Furthermore, final fitted values are:\n alpha_{m} = %8.6f...
      %8.6f \n m_{4} = %8.6f   %8.6f \n ';
fprintf(FormatSpec2, a, a_uncert, b, b_uncert)

%% Plotting
figure('position', [0, 0, 800, 1000])
subplot(3,2,1)
graph=plot(tttq,mass,'o')
xlabel('t^{1/4} (h^{1/4})')
ylabel('mass (mg)')
title('Final Fit')
hold on
andfit=plot(tttq,yfit(ind,:),'k')
legend([graph andfit],{'Data', 'Final Linear Least Squares fit'},...
    'FontSize',8,'FontWeight','bold','Location','southeast')
subplot(3,2,2)
plot(tttq(1:length(tttq)-6,1),pf(1:length(pf)-6,1))
hold on
plot([0 tttq(length(tttq))],[a a],'-k')
plot([0 tttq(length(tttq))],[a+a_uncert a+a_uncert],'--k')
plot([0 tttq(length(tttq))],[a-a_uncert a-a_uncert],'--k')
```

```
xlabel('t^{1/4}')
ylabel('\alpha_{m} (mg.h^{-1/4})')
title('Sequentially-fitted \alpha_{m}')
subplot(3,2,3)
plot(tttq(1:length(tttq)-6,1),pf(1:length(pf)-6,2),'r')
hold on
plot([0 tttq(length(tttq))],[b b],'-k')
plot([0 tttq(length(tttq))],[b+b_uncert b+b_uncert],'--k')
plot([0 tttq(length(tttq))],[b-b_uncert b-b_uncert],'--k')
xlabel('t^{1/4}')
ylabel('m_{4} (mg)')
title('Sequentially-fitted m_{4}')
subplot(3,2,4)
SWS=plot(tttq(1:length(tttq)-2,1),new2,'b')
xlabel('t^{1/4}')
ylabel('probability')
title('Sucessive Hartigans Dip/Shapiro-Wilk Statistics')
hold on
Hart=plot(tttq(1:length(tttq)-2,1),p_valuep,'r')
Final=plot([tttq(ind) tttq(ind)],[0 1],'--k')
legend([SWS Hart Final],{'Shapiro-Wilk p-value', ...
    'Hartigans Dip p-value', 'Mininum Fit Point'},'FontSize',8,...
    'FontWeight','bold','Location','northwest')
subplot(3,2,5)
qqplot(yresid(ind,ind:length(yresid)))
title('Final Fit: QQ plot, Residuals vs Normal Distribution')
box on
subplot(3,2,6)
histogram(yresid(ind,ind:length(yresid)),30)
ylabel('Frequency')
xlabel('Bins')
title('Final Fit: Residuals')
set(gcf, 'Color', 'w');
% export_fig tttq_fits8.eps
```

```
%-------------------------------------------
%% SIMULATION OF REHYDROXYLATION RATE, WITH COOLING EFFECTS.
%-------------------------------------------------------------------------
% Program for simulation of RHX mass gain according to the original model,
% with cooling rate effects, and normally distributed fluctuations in
% temperature.
% A general model with noise is assumed:
%   y(t)=a(T)t^1/4+psi(t)+e(t)
%          At large t, psi -> 0.
% procedure for numerical simulation of RHX kinetics is as follows
```

```
%               1) generate t0, tmax and dt
%               2) generate T(t)
%               3) generate a(T)
%               4) numerically evaluate intergral of [a^(4)dt]^1/4 using
%           trapezoidal rule
% an alternative (but more lenghty) approach solves 4y^3dy=a(T)dt by
% Euler method with initial condition y(0)=0 or similar.
%------------------------------------------------------------------------

clear all
startplot=800;
%%
%--------------------------------------
%% Simulation Parameters - enter as appropriate
% time offset, t_off, and t_0 (hrs)
t_off=0.0;
t_0=0;
t_1=8766;
% t_2=18320;
% maximum time for simulation (hrs)
% Thermal properties of sample: D, sample diameter
D=0.018;
% % Thermal properties of sample: kappa, thermal diffusivity (m^2/s)
% kappa=60*60*3*10^(-7);
% Heat transfer coefficient, H (W/(m^2K))
H=5;
% bulk density (kg/m^3)
rho_b=1800;
% specific heat capacity (J/kg.K)
c=820;
% % thermal conductivity (W/m.K)
% lambda=0.45;
% Initial Temperature, T_1, Final Temperature, T_0
T_1=273.15+100.0;
T_0=273.15+22.6;
T_m=290.561;
% measured RHX rate constant at T_0 (mg.h^-1/4)
alpha_m=9.198;
% m_4 (mg)
m_4=5939;
alpha_0=alpha_m./m_4
% time step for numerical integration (hours)
dt=0.1;
% length n over which to obtain dm/dt (appropriate to experimental dataset)
```

```
n=10;
% timestep spacing of t, original experimental dataset. N.B. this should
% be >>dt
spacing=35;
timestep=spacing*dt;
% noise amplitude scaling factor for temperature function (oK). Set this to
% s.d. of thermal measurements under isothermal chamber conditions.
noiseAmplitude=0.1;
tau=D*rho_b*c/(6*H);
% Activation Energy (J/mol)
E_a=96059;
% Gas Constant (J.K^-1.mol^-1)
R=8.3144621;

%%
%--------------------------------------
% The following simulates noise drawn from a normal distribution
% by Metropolis-Hastings, for addition to T(t).

time=t_0:dt:t_1;

rng default
delta = .5;
pdf = @(x) normpdf(x);
proppdf = @(x,y) unifpdf(y-x,-delta,delta);
proprnd = @(x) x + rand*2*delta - delta;
nsamples = length(time);
x = noiseAmplitude.*mhsample(1,nsamples,'pdf',pdf,'proprnd',proprnd,...
    'symmetric',1);

%%
%--------------------------------------
% Numerical integration using Trapedoizal rule.
T=((T_1-T_0).*exp(-time./(tau./3600)))+T_0+x';

% % Jump at time 2 to 100oC
% time2=t_1+1:dt:t_1+800;
% T2=((T_1-T_0).*exp(-time2./(tau./3600)))+T_0;
%
% time3=horzcat(time,time2);
% T3=horzcat(T,T2);

alpha_p=alpha_m.*exp((E_a./(4.*R)).*((1./T_m)-(1./T)));
alpha_e=(mean(alpha_p.^(4)))^(0.25)
```

```
ELT=(4*R*((E_a/(4*R*T_m))-(log(alpha_e/alpha_m)))/E_a)^(-1)

rhs=cumtrapz(time,(alpha_0.*exp((E_a./(4.*R)).*((1./T_m)-(1./T)))).^4);
y=(rhs).^(0.25);
mass=(m_4.*y)+m_4;

% % Alternative implementation by 1st Order Runge-Kutta method:
% y0=0.001;
% ystar=zeros(size(time));
% ystar(1)=y0;
% for i=1:(length(time)-1)
%     k1=0.25*(a(i)^4)*(ystar(i))^(-3);
%     ystar(i+1)=ystar(i)+k1*dt;
% end
% mass=(m_4.*ystar)+m_4;

% time3p=time3;
% mass3p=mass;
%-------------------------------------
%% plotting

% Uncomment following for an ordinary t.^1/4 plot:
figure(1)
plot(time.^0.25,(mass-m_4)./m_4)
% plot(log(time(1,1:length(time))),log(1,1:length(time)))

% The following will plot a graph of ln(?m/?t) versus ln(t). Timestep is
% that of real data (hrs). Also - set alpha_m, m_4, t_max as appropriate.

% filter=floor(timestep./dt);
% mass=mass';
% time=time';
% for i=1:(length(mass)/filter);
%     mass1(i,1)=mass(filter*i,1);
%     time1(i,1)=time(filter*i,1);
% end
% for i=1:(length(mass1)-n)
%     new1(i,1)=(mass1(i+n,1)-mass1(i,1))./(time1(i+n,1)-time1(i,1));
%     tnew1(i,1)=time1(i+n,1);
% end
%
% fmg=(mass1-mass1(1,1))./mass1(1,1);
%
% figure(2)
```

```
% createfigure(log(tnew1(startplot:length(tnew1),1)+t_off),...
%     log(new1(startplot:length(new1),1)))
```

```
%-------------------------------------------
%MONTE CARLO PROPAGATION OF ERROR IN RHX DATES
%-------------------------------------------
%A program to simulate the pdfs of RHX dates, given
%gaussian error about mean measured quantities m2, m4 and alpham%
%This produces data for Fig. 3 in " (2015), Theoretical constraints..."
%INPUTS:
%   nsamples            Monte Carlo draws.
%   start_mass          m_{4}
%   number_of_points    Specifies the number of repeat simulations to
%                       perform.
%   alpha_m             Measured RHX rate constant
%   ELT                 Effective lifetime temperature
%   measured_temp       Measurement temperature T_{m}
% To set uncertainties in all quantities, edit lines 39 to 44
% appropriately.

clear all;

nsamples=1000000;
start_mass=1.412509;
number_of_points=130
alpha_m=0.000256200
ELT=286.0
measured_temp=287.0

e=exp(1);
R=8.3144621;
final_mass=start_mass+0.02*start_mass;
spacing=(0.02*start_mass)/number_of_points;

mu = (start_mass:spacing:final_mass)';
mu2 = repmat(mu,[1,nsamples]);
mu4 = start_mass * ones(size(mu2));
mua = alpha_m * ones(size(mu2));
muEa = 70000 * ones(size(mu2));
muTe = ELT * ones(size(mu2));
muTm = measured_temp * ones(size(mu2));
m2 = normrnd(mu2, 0.00001);
m4 = normrnd(mu4, 0.00001);
alpham = normrnd(mua, 0.000001);
Ea = normrnd(muEa,2000);
```

```
Te = normrnd(muTe,0.18);
Tm = normrnd(muTm,0.1);

ta=(((e.^(Ea./(R.*Te))).^(e.^(Ea./(R.*Tm)))).*((m2-m4)./alpham).^(4))./...
    (365.242*24);

bounds = [];

for i=1:size(ta,1)
    bounds_ = prctile(ta(i,:), [15.9 50 84.1])
    bounds = [bounds; bounds_];
end

lower=bounds(:,1);
meanta=bounds(:,2);
upper=bounds(:,3);

%relative percentage error, shaded
upperpercent=((upper-meanta)./meanta)*100;
lowerpercent=((lower-meanta)./meanta)*100;
area(meanta,upperpercent,'FaceColor',[1 1 0])
hold on;
area(meanta,lowerpercent, 'FaceColor',[1 1 0])

%write the data to .txt format. "up" and "bott" are the 1 sigma upper and
%lower bounds. "midd" is ta.
dlmwrite('up.txt',upperpercent,'delimiter','\t','precision',7);
dlmwrite('midd.txt',meanta,'delimiter','\t','precision',7);
dlmwrite('bott.txt',lowerpercent,'delimiter','\t','precision',7);

%uncomment the following to obtain the data for Fig. 2 in Hare (2015)
%dlmwrite('hist2.txt',ta(137,:),'delimiter','\t','precision',10);
```

```
#-----------------------------------------------
#CHI-SQUARE FITTING OF 1/N
#-----------------------------------------------
#A python program determine the power 1/N via gradient approximation.

import numpy as np
import matplotlib.pyplot as plt
import matplotlib.gridspec as gridspec  # for unequal plot boxes
import scipy.optimize

# define fitting function
def GaussPolyBase(f, a, b):
```

```
    return a + b*f

# read in spectrum from data file
# f=frequency, s=signal, ds=s uncertainty
f, s, sig = np.loadtxt("beta.txt", skiprows=4, unpack=True)

#multiplication factor for errors
ds=sig*0.01

# initial guesses for fitting parameters
a0, b0 = 5., 4.

# fit data using SciPy's Levenberg-Marquart method
nlfit, nlpcov = scipy.optimize.curve_fit(GaussPolyBase,
                f, s, p0=[a0, b0], sigma=ds)

# unpack fitting parameters
a, b = nlfit
# unpack uncertainties in fitting parameters from diagonal
# of covariance matrix
da, db = \
          [np.sqrt(nlpcov[j,j]) for j in range(nlfit.size)]

# create fitting function from fitted parameters
f_fit = np.linspace(0.0, 25., 128)
s_fit = GaussPolyBase(f_fit, a, b)

# Calculate residuals and reduced chi squared
resids = s - GaussPolyBase(f, a, b)
redchisqr = ((resids/ds)**2).sum()/float(f.size-6)

#calculate N
N=1/(b+1)

dN=N*db/b

# Create figure window to plot data
fig = plt.figure(1, figsize=(8,8))
gs = gridspec.GridSpec(2, 1, height_ratios=[6, 2])

# Top plot: data and fit
ax1 = fig.add_subplot(gs[0])
ax1.plot(f_fit, s_fit)
ax1.errorbar(f, s, yerr=ds, fmt='or', ecolor='black')
```

```
ax1.set_xlabel('$ln(t)$', fontsize=12)
ax1.set_ylabel('$ln(\Delta m/\Delta t)$', fontsize=12)
ax1.set_xlim(12.5, 15)
ax1.set_ylim(-26, -19)
ax1.text(0.15, 0.3, '$c$ = {0:0.1f}$\pm${1:0.1f}'
         .format(a, abs(da)), transform = ax1.transAxes)
ax1.text(0.15, 0.25, '$N$ = {0:0.1f}$\pm${1:0.1f}'
         .format(abs(N), abs(dN)), transform = ax1.transAxes)
ax1.text(0.15, 0.2, '$\chi_r^2$ = {0:0.2f}'
         .format(redchisqr),transform = ax1.transAxes)
ax1.set_title('$ln(\Delta m/\Delta t)=(N^{-1}-1)ln(t)-c$')

# Bottom plot: residuals
ax2 = fig.add_subplot(gs[1])
ax2.errorbar(f, resids, yerr = ds, ecolor="black", fmt="ro")
ax2.axhline(color="gray", zorder=-1)
ax2.set_xlabel('$ln(t)$', fontsize=12)
ax2.set_ylabel('residuals')
#ax2.set_ylim(-20, 20)
#ax2.set_yticks((-20, 0, 20))
ax2.set_xlim(12.5, 15)

plt.savefig('RHX_fits_1.pdf', dpi=1200)
plt.show()
```

Appendix D

Index of Samples

TABLE D.1: Index of samples discussed in this thesis. The final column is the page number where the sample first appears in this thesis.

Sample	Material	Location	Age (a)	pg.
CPδ-A5	Brick	Cape Town, South Africa	61	85,86,93,153
PBγ-A2	Brick	Cape Town, South Africa	mod.	85,86,93,95,100,153
OGα-A1	Brick	Cape Town, South Africa	150	86,87,93,95,153
GAγ-A6	Brick	Cape Town, South Africa	350	85,93,96,153
ECα-A9	Brick	Cape Town, South Africa	168	86,93,96,153
KCα-A3	Brick	Keble College, Oxford	142	85,86,93, 97,100, 153
X3880-A4	Brick	U.K.	349	86,93,97,153
RB-A7	Tile	U.K.	1800	86,93,98,153
A8	Brick	Cape Town, South Africa	300	98,153
MAN038	Earthenware	Enkhuizen, Netherlands	416	74,76,86,87
MAN037	Earthenware	Enkhuizen, Netherlands	416	74,76,86,87,93,115,116,120-122,143
MAN037/2	Earthenware	Enkhuizen, Netherlands	416	74,76
Chester Red	Brick	U.K.	mod.	93
MAN005	Pottery (Samian)	Unknown	1950	92,93
Samian (RLAHA)	Pottery	Unknown	unkown	92,93
Megiddo	Earthenware	Israel	4000	91,92,93
MAN088	Opus spicatum tile	U.K.	1950	93
Terracotta (3 sizes)	Terracotta	N/A	fresh	76,89-93
T (no SFE)	Terracotta	N/A	fresh	112,113,120,122,125-127,147
T (SFE)	Terracotta	N/A	fresh	112,113,120,122,125-127,147
T (lipid, SFE)	Terracotta	N/A	fresh	112,113,120,122,125-127,147
K7	Kaolinite	N/A	fresh	111,119,120,123,125
K2	Kaolinite	N/A	fresh	111,118-120,87,88,123,124,130-134,141
K1	Kaolinite	N/A	fresh	111,119,120-124
M20	Montmorillonite K-10	N/A	fresh	89,111,118,120,121,123,124,130-134,139,140
M23	Montmorillonite K-10	N/A	fresh	111,118,120,121,123,125
M21	Montmorillonite K-10	N/A	fresh	89,111,117-120,121,123,124

Bibliography

Aitken, M. J., 2013. Science-based dating in archaeology. *Routledge*, London.

Barrett, G. T., 2013. Rehydroxylation dating of fired clays: an improved *time-offset* model to account for the effect of cooling on post-reheating mass gain. *Journal of Archaeological Science* **40**, 3596-3603.

Beecher, M. F., 1916. A note on the methods for saturating clay trials for absorption and porosity determinations. *Transactions of the American Ceramic Society* **18**, 73.

Bergaya, F., Theng, B. K. G., Lagaly, G. (Eds.), 2006. Handbook of clay science: developments in clay science, Vol. 1. *Elsevier*, United Kingdom.

Bevington, P. R., Robinson, D. K., 2003. Data reduction and error analysis for the physical sciences. *McGraw-Hill*, New York.

Bird, M. J., Gröcke, D., R., 1997. Determination of the abundance and carbon isotope composition of elemental carbon in sediments. *Geochimica et Cosmochimica Acta* **61**, 3413-3423.

Bowen, P. K., Ranck, H. J., Scarlett, T. J., Drelich, J. W., 2011. Rehydration/rehydroxylation kinetics of reheated XIX-Century Davenport (Utah) ceramic. *Journal of the American Ceramic Society* **94**, 3651-3654.

Bowen, P. K., Drelich, J., Scarlett, T. J., 2013. Modeling rehydration/rehydroxylation mass-gain curves from Davenport ceramics. *Journal of the American Ceramic Society* **96**, 885-891.

Bronk Ramsey, C., 2009. Bayesian analysis of radiocarbon dates. *Radiocarbon* **51**, 337-360.

Burakov, K. S., Nachasova, I. E., 2013. Archaeomagnetic study and rehydroxylation dating of fired-clay ceramics. *Izvestiya, Physics of the Solid Earth* **49**, 105-112.

Bullin, L., Green, K., 1954. Crazing of wall tiles. *Transactions of the British ceramic society* **53**.

Campbell, J. W. P., Pryce, W., 2003. Brick: A world history. *Thames and Hudson*, London.

Carvalho, M. A., Segades, A. M., 2004. Moisture expansion: Activation energy versus firing temperature. *Key Engineering Materials* **264**, 1581-1584.

Clegg, F., Breen, C., Carter, M. A., Ince, C., Savage, S. D., Wilson, M. A., 2012. Dehydroxylation and rehydroxylation mechanisms in fired clay ceramic: A TG-MS and DRIFTS Investigation. *Journal of the American Ceramic Society* **95**, 416-422.

Cole, W. F., 1961. Moisture expansion relationships for a fired kaolinite-hydrous mica-quartz clay. *Nature* **192**, 737-739.

Cole, W. F., 1962. Possible siginificance of linear plots of moisture expansion against log of a time function. *Nature* **196**, 431-433.

Cole, W. F., 1967. Changes in a 50 m mural tape standardizing base. *The Engineer* **223**, 769-770.

Cole, W. F., Birtwistle, R., 1969. Kinetics of moisture expansion of ceramic bodies. *Bulletin of the American Ceramic Society* **48**, 1128-1132.

Craig, O. E., Love, G. D., Isaksson, S., Taylor, G., Snape, C. E., 2004. Stable carbon isotopic characterisation of free and bound lipid constituents of archaeological ceramic vessels released by solvent extraction, alkaline hydrolysis and catalytic hydropyrolysis. *Journal of analytical and applied pyrolysis* **71**, 613-634.

Crank, J., 1956. The mathematics of diffusion. *Oxford University press, Oxford.*

Crumpton, D. M., Laitinen, R. A., Smieja, J., Cleary, D. A., 1996. Thermal analysis of carbon allotropes. *Journal of chemical education*, **73**, 590-591.

Cultrone, G., Sebastian, E., Elert, K., de la Torre, M. J., Cazalla, O., Rodriquez-Navarro, C, 2004. Influence of mineralogy and firing temperature on the porosity of bricks. *Journal of the European Ceramic Society*, **24**, 547-564.

De Keyser, A., 1939. A study of kaolin and some Belgian clays. *Annales Mines Belgique*, **40**, 711-806.

Dellisanti, F., Valdré, G., 2008 Linear relationship between thermo-dehydroxylation and induced-strain by mechanical processing in vacuum: The case of industrial kaolinite, talc and montmorillonite. *Int. J. Miner. Process.* **88**, 94-99.

Derkowski, A., Drits, V. A., McCarty, D. K., 2012. Nature of rehydroxylation in dioctahedral 2:1 layer clay minerals. *American Mineralogist* **97**, 610-629.

Dobson, G., 2001. Spectroscopy and spectrometry of lipids - Part 1. *Eur. J. Lipid. Sci. Technol.* **103**, 815-840.

Drozdov, A. D., de Christiansen, J., Gupta, R. K., Shah, A. P., 2003. Model for anomalous moisture diffusion through a polymer-clay nanocomposite. *Journal of Polymer Science* **41**, 476-492.

Dunn, W. L., Shultis, J. K., 2012. Exploring monte carlo methods. *Academic press*, Amsterdam, Netherlands.

Farmer, V. C., 1974. The layer silicates. In Farmer, V.C. (Ed.) The infrared spectra of minerals. Mineralogical Society monograph 4. *Mineralogical Society, London*, 227-284.

Farmer, V. C., Russell, J. D., 1964. The infra-red spectra of layer silicates. *Spectrochimica Acta.* **20**, 1149-1173.

Freestone, I. C., 2001. Post-depositional changes in archaeological ceramics and glass. In Brothwell, D. R., Pollard, A. M., (Eds.) 2001. *Handbook of Archaeological Sciences*, *Wiley*, Chichester, 615- 625.

Friedman, I., Long, W. D., 1976. Hydration rate of obsidian. *Science* **191**, 347-352.

Frost, R. L., Kristof, J., 2004. Raman and infrared spectroscopic studies of kaolinite surfaces modified by intercalation. In Wypych, Fernando Satanarayana, Kestur Gundappa (Eds.) 2004. Clay surfaces: fundamental and applications. *Elsevier*, Amsterdam, Netherlands, p. 184-215.

Gallet, Y., Le Goff, M., 2015. Rehydration and rehydroxylation in ancient ceramics: new constraints from mass gain analyses versus annealing temperatures. *Journal of the American Ceramic Society* **98**, 2738-2744.

Geller, R. F., Creamer, A. S., 1940. Notes on moisture expansion of ceramic whiteware in storage and in service. *Journal of the American Ceramic Society* **24**, 77-79.

Grim, R. E., Bradley, W. F., 1948. Rehydration and dehydration of the clay minerals. *The American Mineralogist* **33**, 50-59.

Grim, R. E., 1968. Clay Mineralogy. *McGraw-Hill*, New York.

Hahn, K., Kärger, J., Kukla, V., 1996. Single-file diffusion observation. *Phys. Rev. Lett.* **76**, 2762-2765.

Hahn, K., Kärger, J., 1998. Deviations from the normal time regime of single-file diffusion. *J. Phys. Chem. B* **102**, 5766-5771.

Hall, C., Wilson, M. A., Hoff, W. D., 2011. Kinetics of long-term moisture expansion in fired-clay brick. *Journal of the American Ceramic Society* **94**, 3651-3654.

Hall, C., Hoff, W. D., 2012. Moisture Expansivity of Fired-Clay Ceramics. *Journal of the American Ceramic Society* **95**, 1204-1207.

Hall, C., Hamilton, A., Wilson, M. A., 2013. The influence of temperature on rehydroxylation [RHX] kinetics in archaeological pottery. *Journal of Archaeological Science* **40**, 305-312.

Halsey, G. D., 1951. The rate of adsorption on a nonuniform surface. *Journal of Physical Chemistry* **55**, 21-26.

Hamilton, A., Hall, C., 2012. A review of rehydroxylation in fired-clay ceramics. *Journal of the American Ceramic Society* **95**, 2673-2678.

Hare, V. J., 2015. Theoretical constraints on the precision and age range of rehydroxylation dating. *Royal Society Open Science* **2**, 140372.

Hare. V. J., 2012. Rehydroxylation measurements of historical fired-clays. *MSc Dissertation*, Research Laboratory for Archaeology and the History of Art, University of Oxford, U.K.

Hare. V. J., Kärger, J., Moinester, M., Piasetzky, E., 2016. Testing the $(\text{time})^{1/4}$ diffusion law of rehydroxylation in fired clays: evidence for single-file diffusion in porous media? *Diffusion Fundamentals* **2**, Diffusion Fundamentals VI - part 2. Available at http://www.qucosa.de/fileadmin/data/qucosa/documents/20118/diff_fund_25(2016)5.pdf

Harris, T. E., 1965. Diffusion with "collisions" between particles. *Journal of Applied Probability* **2**, 323-338.

Harry, K. A., Johnson, A., 2004. A non-destructive technique for measuring ceramic porosity using liquid nitrogen. *Journal of Archaeological Science* **31**, 1567-1575.

Heimann, R. B., Maggetti, M., 1981. Experiments on simulated burial of calcareous terra sigillata. In Hughes, M. J., (Ed.) *Scientific studies in ancient ceramics*, Occasional Paper 19, British Museum, London, 163-177.

Heller, L., Farmer, V. C., Mackenzie, R. C., Mitchell, B. D., Taylor, H. F. W., 1962. The dehydroxylation and rehydroxylation of triphormic dioctahedral clay minerals. *Clay Minerals Bulletin* **5**, 56-72.

Heller-Kallai, L., 2006. 'Thermally modified clay minerals', in Bergaya, F., Theng, B. K. G., Lagaly, G. (Eds.), 2006. Handbook of clay science: developments in clay science, Vol. 1. *Elsevier*, United Kingdom.

Hillel, D., 1982. Introduction to soil physics. *Academic Press*, San Diego, CA.

Holdridge, D. A., 1959. Composition variation in ball clays. *Transactions of the British ceramic society* **11**, 645-659.

Hosking, J. S., Hueber, H. V., 1958. Permanent moisture expansion of clay products on autoclaving. *Nature* **182**, 509.

Hosking, J. S., Heuber, H. V., 1959. Permanent moisture expansion of clay products on natural exposure. *Nature* **184**, 1373-1375.

Howden, M. G., 1977. Activation energy of moisture expansion of some fired clay bricks. *Transactions and Journal of the British Ceramic Society* **76**, 27-30.

Hueber, H. V., Milne, A. A., 1955. Expansion and Deterioration of Ceramic Bodies. *Nature* **176**, 509.

Hughes, R. E., Bargh, B. L., 1982. The Weathering of Brick: Causes, Assessment and Measurement. *A Report of the Joint Agreement between the U.S. Geological Survey and the Illinois State Geological Survey.*

Ince, C., 2008. Water transport kinetics in mortar-masonry systems. *PhD Thesis*, School of Mechanical, Aerospace and Civil Engineering, University of Manchester.

Joint Committee for Guides in Metrology, 2008. Evaluation of measurement data - Guide to the expression of uncertainty in measurement (First Edition). Available online: http://www.bipm.org/utils/common/documents/jcgm/JCGM_100_2008_E.pdf Accessed 5 Sep 2012.

Johnson, J. S., Clark, J., Miller-Antonio, S., Robins, D., Schiffer, M. B., Skibo, J. M., 1987. Effects of firing temperature on the fate of naturally occurring organic matter in clays. *Journal of Archaeological Science* **15**, 403-414.

Kalinkin, A.M., Kalinkina, E.V., Zalkind, O.A., Makarova, T.I., 2005. Chemical interaction of calcium oxide and calcium hydroxide with CO_2 during mechanical activation. *Inorganic Materials* **41**, 1218-1224.

Kärger, J., Ruthven, D. M., Theodorou, D. N., 2012. Diffusion in nanoporous materials, *Wiley-VCH*, Weinheim, Germany.

Kukla, V., Kornatowski, J., Demuth, D., Girnus, I., Pfeifer, H., Rees, L. V. C., Schunk, S., Unger, K. K., Kärger, J., 1996. NMR studies of single-file diffusion in unidimensional channel zeolites. *Science* **272**, 702-704.

Laird, J. S., Geller, R. F., 1919. The rehydration of calcined clays. *Journal of the American Ceramic Society* **2**, 828-832.

Le Chatelier, H., 1887. De l'action de la chaleur sur les argiles. *Bulletin de la Société Française de Minéralogie et de Cristallographie* **10**, 204-211.

Levitt, D. G., 1973. Dynamics of a single-file pore: non-Fickian behaviour. *Physical Review A* **8**, 3050-3054

Le Goff, M., Gallet, Y., 2014. Evidence for complexities in the RHX dating method. *Journal of the American Ceramic Society* **57**, 897-910.

Le Goff, M., Gallet, Y., 2014. Evaluation of the rehydroxylation dating method: Insights from a new measurement device. *Quaternary Geochronology* **20**, 89-98.

Le Goff, M., Gallet, Y., 2014. Experimental variability in kinetics of moisture expansion and mass gain in ceramics. *Journal of the American Ceramic Society* **98**, 398-401.

Low, M. J. D., 1960. Kinetics of chemisorption of gases on solids. *Chemical Reviews* **60**, 267-312.

Luca, V., Cardile, C.M., 1988. Thermally induced cation migration in Na and Li montmorillonite. *Phys Chem Minerals* **16**, 98-103.

Macht, F., Eusterhues, K., Pronk, G. J., Totsche, K. U., 2011. Specific surface area of clay minerals: Comparison between atomic force microscopy measurements and bulk-gas (N_2) and liquid (EGME) adsorption methods. *Applied Clay Science* **53**, 20-26.

Madejová, J, Komandel, P., 2001. Baseline studies of the Clay Minerals Society source clays: Infrared methods. *Clays and Clay Minerals* **49**, 410-432.

Madejová, J., 2003. FTIR techniques in clay mineral studies. *Vibrational Spectroscopy* **31**, 1-10.

Magetti, M., 1982. Phase analysis and its significance for technology and origin. In Olin, J.S., Franklin, J. D. (Eds), 1982. Archaeological Ceramics, *Smithsonian Institution Press*, Washington D.C., p. 121-133.

Mata, M. P., Peacor, D. R., Gallart-Marti, M. D., 2002. Transmission electron microscopy (TEM) applied to ancient pottery. *Archaeometry* **44**, 155-176.

Mattyasovszky-Zsolnay, L., 1946. Investigations on crazing, I-III. *Journal of the American Ceramic Society* **29**, 200-204.

Mazzucato E., Artioli, G., Gualtieri, A., 1999. High temperature dehydroxylation of muscovite-$2M_1$: a kinetic study by in situ XRPD. *Phys. Chem. Minerals* **26**, 375-381.

McBurney, J. W., 1954. Masonry cracking and damage caused by moisture expansion of structural clay tile. *American Society for Testing Materials Proceedings* **54**, 1219-1241.

Meier, L. P., Menegatti, A. P., 1997. A new, efficient, one-step method for the removal of organic matter from clay-containing sediments. *Clay minerals*, **32**, 557-563.

Mellor, J. W., Holdcroft, A. D., 1911. The chemical constitution of the kaolinite molecule. *Transactions of the English Ceramic Society* **9**, 94-120.

Mesbah, H., Wilson. M. A., Carter., M. A., 2010. The role of the kaolinite-mullite reaction sequence in moisture mass gain in fired kaolinite. *Paper presented at the CIIMTEC Ceramic Conference, Italy.*

Michels, J. W., Tsong, I. S. T., Smith, G. A., 1983. Experimentally derived hydration rates in obsidian dating. *Archaeometry* **25**, 107-117.

Mitchell, B. D., Smith, B. F. L., 1974. The removal of organic matter from soil extracts by bromine oxidation. *Journal of Soil Science* **25**, 239-241.

Moinester, M, Piasetzky E., Braverman, M., 2014. RHX dating of archaeological ceramics via a new method to determine effective lifetime temperature. *Journal of the American Ceramic Society* **98**, 913-919.

Molina-Montes, E., Timon, V., Hernandez-laguna, A., Ignacio Sainz-diaz, C., 2008. Dehydroxylation mechanisms in Al^{3+}/Fe^{3+} dioctohedral phyllosilicates by quantum mechanical methods with cluster models. *Geochimica et Cosmochimica Acta* **72**, 3929-3938.

Moore, D.M., Reynolds, R.C., 1997. X-Ray diffraction and the identification and analysis of clay minerals (2^{nd} Ed.), *Oxford University Press*, Oxford.

Mulla, D. J., Low, P. F., Roth, C. B., 1985. Measurement of the specific surface area of clays by internal reflectance spectroscopy. *Clays and Clay Minerals*, **33**, 391-396.

Muller, F., Plancon, A., Drits, V. A., 2000. Studies of the dehydroxylated-rehydroxylated montmorillonite: Structure of the layers and intercalation of water molecules. *Journal de Physique IV* **10**, 481-487.

Nachasova, I. E., Burakov, K. S., 2012. Variations in geomagnetic intensity and temperature in the Second Millennium B.C. in Spain. *Izvestiya, Physics of the Solid Earth* **48**, 434-440.

Nield, D. A., Bejan, A., 2006. Convection in porous media. *Springer*, USA.

Numrich, M., Kutschera, W., Steier, P., Sterba, J.H., Golser, R., 2015. On the effect of organic carbon on rehydroxylation (RHX) dating. *Journal of Archaeological Science* **57**, 92-97.

Nuñez, R., Capel, J., Reyes, E., Delgado, A., 2002. Hydrolysis of ceramics materials: neoformation or rehydroxylation of clay minerals. Oxygen stable isotope analysis. *Clay Minerals* **37**, 345-349.

Ostrom, M.E., 1961. Separation of clay minerals from carbonate rocks by using acid. *J. Sediment. Petrol.* **31**, 123-129.

Parfitt, R. L., Fraser, A. R., Farmer, V. C., 1977. Adsorption on hydrous oxides. III. Fulvic acid and humic acid on goethite, gibbsite, and imogolite. *The Journal of Soil Science* **28**, 289-296.

Pask, J.A., Davies, B. 1945. Thermal analysis of clays and acid extraction of alumina from clays. *U.S. Bur. Mines, Tech. Paper* **664**, 56-78.

Pollard, A. M., Heron, C., 2008. Archaeological Chemistry (2^{nd} Ed.). *RSC publishing*, Cambridge.

Rouxhet, P. G., 1970. Kinetics of dehydroxylation and of OH-OD exchange in macrocrystalline micas. *Am. Mineral*, **55**, 841-853.

Savage, S. D., Wilson, M. A., Carter, M. A., McKay, B., Hoff, W. D., 2008. Mass gain due to the chemical recombination of water in fired clay brick. *Journal of the European Ceramic Society* **91**, 3396-3398.

Schurecht, H. G., 1928. Methods for testing crazing of glazes caused by increases in size of ceramic bodies. *Journal of the American Ceramic Society* **11**, 271-277.

Schurecht, H. G., Pole, G.R., 1929. Effect of water in expanding ceramic bodies of difference compositions. *Journal of the American Ceramic Society* **82**, 596-604.

Secco, M., Maritan, L., Mazzoli, C., Lampronti, G. I., Zorzi, F., Nodari, L., Russo, U., Mattioli S. P., 2011. Alteration processes of pottery in lagoon-like environments. *Archaeometry* **53**, 809-829.

Serratosa, J.M., 2013. Dehydration and rehydration studies of clay minerals by infrared absorption spectra, Proceedings of the 9th National Clay Conference. *Pergamon Press*, New York.

Shoval, S. Paz, Y., 2013. A study of the mass-gain of ancient pottery in relation to archaeological ages using thermal analysis. *Applied Clay Science* **82**, 113-120.

Shoval, S., Beck, P., Kirsh, Y., Levy, D., Gaft, M., Yadin, E., 1991. Rehydroxylation of clay minerals and hydration in ancient pottery from the 'Land of Geshur', *Journal of Thermal Analysis* **37**, 1579-1592.

Sposito, G., 2008. The chemistry of soils, 2^{nd} Ed. *Oxford University Press*, Oxford.

Stevenson, C. M., Gurnick, M., 2016. Structural collapse in kaolinite, montmorillonite and illite clay and its role in the ceramic rehydroxylation dating of low-fired earthenware. *Journal of Archaeological Science* **69**, 54-63.

Theng, B. K. G., 1979. Formation and properties of clay-polymer complexes. *Elsevier*, Amsterdam.

Tokiwai, K., Nakashima, S., 2010. Dehydration kinetics of muscovite by in situ infrared microspectroscopy. *Phys. Chem. Minerals* **37**, 91-101.

Tosheva, L., Mihailova., B., Wilson, M. A., Carter, M. A., 2010. Gravimetric and spectroscopic studies of the chemical combination of moisture by as-fired and reheated terracotta. *Journal of the European Ceramic Society* **30**, 1867-1872.

Troell, E. 1931. The use of sodium hypobromite for the oxidation of organic matter in the mechanical analysis of soils. *The Journal of Agricultural Science* **21**, 476-483.

Van Ham-Meert, A., 2015. Supercritical fluid extraction of organics from ceramics. *MSc Dissertation*, Research Laboratory for Archaeology and the History of Art, University of Oxford, U.K.

Vyazovkin, S., Wight, C. A., 1997. Kinetics in solids. *Annual Reviews in Physical Chemistry* **48**, 125-149.

Washburn, E. W., Footitt, F. F., 1921. Porosity: III. Water as an absorption liquid. *Journal of the American Ceramic Society* **4**, 961982.

Weisstein, E. W., 2012. Error Propagation. From MathWorld - A wolfram web resource. http://mathworld.wolfram.com/ErrorPropagation.html Accessed 5 Feb 2012.

White, W.B., 1974. The carbonate minerals. In Farmer, VC (Ed.) The infrared spectra of minerals. Mineralogical Society Monograph 4. *Mineralogical Society, London,* 227-284.

Wilson, M. A., Hoff, W. D., Hall, C., McKay, B., Hiley, A., 2003. Kinetics of moisture expansion in fired clay ceramics: A $(\text{Time})^{1/4}$ law. *Physical Review Letters* **90**, 125503.

Wilson, M. A., Carter, M. A., Hall, C., Hoff., W. D., Ince, C., Savage, S. D., McKay, B., Betts, I. M., 2009. Dating fired-clay ceramics using long-term power law rehydroxylation kinetics. *Proceedings of the Royal Society A* **465**, 2407-2415.

Wilson, M. A., Hamilton, A., Ince, C., Carter, M. A., Hall, C., 2012. Rehydroxylation (RHX) dating of archaeological pottery. *Proceedings of the Royal Society A* **468**, 3476-3493.

Wilson, M. A., Clelland, S., Carter, M. A., Ince, C., Hall, C., Hamilton, A., 2013. Rehydroxylation of fired-clay ceramics: factors affecting early-stage mass gain in dating experiments. *Archaeometry* **56**, 689-702.

Wolff, R.G., 1963. Structural aspects of kaolinite using infrared absorption. *American Mineralogist* **48**, 390-399.

Zaitseva, G., Skripkin, V., Kovaliukh, N., Possnert, G., Dolukhanov, P., Vybornov, A., 2009. Radiocarbon dating of neolithic pottery. *Radiocarbon* **51**, 795-801.

Zhao, S., Bowen, P. K., Drelich, J. W., Scarlett, T. J., 2015. Reproducibility in rehydroxylation of ceramic artifacts. *Journal of the American Ceramic Society* **98**, 3367-3372.

Zsembery, S., Waechter, R. T., McNeilly, T. H., 2004. The Expansion of clay bricks after 30 years and a method for its prediction. *Proceedings of the Seventh Australian Masonry Conference, Newcastle*, 182-191.